Title
Bio-inspired Control of Robots to Assist Humans with Repetitive Movement Tasks

Author
Zhao, Jinxin

Publication Date
2017

Peer reviewed|Thesis/dissertation

UNIVERSITY OF CALIFORNIA

Los Angeles

Bio-inspired Control of Robots to Assist Humans with Repetitive Movement Tasks

A dissertation submitted in partial satisfaction
of the requirements for the degree
Doctor of Philosophy in Mechanical and Aerospace Engineering

by

Jinxin Zhao

2017

ABSTRACT OF THE DISSERTATION

Bio-inspired Control of Robots to Assist Humans
with Repetitive Movement Tasks

by

Jinxin Zhao
Doctor of Philosophy in Mechanical and Aerospace Engineering
University of California, Los Angeles, 2017
Professor Tetsuya Iwasaki, Chair

Oscillatory movements play important roles in human life, various movements in human life, such as walking, bicycling, cleaning, chewing, swimming, etc., are periodic or repetitive. A robotic device that can assist human with such motion tasks would be of utterly significance. This research work addresses the control design problem for such robotic devices and investigates the methods for designing feedback controllers for a robotic system to help a human with periodic motion tasks. The control objective is to stabilize a human-intended oscillatory movement while reducing the required human effort.

To approach this problem, two mathematical models are studied and formed as controllers accordingly for a general mechanical system. First, a biological neural circuit model, central pattern generator (CPG), is adopted. Animal locomotions under CPG control are capable of complying with various environment dynamics to yield different oscillatory movements. A mathematical model of reciprocal inhibition oscillator (RIO), a simple-structured and well-studied type of CPG, is taken advantage of. The RIO controller acts as a nonlinear damping compensator and removes part of the resistive forces in the system, thereby reducing the human effort. It is shown that the resulting human-intended oscillation is a locally stable periodic solution of the closed-loop system, assuming a simple human intention motor control. The result is first presented for a single degree-of-freedom (DOF) mechanical system and then extended to a multi-DOF system.

Alternatively, a nonlinear oscillator model, Andronov-Hopf Oscillator (AHO), is selected. Nonlinear oscillators are appropriate candidates for controlling such systems since they are capable of generating stable rhythm signals. Here I consider the problem of designing a nonlinear adaptive feedback controller for uncertain linear mechanical systems so that convergence to a natural mode of oscillations is achieved for the closed-loop system. A controller is proposed based on the Andronov-Hopf oscillator with additional adaptation mechanisms for estimating the unknown natural frequency and damping parameters. It is proven that, with sufficiently slow adaptation, the estimated parameters locally converge to their true values and entrainment to the natural oscillation is achieved as part of an orbitally stable limit cycle. Numerical examples demonstrate that adaptation and convergence can in fact be fast.

To examine the research results, a four-linkage robotic arm system is designed and prototyped. With the hardware set-up, the proposed human intention motor control is validated by first identifying the control parameters and then replacing human to control the robotic arm. Furthermore, it is experimentally shown that robotic arm under RIO control is able to stabilize human-intended oscillatory movements and reduce the human effort.

The dissertation of Jinxin Zhao is approved.

Lieven Vandenberghe

Jacob Rosen

Tsu-Chin Tsao

Tetsuya Iwasaki, Committee Chair

University of California, Los Angeles

2017

To my parents, my wife and the unnamed ...

TABLE OF CONTENTS

LIST OF FIGURES

LIST OF TABLES

ACKNOWLEDGMENTS

I would first thank my advisor Professor Iwasaki. I am utterly grateful that he selected me as his student in 2014. During this research project, his patient advising has been guiding me through the mist of unknowns. His profound knowledge sets a target for me to pursue and also will motivate me to keep chasing in future. Meanwhile, I am thankful that he gave me the freedom of choosing the directions of the research project and always supported my decisions.

I would like to thank my committee members Professor Rosen, Professor Tsao and Professor Vandenberghe. Professor Rosen provided tremendous helpful advises through our meaningful discussions about the robotic arm design. Professor Tsao's question during my oral exam inspired me the idea of human modeling. I formulated many least-square problem to identify various parameters during this project, and the idea came from Professor Vandenberghe's suggestion of using off-line optimization. I would like to thank Professor Hopkins for the generous support of 3-D printing and the help from his student Luke. I would also thank all the former and present members of our Cybernetic Control Lab, together who created and maintained such a pleasant lab culture. Our department staff offered me huge assistance on my way of completing this project and I would particularly thank Angie, Abel, Lance and Samantha.

Moreover, I would like to thank my wife Dan Li, who always supports me and encourages me. I cannot stop thinking how lucky I am to meet her. I would like to give enormous thanks to my parents, who make this chance of education possible.

Hanging out with Yuwei, Poting and Michael was always a relaxing experience but in the meantime the conversations sparked new ideas of research. Hence I would like thank all of them.

VITA

2011	B.Sc, Mechanical Engineering, Zhejiang University, China
2011-2013	Research Assistant, Aerospace Engineering, University of Michigan, Ann Arbor
2012-2013	Teaching Assistant, Aerospace Engineering, AERO201 Introduction to Aerospace Engineering, University of Michigan, Ann Arbor
2013	M.Sc, Aerospace Engineering, University of Michigan, Ann Arbor
2013-present	Research Assistant, Mechanical and Aerospace Engineering, University of California, Los Angeles
2015-2016	Teaching Assistant, Mechanical and Aerospace Engineering, MAE171 Dynamic Systems Control, MAE273A Robust Control, University of California, Los Angeles

PUBLICATIONS

Jinxin Zhao, Tetsuya Iwasaki, "CPG-Controlled Assistive Robot and Human motor control Identification," IEEE Transactions on Control System Technology. (Under review as a regular paper)

Jinxin Zhao, Tetsuya Iwasaki, "Natural Entrainment via Adaptive Andronov-Hopf Oscillator," IEEE Transactions on Automatic Control. (Under review as a regular paper)

Jinxin Zhao, Florian Dörfler, "Distributed control and optimization in DC microgrids", Automatica, Volume 61, November 2015, Pages 18-26, ISSN 0005-1098.

Jinxin Zhao, Tetsuya Iwasaki, "Adaptive natural entrainment via Andronov-Hopf oscillator", American Control Conference (ACC), 2017, 1257-1262

J. Zhao and T. Iwasaki, "CPG control for assisting human with periodic motion tasks," 2016 IEEE 55th Conference on Decision and Control (CDC), Las Vegas, NV, 2016, pp. 5035-5040.

Jinxin Zhao, Florian Dörfler, "Distributed control, load sharing, and dispatch in DC microgrids," 2015 American Control Conference (ACC), Chicago, IL, 2015, pp. 3304-3309.

J. Zhao, J. Seok, J. Selvakumar, R. Bencatel, P. Kabamba and A. Girard, "A greedy policy for feet-level radar resource management," 52nd IEEE Conference on Decision and Control, Firenze, 2013, pp. 3160-3165.

J. Seok, J. Zhao, J. Selvakumar, E. Sanjaya, P. T. Kabamba and A. Girard, "Radar resource management: Dynamic programming and dynamic finite state machines," 2013 European Control Conference (ECC), Zurich, 2013, pp. 4100-4105.

CHAPTER 1

Introduction

Repetitive body movements, such as the swing motion of legs and arms during human locomotion, are essential in human life. Inventions of mechanical devices that help human achieve those movements (e.g., exoskeleton) would be of significant benefit to the human with disability due to aging, injury, neurological disorder, etc. Human assistive system has drawn decent amount of attention from robotics researchers. This kind of devices can provide assistive forces to the operator, thereby reducing his/her effort and stabilizing the desired oscillatory movements. Studies e.g. [28, 45] have shown that such devices can be used for neuro-rehabilitation to improve motor control capability.

Hence designing the control strategy is of utterly significance for the successful design of such robotic devices. The objective of this project is to establish a method for designing a feedback controller for a general robotic system interacting with human to stabilize the intended oscillation and reduce the human burden by providing assistive forces. We can learn from the biological observation when we focus on the oscillatory movements. Studies in biology and zoology have shown that resonance or natural oscillations are exploited for rhythmic movements during animal locomotion to achieve high energy efficiency [2, 3]. Various mechanisms are discussed in [3] for adjusting the natural body dynamics to set a resonance frequency appropriately for a desired speed of locomotion. A model-based study of experimental data in fish swimming [27] suggests that the tail beat frequency is aligned with hydrodynamic resonance, while the muscle stiffness is actively adjusted by co-contraction to exploit overall body-fluid resonance. Similar observations of resonance exploitation have been made in human movements. Human subjects, asked to move their forearm periodically with different mass and spring loads, tend to tune the movement frequency into the natural

frequency of the mechanical loads [51].

The fact that animal is exploiting resonance has attracted interests from engineers in the field of robotics. And control algorithms for human assistive devices have been studied and some effective methods are proposed. The most commonly-used control strategy in assistive device is a combination of predefined trajectory with impedance control [32]. For a lower limb orthosis called ATLAS [44], the gait pattern is first analyzed and pre-generated, then a passive PD controller regulates the actual movement to the pre-defined trajectory through a restoring force emulating a mechanical impedance. A similar approach is used in robot suit HAL [45], where the reference gait pattern is generated off-line, the human intended walking phase is estimated in real time to generate a command signal, and then a PD controller achieves the regulation. However, classical methods were not ready to address this important issue. Robotic actuators used to be highly stiff and is controlled by servo controllers to achieve fast and precise motion. Such robot architecture and control algorithm are useful for industrial manipulators, and have also been implemented in other tasks such as legged locomotion [43, 47] and human assistive exoskeleton [24, 37]. In these applications, dedicated trajectory planning and high gain servo tracking are required. As a result, such robotic devices are not adaptive nor compliant to varying environment and have high energy consumption [29]. Another control method, admittance control, is often employed to provide assistive power for large payload, where the controllers modify the apparent payload felt by the human through force feedback [17, 38].

A major challenge for controlling assistive devices is the detection of the human intention. A seminal work [42] is based on measured electromyography (EMG) signals, which indicate the electrical activity of skeletal muscles. Such signals can be used as an explicit indication of human intention. The detected EMG signal is passed through a Hill-type muscle model to estimate the intended joint moment, which is then used as a reference command for a moment servo controller to drive an exoskeleton. This powerful technique provides numerous possibilities in clinical/biomedical applications for assisting humans; see e.g. [13]. However, EMG signals may not perfectly correlate with human intention without careful calibrations due to the complex musculo-skeletal structure and activation dynamics. Other methods for

detecting human intention, in addition to EMG signals, include the direct sensing of the forces applied by the human [53], and electroencephalogram (EEG) signals [8]. While these methods have been shown to be effective to some extent, none of these is accepted as the best and ongoing researches still seek for improved methods.

Most existing methods for controlling human assistive devices apply to general, possibly non-repetitive movement tasks. When we consider periodic motions such as walking, however, we can exploit biological knowledge at the neuronal level for developing control algorithms. Neuroscience researches have shown that periodic body movements in animal locomotion are controlled by neuronal circuits called the central pattern generators (CPGs), which are nonlinear oscillators producing rhythmic pattern outputs for commanding muscle contractions [36]. The CPG mechanisms in [39] have been adopted for walking rehabilitation to generate reference trajectories of kinematic variables, modulated by EEG signals indicating the gait cycle phase [8]. Similar approaches have been taken for walking assistance by exoskeletons using adaptive frequency oscillators with encoder feedback [41, 46], and phase estimators based on position and ground force measurements [33].

While the CPG-based approaches mentioned above employ explicit learning mechanisms for adapting the CPG parameters to kinematic motion variables, the CPG has an ability, without such parameter adaptation, to comply with varying environmental dynamics through sensory feedback [23]. In particular, a CPG can detect the resonance frequency of a mechanical system through position measurements and achieve a natural mode of oscillation as a stable limit cycle of the closed-loop control system [15, 16, 21]. If we view the human action as shaping of the natural dynamics, the CPG mechanisms appear to be useful for assistive control by complying with human intention. However, whether this idea works or not depends on the dynamics of human motor control.

To control a mechanical system and exploit a resonance, the controller needs to have the essential capability of detecting and entraining to the natural oscillation. In [40], a dynamic Hebbian learning method is introduced for an Andronov-Hopf oscillator (AHO) to adapt its frequency to match the frequency of a rhythmic input signal. The learning algorithm is implemented in a quadruped robot to exploit a resonance [7]. Simulation results for the

adaptive frequency oscillators displayed slow convergence of the frequency parameter, but the method is effective once the frequency is learned. A biological control system, called the central pattern generator (CPG), has been shown to have the ability to detect and tune into the mechanical resonance [19,21,48–50]. CPG parameters are fixed constant and no learning process involving explicit parameter estimation is required, resulting in very fast convergence. The underlying mechanisms have been used for designing bio-inspired controllers to achieve adaptive entrainment to a natural mode of oscillations for mechanical systems [15, 16] or provide assistive force to help human make oscillatory movement [52]. While the methods were found effective for certain cases, no theoretical guarantee for convergence was provided. A more recent result [11] used the feedback resonance [14] to achieve finite-time convergence to an oscillation at a natural frequency for a class of mechanical systems. Unlike the results mentioned earlier, convergence was rigorously proven, but the control law is discontinuous and the system is restricted to those with Rayleigh damping.

Understanding how human chooses the motor control command would provide a guidance for helping impaired patients to regain certain motor capability, as well as for designing assistive and rehabilitation devices. To explain the visual-guided reaching movement mechanism, different models have been proposed, including feedforward, feedback, and hybrid models, and there has been an ongoing controversy among these three models [9]. The feedforward model suggests that human motor command is pre-planned based on the target and initial states, while fine adjustment through feedback only happens during the end of the task [25,34]. The feedback model assumes that the muscle command is produced during the movement based on the difference between target and current states [12, 20]. An improved feedback model is discussed in [18], where an inner observer is added to the control loop. The hybrid model combines the feedforward and feedback model, and a validation of such model has been conducted in [9]. As described in [35], the feedforward part of a hybrid model can be learned by a neural network.

The dissertation is organized as follows. In chapter 2, the CPG based control design approach is discussed. This research seeks to create a method of control designing for assistive robotic devices. The study starts with the formulation of a single-DOF problem in section 2.2.

In section 2.3, the mathematical of reciprocal inhibition oscillator (RIO), one type of CPG, is exploited to construct the controller. The conditions on the controller parameters, when the controller can stabilize the human intended oscillation and provide human assistance to compensate the system damping, are investigated and provided in section 2.4. In this analysis, a human motor control model is proposed, which would be validated in the later experiments. The result of single-DOF case is then extended to multi-DOF system in section 2.5, with the assumption of Rayleigh damping. Before the implementation of the controller, its performance is first justified by multiple simulations in section 2.6, testing the system stability and amount of human effort reduction with respect to different plant systems and human intended oscillations. This assistive control method could be robust and insensitive to plant and human intention changes. However, the amount of human assistance may reduce when the estimated damping is away the true system damping.

In chapter 3, an AHO adaptive controller is introduced for natural oscillation entrainment. For this problem, the design starts with developing a novel stability analysis method for linear periodic system in section 3.2. Then a external signal synchronization problem is studied in section 3.3. It is shown that an adaptive oscillator can serve as an intrinsic model of generator of a periodic signal. The problem of exact natural oscillation entrainment problem was considered and formulated in section 3.4. The controller was designed through following steps. First, an Andronov-Hopf oscillator (AHO) was chosen to act as the intrinsic model of the plant and it was expected to synchronize with the plant at the limit cycle. Additional dynamics of natural frequency adaptation was added to the control structure for the sake of natural frequency estimation. Moreover, another dynamics of damping estimation was attached. As before, the result was first developed for a general single-DOF second-order mechanical system and followed by extension to multi-DOF system in section 3.5. The controller capability is justified by multiple simulations in section 2.6, where the controller is fixed, while the plant system impedance parameters vary.

The experiment process is designed and the requirements of hardware are summarized first in chapter 4. A robotic arm is then designed accordingly and control scheme of the system is also explained here. Following in chapter 5, through multiple experiments that a

human subject performs tracking tasks, the parameters of human intention motor control model are identified. Note that the human motor control model was proposed for the analysis of closed-loop system with RIO assistive control. This model is validated then by comparing the resulted trajectories between under human subject control and under intention model control. In chapter 6, the assistive controller is implemented and human effort is compared under different payload settings with or without the assistive control, in order to verify the controller capacity. Finally, the results are concluded in chapter 7 and ideas of future research work are discussed.

Notation: Let $\text{diag}(x_1, ...x_n)$ and $\text{col}(x_1, ...x_n)$ represent the diagonal matrix and column vector with entries $x_1, \ldots, x_n$. For a matrix-valued function $V(t)$, the maximum norm $\|V(t)\|$ over time is denoted by $\|V\|_\infty$.

CHAPTER 2

Central Pattern Generators (CPG) control

2.1 Overview

In this chapter, the ability of a CPG control is first examined, without explicit learning mechanisms, to drive a mechanical system interacting with a human, and assist with oscillatory movement tasks. I adopt the reciprocal inhibition oscillator (RIO) for the control architecture, which is a simple and well-studied type of CPG. The situation was first considered where a human applies a force to a single degree-of-freedom (DOF) robotic system, loaded by a resistive environment, to achieve an intended periodic motion. A design problem is formulated in section 2.2 for the RIO control to drive the system and stabilize the human-intended oscillation, while reducing the human burden. Motivated by the mechanism of the RIO to achieve robust entrainment to a natural oscillation [16,21], in section 2.3 I first derive a condition for the RIO controller to achieve a damping compensation approximately. In section 2.4, the nonlinear closed-loop robot-RIO-human system is then analyzed to give a sufficient condition for stability of the human-intended periodic motion, assuming that the human motor control can be modeled as a combination of feedforward and feedback terms. It is shown that the control design does not require knowledge of the human model, and the stability is guaranteed if the human control satisfies a certain qualitative property. Section 2.5 discusses the expended results in multi-DOF system. The proposed RIO control scheme is validated through simulation in section 2.6 and physical experiments on a simple robotic arm in latter chapter.

2.2 Problem Formulation

I consider a situation where a human is tasked to achieve a repetitive movement of a mechanical system by applying a force input v as shown in Fig. 2.1a. Our objective is to develop a systematic method for designing a feedback controller, labeled as "CPG" in Fig. 2.1b, that assists the human by applying a force input u so that the human-intended periodic motion is achieved while the human control effort is reduced. To formalize the problem and provide a theoretically justified solution, let us focus on a one-DOF mechanical system.

Consider a mechanical system described by

$$m\ddot{z} + d\dot{z} + kz = v + u \tag{2.1}$$

where $m, d, , k \in \mathbb{R}$ are positive parameters representing the mass, damping, and stiffness, $v(t) \in \mathbb{R}$ and $u(t) \in \mathbb{R}$ are the force inputs from a human and an actuator driven by a feedback controller, and $z(t) \in \mathbb{R}$ is the resulting displacement. Suppose the human intends to achieve an oscillatory movement

$$z_d(t) = a_d \sin \omega_d t. \tag{2.2}$$

Without help from the controller ($u = 0$), the human input must satisfy $v = v_o$ when achieving $z = z_d$, where

$$v_o := m\ddot{z}_d + d\dot{z}_d + kz_d. \tag{2.3}$$

To generate this input signal v_o, the human may use a general control strategy of state feedback and feedforward so that the desired oscillation z_d is stabilized. In this chapter, the following form is assumed:

$$v = \alpha\dot{z} + \beta z + \gamma, \tag{2.4}$$

where α and β are constant gains, and $\gamma(t)$ is a feedforward signal dependent on the target oscillation z_d.

The target is to design a feedback controller that generates input u based on measured output z to help the human so that the human effort is reduced while achieving the desired

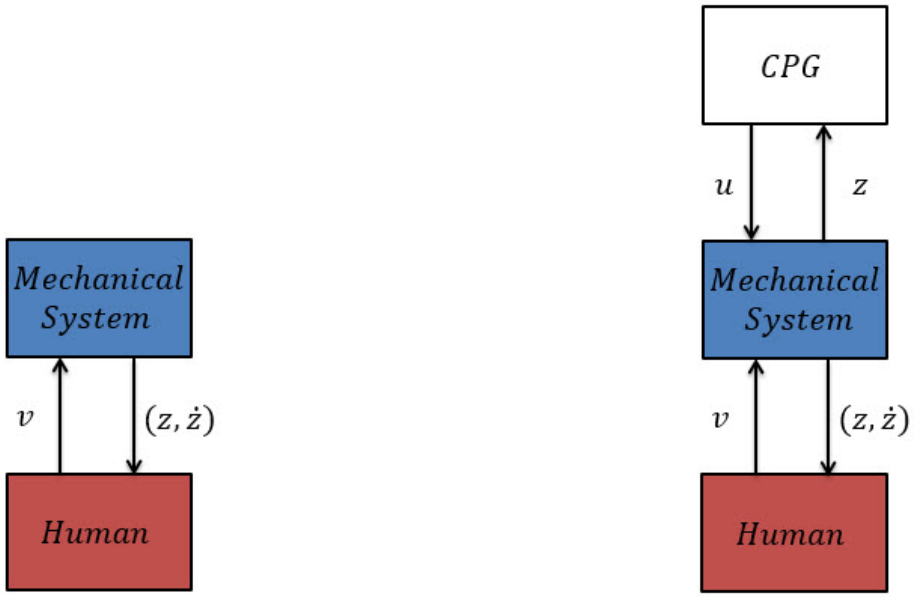

(a) Without assistive control

(b) With assistive control

Figure 2.1: Human operation with/without assistive control

oscillation. In particular, a controller is considered of the form

$$u = \mathsf{g}(p), \quad \dot{p} = \mathsf{h}(p, z). \tag{2.5}$$

The human would see the controlled mechanical system, (2.1) and (2.5), as the "plant," and adjust the control law (2.4) to achieve the desired oscillation $z = z_d$ by generating $v = v_o - u_d$ *in the steady state*, where u_d is the control input u resulting from the feedback signal $z = z_d$ through (2.5). This is achieved by a control of the form (2.4) by selecting an appropriate signal $\gamma(t)$; in particular,

$$v = v_o - u_d + \alpha(\dot{z} - \dot{z}_d) + \beta(z - z_d). \tag{2.6}$$

Assuming this human control action, $z = z_d$ is a solution to the closed-loop system defined by (2.1), (2.5), and (2.6).

The human burden can be reduced by a simple damping compensator $u = \delta\dot{z}$. With this control, the steady state input from the human should be $v = v_\delta$ where

$$v_\delta = m\ddot{z}_d + (d - \delta)\dot{z}_d + kz_d.$$

It can readily be shown that

$$\|v_o\|_\infty^2 - \|v_\delta\|_\infty^2 = \delta(2d - \delta)(a_d\omega_d)^2.$$

Thus the human effort as measured by the amplitude of input force is reduced when $0 < \delta < 2d$, with the maximum reduction $(da_d\omega_d)^2$ at $\delta = d$. However, the controller $u = d\dot{z}$ would make the augmented plant, seen by the human, marginally stable, and a small perturbation of d due to e.g. uncertain damping coefficient could destabilize the controlled plant. In this case, the burden of stabilization is on the human control, requiring an extra human effort.

It is preferred that the controller not only to achieve the reduction of human effort but also to stabilize the desired oscillation z_d. To this end, let us precisely define the stability property.

Definition 1. *Consider the system given by* (2.1), (2.5), *and* (2.6). *The trajectory* $z_d(t)$ *is said to be stable if there exists* $\varepsilon > 0$ *such that*

$$||z(0) - z_d(0)|| < \varepsilon \quad \Rightarrow \quad \lim_{t\to\infty} ||z(t) - z_d(t)|| = 0.$$

The problem addressed in this chapter can now be formally stated as follows.

Problem 1. *Consider the mechanical system in* (2.1) *with human control* (2.6) *and assistive control* (2.5). *Given a desired oscillation* $z_d(t) = a_d \sin(\omega_d t)$, *design a controller* (2.5) *such that* $\|v\|_\infty < \|v_o\|_\infty$ *and* $z_d(t)$ *is a stable trajectory of the closed-loop system.*

In the next section, I will characterize a class of nonlinear controllers that approximately achieve $u = \delta\dot{z}$. A condition on the controller parameters will then be given to guarantee stability of the desired oscillation z_d in the section that follows.

2.3 CPG Control for Damping Compensation

For the architecture of controller (2.5), I adopt a rather simple and well-studied CPG, called the reciprocal inhibition oscillator (RIO). A mathematical description of the RIO controller

is given by (see [15, 21])

$$q = b(s)(L\Psi(q) + Hz), \quad u = G\Psi(q), \tag{2.7}$$

with $q(t) \in \mathbb{R}^2$ being the variable, and

$$b(s) = \frac{2\varpi s}{(s+\varpi)^2}, \quad l = \begin{bmatrix} 1 \\ -1 \end{bmatrix}, \quad \begin{matrix} G = gl^{\mathsf{T}}, \\ H = hl, \end{matrix} \tag{2.8}$$

$$\Psi(q) = \begin{bmatrix} \psi(q_1) \\ \psi(q_2) \end{bmatrix}, \quad L = -\mu \begin{bmatrix} 0 & 1 \\ 1 & 0 \end{bmatrix},$$

where $g, h, \mu, \varpi \in \mathbb{R}$ are design parameters, $\psi(x)$ is a sigmoid (bounded, increasing, odd) function capturing the synaptic threshold effect, and $b(s)$ is a band-pass filter representing the time lag and adaptation in neuronal dynamics. The parameters μ and ϖ are assumed positive, and I use $\psi(x) := \tanh(x)$. The RIO exhibits anti-phase oscillations of q_1 and q_2 with a frequency near ϖ in the absence of input ($z = 0$) when the coupling strength is sufficiently large ($\mu > 1$). With an arbitrary input z, it is proven [15] that the anti-phase property is preserved in the steady state, i.e., $q_1 + q_2$ converges to zero as $t \to \infty$.

In what follows, I will derive a condition under which the RIO control in (2.7) compensates for the damping so that $u \cong \delta \dot{z}$ for a fixed parameter δ, where the equality holds only approximately due to the nonlinearity in (2.7). A classical tool for approximating a static nonlinearity in the context of oscillation analysis is the describing function [26]. While describing functions provide fairly accurate predictions of oscillatory behaviors [22], it is difficult to guarantee dynamical properties with proofs when they are used for analyses. Here I propose another approximation method that turns out later to allow for a rigorous stability analysis. In particular, for a T-periodic signal $x(t)$, I approximate $\psi(x)$ using the average slope:

$$\psi(x) \cong \kappa(x)x, \quad \kappa(x) := \frac{1}{T}\int_0^T \psi'(x(t))dt$$

where ψ' is the derivative of ψ.

Now, consider the control input u generated by a T-periodic input z through (2.7), where I assume that q and u are also T-periodic. The existence of a periodic solution q to (2.7) can

be justified by Lemma 3 in the appendix when $|h|$ is sufficiently small. Since $q_1 + q_2 = 0$ in the steady state, q can be expressed as $q = xl$ for some T-periodic signal $x(t) \in \mathbb{R}$. In this case, the dynamical relationship in (2.7) reduces to

$$u = 2g\psi(x), \quad x = b(s)(\mu\psi(x) + hz).$$

To obtain a linear approximation of the system near the target oscillation $z = z_d$, let x_d be the solution to the above equation when the input to the controller is $z = z_d$. Employing the average slope method, $\psi(x)$ can be approximated as $\psi(x) \cong \kappa(x_d)x$ in the neighborhood of $x = x_d$. In this case, the RIO control in (2.7) is approximately given by

$$u \cong K(s)z, \quad K(s) := \frac{2gh\kappa(x_d)b(s)}{1 - b(s)\mu\kappa(x_d)}. \tag{2.9}$$

The following result gives a condition for this approximate controller to compensate for the damping.

Theorem 1. Consider the RIO control (2.7). Let $\delta \in \mathbb{R}$ be a positive scalar and $z_d(t)$ be given by (2.2). Suppose there exists a T-periodic solution $x_d(t)$ to

$$x_d = b(s)(\mu\psi(x_d) + hz_d) \tag{2.10}$$

where $T = 2\pi/\omega_d$, and define $K(s)$ as in (2.9). Then, the RIO control achieves the damping compensation approximately, i.e., $K(s) = \delta s$ for $s = j\omega_d$, if and only if

$$\frac{4gh\varpi\kappa(x_d)}{\varpi^2 - \omega_d^2} = \delta, \tag{2.11a}$$

$$\mu\kappa(x_d) = 1, \tag{2.11b}$$

are satisfied.

Proof. The result follows by noting that

$$K(s) = \frac{4gh\varpi\kappa(x_d)s}{s^2 + 2\varpi(1 - \mu\kappa(x_d))s + \varpi^2} \tag{2.12}$$

and verifying that $K(j\omega_d) = j\omega_d\delta$ is equivalent to (2.11). □

Lemma 3 in the appendix guarantees the existence of T-periodic x_d satisfying (2.10) when $|h| \neq 0$ is sufficiently small and $\mu \neq 1$. In this case, $q_d := x_d l$ is a solution to (2.5) with $z = z_d$, and the corresponding control input u is well defined. Theorem 1 characterizes the parameters of the RIO control such that the damping compensation $u = \delta \dot{z}$ is achieved approximately near the target operating condition $z = z_d$, thereby reducing the human effort. A benefit of the nonlinear RIO controller over the simple linear compensation $u = \delta \dot{z}$ is the stability felt by the human. With the linear control, the closed-loop system of (2.1) and $u = \delta \dot{z}$, which receives the human force v as the input, is stable when $\delta < d$ but becomes unstable when $\delta > d$. With the RIO control, however, the free response of the closed-loop system of (2.1) and (2.7) is convergent for both cases. The stability properties are illustrated by the initial state responses simulated with $v = 0$ in Fig. 2.2, where the system parameters are fixed, using Theorem 1, to

$$\begin{aligned} &(m, d, k) = (1, 10, 2), && \omega_d = 1, \\ &(h, \mu, \varpi) = (0.5, 1.01, 5), && g = \delta\mu(\varpi^2 - \omega_d^2)/(4h\varpi), \end{aligned}$$

with two cases of damping compensation $\delta = 11$ and 9 (the blue curve for the case $\delta = 11$ plots $z/100$ to show the divergence behavior). With the stability, the damping parameter δ in the RIO control can be safely tuned on the experimental site to match with the uncertain loading d.

The next section will explore further conditions on the RIO parameters to guarantee stability of the human-intended oscillation z_d as a solution to the closed-loop system.

2.4 Stability of the Periodic Solution

Consider the closed-loop system consisting of the plant (2.1), human control (2.4), and the RIO control (2.7). I assume that the human control is chosen as in (2.6) to make the target oscillation z_d in (2.2) a solution of the closed-loop system. Assuming the knowledge of the human control parameters (α, β), I will show how the RIO control parameters (g, h, μ, ϖ) can be chosen to stabilize z_d. After a formal statement of the stability condition, I will discuss robustness against uncertainties in (α, β).

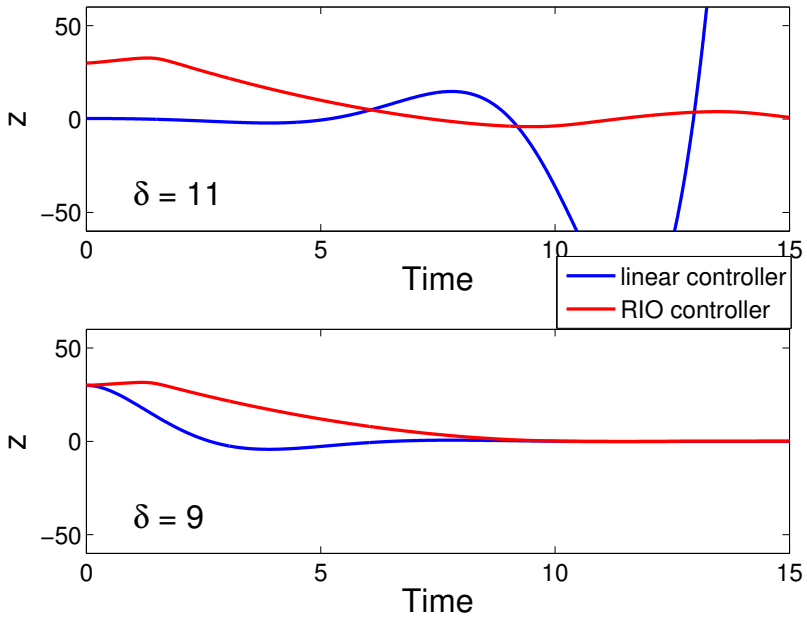

Figure 2.2: Mechanical-RIO system behavior without human input

First note that the closed-loop system can be expressed as

$$\begin{aligned} \ddot{z} &= G\Psi(\dot{p})/m + \gamma/m - d_\alpha \dot{z} - k_\beta z \\ \ddot{p} &= 2\varpi(L\Psi(\dot{p}) + Hz - \dot{p}) - \varpi^2 p \end{aligned} \tag{2.13}$$

where $p \in \mathbb{R}^2$ is a state associate with the transfer function $b(s)$ and is related to q by $\dot{p} = q$, and

$$k_\beta := (k - \beta)/m, \quad d_\alpha := (d - \alpha)/m.$$

It can be verified that $(z, p) = (z_d, p_d)$ is a solution of (2.13) where p_d is a periodic signal such that $\dot{p}_d = x_d l$ and the average of p_d over a cycle is zero, with x_d being a periodic solution to (2.10). The linearization of (2.13) around $(z, p) = (z_d, p_d)$ is given by the linear T-periodic system

$$\dot{\eta} = A(t)\eta \tag{2.14}$$

where $T := 2\pi/\omega_d$ and

$$\eta := \mathrm{col}(z_e, \dot{z}_e, p_e, \dot{p}_e), \quad z_e := z - z_d, \quad p_e := p - p_d,$$

$$A = \begin{bmatrix} 0 & 1 & 0 & 0 \\ -k_\beta & -d_\alpha & 0 & (g/m)\psi'(x_d)l^\intercal \\ 0 & 0 & 0 & I \\ 2\varpi hl & 0 & -\varpi^2 I & 2\varpi(\psi'(x_d)L - I) \end{bmatrix}, \tag{2.15}$$

As is well known [26], exponential stability of the trajectory (z_d, p_d) for the original nonlinear system (2.13) is equivalent to exponential stability of the linearized system (2.14). According to a result in [5] (Theorem 2 on page 36), the linear periodic system (2.14) is asymptotically stable if $\bar{A}$ is Hurwitz and $\|\mathscr{E}\|_\infty$ is sufficiently small, where

$$\bar{A} := \frac{1}{T}\int_0^T A(t)dt, \quad \mathscr{E}(t) := A(t) - \bar{A},$$

and $\|\mathscr{E}\|_\infty$ is the maximum of $\|\mathscr{E}(t)\|$ over a cycle. Based on this stability condition, The following result can be reached.

Theorem 2. Consider the closed-loop system consisting of the plant (2.1), human control (2.6), and RIO control (2.7). Suppose the human chooses (α, β) such that

$$k_\beta := \frac{k - \beta}{m} > 0, \quad d_\alpha := \frac{d - \alpha}{m} > 0. \tag{2.16}$$

Then $z_d(t)$ in (2.2) is a solution of the closed-loop system. Let positive scalars $\delta, \varpi \in \mathbb{R}$ be given such that

$$0 < \frac{\omega_d^2 - \varpi^2}{\omega_n^2 - \varpi^2} < r := \frac{d - \alpha}{\delta}, \quad \omega_n := \sqrt{k_\beta} \tag{2.17}$$

Then, for each $\mu > 1$ with sufficiently small $\mu - 1$, there exists an h with sufficiently small $|h|$ such that a T-periodic solution x_d to (2.10) exists and $z_d(t)$ is a stable solution of the closed-loop system, where the remaining RIO parameter g is chosen to satisfy (2.11a).

Proof. I will prove stability of the linearized system (2.14) by showing that the average dynamics $\bar{A}$ is Hurwitz and the periodic perturbation $\mathscr{E}(t) := A(t) - \bar{A}$ is small. Since we consider the RIO control satisfying (2.11a), we shall regard (δ, h, μ, ϖ) as the design parameters instead of (g, h, μ, ϖ).

First, I show that $\bar{A}$ is Hurwitz in the limiting case where $\mu \to 1$ and $|h| \to 0$, provided (δ, ϖ) satisfies (2.17). Noting that $\bar{A}$ is given by $A(t)$ in (2.15) with $\psi'(x_d)$ replaced by $\kappa(x_d)$,

the characteristic polynomial $p(\lambda) := \det(\lambda I - \bar{A})$ is obtained as

$$p(\lambda) = (\lambda^2 + c_1\lambda + \varpi^2)(\lambda^4 + c_2\lambda^3 + c_3\lambda^2 + c_4\lambda + c_5) \tag{2.18}$$

$$\begin{aligned}
&c_1 := 2(2-\zeta)\varpi, \quad c_2 := 2\varpi\zeta + d_\alpha, \quad c_5 := k_\beta\varpi^2,\\
&c_3 := \varpi^2 + 2\varpi\zeta d_\alpha + k_\beta, \quad c_4 := \varpi^2 d_\alpha + 2k_\beta\varpi\zeta - \chi,\\
&\chi := (\delta/m)(\varpi^2 - \omega_d^2), \quad \zeta := 1 - \mu\kappa(x_d),
\end{aligned}$$

where χ is expressed in terms of δ by solving (2.11a) for g and substituting the result to remove the explicit dependence of χ on g. Applying the Routh stability criterion, the characteristic polynomial with $\zeta = 0$ is Hurwitz if and only if

$$\varpi > 0, \quad d_\alpha > 0, \quad k_\beta > 0, \tag{2.19a}$$

$$\varpi^2 d_\alpha > \chi > -d_\alpha k_\beta, \quad \chi(\varpi^2 d_\alpha - d_\alpha k_\beta - \chi) > 0. \tag{2.19b}$$

It is tedious but straightforward to verify that condition (2.19b) is equivalent to (2.17). Thus, for the given (δ, ϖ), the characteristic polynomial with $\zeta = 0$ is Hurwitz. By continuity, there exists $\varepsilon > 0$ such that the original characteristic polynomial is Hurwitz for all ζ such that $|\zeta| < \varepsilon$. Let μ be chosen to satisfy $1 < \mu < 1 + \varepsilon$. Then $-\varepsilon < 1 - \mu < 0$ and hence $|\zeta| < \varepsilon$ if $\kappa(x_d)$ is sufficiently close to 1, which is the case when $|h|$ is sufficiently small for the following reason. In Lemma 3, $b_\mu(s)$ has no poles on the imaginary axis if and only if $\mu \neq 1$ when $b(s)$ is given by (2.8). Hence, when $|h|$ is sufficiently small, there exists a T-periodic solution $x_d(t)$ to (2.10) with its peak value $\|x_d\|_\infty$ converging to zero as $|h| \to 0$. In this case, $\kappa(x_d)$ approaches 1 as $|h|$ approaches zero. Thus stability of the average dynamics dictated by $\bar{A}$ is proven.

Now I can show that $\|\mathscr{E}\|_\infty$ approaches 0 as $|h| \to 0$. Let us denote x_d by x_h to show its dependence on h explicitly. There are only two nonzero entries of $\mathscr{E}(t)$, which are

$$\mathscr{E}_{24} := \frac{\chi l^\intercal}{4\varpi} \cdot \frac{\psi'(x_h) - \kappa(x_h)}{h} \cdot \frac{1}{\kappa(x_h)}$$

for the (2,4) entry and

$$\mathscr{E}_{44} := 2\varpi L(\psi'(x_h) - \kappa(x_h))$$

for the (4,4) entry. From Lemma 3,

$$\lim_{h\to 0} \mathscr{E}_{24} = \frac{\chi l^{\mathsf{T}}}{4\varpi} \cdot 0 \cdot 1 = 0$$

$$\lim_{h\to 0} \mathscr{E}_{44} = 2\varpi L \cdot 0 = 0.$$

Thus we have $\|\mathscr{E}\|_\infty \to 0$ as $h \to 0$. □

If the human control parameters (α, β) and the intended oscillation $z_d(t)$ were precisely known in advance and satisfied (2.16), then Theorem 2 and its proof suggest the following design procedure for the RIO control. First, choose positive scalars $\delta, \varpi \in \mathbb{R}$ satisfying (2.17). Grid the ζ parameter space and numerically calculate the roots λ_i of the characteristic equation $\det(\lambda I - \bar{A}) = 0$ to plot the largest real part $\max \Re[\lambda_i]$ as a function of ζ. Theorem 2 guarantees that the value at $\zeta = 0$ is negative, and hence by continuity there exists $\varepsilon > 0$ such that $\max \Re[\lambda_i] < 0$ for all $|\zeta| < \varepsilon$. Fix $\mu \in \mathbb{R}$ within the interval $1 < \mu < 1 + \varepsilon$. Grid the h parameter space and numerically calculate the maximum Floquet multiplier τ of the linearized system as a function of h, where

$$\tau(h) := \max |\mathrm{eig}(\Phi(T))|, \quad \dot{\Phi} = A\Phi, \quad \Phi(0) = I.$$

Theorem 2 guarantees that $|\tau(h)| < 1$ and the linearized system is stable when $|h|$ is sufficiently small. Choose a value of such h. The resulting RIO control stabilizes $z_d(t)$.

In reality, the human control parameters (α, β) are uncertain, and the intended oscillation $z_d(t)$ may not be decided in advance or may vary over time. Thus, the design procedure described above does not apply exactly. However, the RIO control may be designed to maintain stability of $z_d(t)$ robustly against uncertainties in (α, β) and $z_d(t)$. In particular, Fig. 2.3 shows the region on the (ϖ^2, r) plane in which the stability condition (2.17) is satisfied. We see that if $r \geq 1$, then the stability condition is met as long as

$$\omega_n < \omega_d < \varpi \quad \text{or} \quad \varpi < \omega_d < \omega_n \tag{2.20}$$

is satisfied. Moreover, if ϖ is chosen close to ω_d within the interval, then stability is maintained even when $r < 1$.

Ideally, the human specifies the intended oscillation $z_d(t)$ by the open-loop input $\gamma(t)$ without taking the burden of stabilization ($\alpha = \beta = 0$), while the RIO control stabilizes $z_d(t)$ and reduces the human effort through the damping compensation $u \cong \delta \dot{z}$. To achieve this operation, the values of the RIO control parameters may be tuned on site. Set h and μ such that $|h|$ and $\mu - 1$ are sufficiently small, and choose ϖ near a rough estimate of ω_d in accordance with (2.20). Gradually increase the value of δ from zero and search for the "comfortable zone" for the human, which may be done by direct human evaluation, or based on measurements of force sensors to monitor the human effort. It is expected that experiments will clarify the utility of the RIO control, but such full justification is out of the scope of this chapter. Instead, a numerical example is provided in a later section.

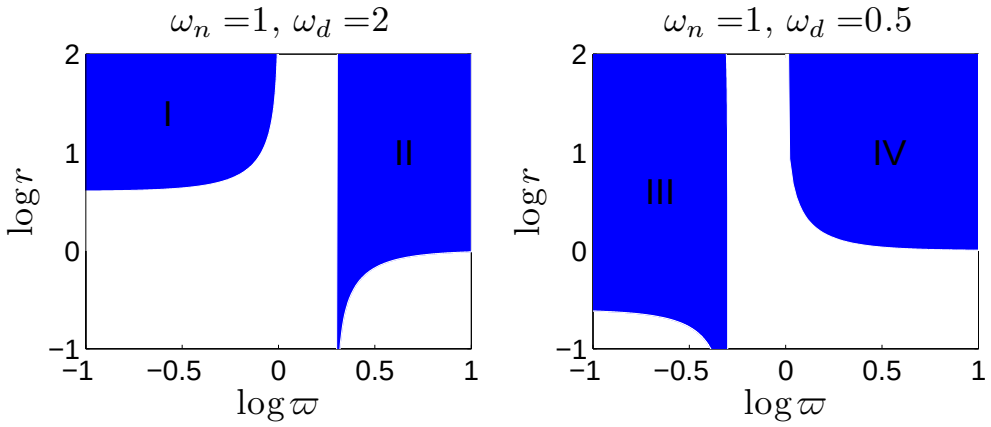

Figure 2.3: Stability regions (shaded) for (ϖ, r) satisfying (2.17).
Case $\omega_n < \omega_d$ (left) and Case $\omega_d < \omega_n$ (right). The vertical asymptotes are at $\varpi = \omega_n$ and ω_d, while the horizontal asymptotes are at $r = 1$ and $(\omega_d/\omega_n)^2$.

2.5 Extension to Multi-DOF System

In this section, the result in the previous sections will be extended to the case where the plant is a multi-DOF mechanical system. It is assumed that the damping is Rayleigh damping and full actuation for the plant, and the extension will be straightforward through the modal decomposition. Full extension to general mechanical systems will be left for further study.

Consider an n-DOF mechanical system controlled by a human with or without help from

an additional feedback controller

$$M\ddot{\mathsf{z}} + D\dot{\mathsf{z}} + K\mathsf{z} = \boldsymbol{\nu} + \mathfrak{u}, \tag{2.21}$$

where $\mathsf{z} \in \mathbb{R}^n$ is the generalized coordinates, $\boldsymbol{\nu} \in \mathbb{R}^n$ and $\mathfrak{u} \in \mathbb{R}^n$ are the force inputs from the human and the controller, respectively. Here I assumed that the system is fully actuated, i.e., there are n actuators that can independently control all the degrees of freedom, and the force inputs are defined so that each input actuates one of the generalized coordinates. I also assume that J and K are symmetric positive definite, which are standard in general mechanical systems without rigid body modes. In addition, I assume Rayleigh damping, i.e., $D = \rho K$ for some $\rho > 0$, which is a common way to model dissipation effects in structural dynamics.

The human desires to achieve an oscillation $\mathsf{z} = \mathsf{z}_d$ specified by

$$\mathsf{z}_d(t) = \Re[\xi e^{j\omega_d t}], \quad \xi_i = a_i e^{jb_i}. \tag{2.22}$$

Note that the i^{th} entry of $\mathsf{z}_d(t)$ is the harmonic oscillation with frequency ω_d, amplitude a_i, and phase b_i. Without the assistance from the controller ($\mathfrak{u} = 0$), the human input is $\boldsymbol{\nu} = \boldsymbol{\nu}_o$, where

$$\boldsymbol{\nu}_o := M\ddot{\mathsf{z}}_d + D\dot{\mathsf{z}}_d + K\mathsf{z}_d. \tag{2.23}$$

It is desired to design a controller that generates $\mathfrak{u}$ based on the measurement z to help human achieve the desired oscillation z_d. The controller is of the form

$$\mathfrak{u} = \mathsf{g}(\mathsf{p}), \quad \dot{\mathsf{p}} = \mathsf{h}(\mathsf{p}, \mathsf{z}). \tag{2.24}$$

I assume that the human control $\boldsymbol{\nu}$ achieves $\mathsf{z} = \mathsf{z}_d$ by generating $\boldsymbol{\nu} = \boldsymbol{\nu}_o - \mathfrak{u}_d$, where $\mathfrak{u}_d$ is the control input resulting from the feedback control (2.24) with sensory signal z_d. As mentioned earlier, it is our best interest to let the controller, rather than human, take care of the burden for stabilization of z_d. Therefore, I consider the open-loop control by human, where it is assumed that the human generates fixed force input $\boldsymbol{\nu}_o - \mathfrak{u}_d$.

The general idea for the control design is to transform the mechanical system into the modal coordinates and apply the RIO control for each mode separately. As a result, we will

obtain a feedback controller of the form (2.24) consisting of n RIO controllers multiplexed through the mode shape transformation. The details are now given below.

Let the modal decomposition of (M, K) be given by

$$(\lambda_i M + K)e_i = 0, \quad e_i \neq 0, \quad i = 1, \dots, n$$

where $e_i \in \mathbb{C}^n$ and $\lambda_i \in \mathbb{C}$ are generalized eigenvectors and eigenvalues, with the magnitude of e_i normalized such that $e_i^* M e_i = 1$. Since M and K are real symmetric positive definite, both e_i and λ_i are real, e_i are linearly independent, and $\lambda_i < 0$. Through the coordinate transformation

$$\mathfrak{z} = Ez, \quad \mathfrak{v} = MEv, \quad \mathfrak{u} = MEu, \quad E := \begin{bmatrix} e_1 & \cdots & e_n \end{bmatrix},$$

the system (2.21) can be described as

$$\ddot{z}_i + \rho\omega_i^2 \dot{z}_i + \omega_i^2 z_i = v_i + u_i, \quad i = 1, \dots, n \tag{2.25}$$

where $\omega_i := \sqrt{-\lambda_i}$ is the undamped natural frequency of the i^{th} oscillation mode.

I apply the RIO control of the form (2.7) for each mode (2.25), resulting in the overall controller described by

$$\mathfrak{u} = MEu, \quad z = E^{-1}\mathfrak{z}, \tag{2.26a}$$

$$q_i = b_i(s)(L_i\Psi(q_i) + H_i z_i), \quad u_i = G_i\Psi(q_i), \tag{2.26b}$$

for $i = 1, \dots, n$, where the parameters are defined by (2.8) with subscript i added, and (g, h, μ, ϖ) replaced by $(g_i, h_i, \mu_i, \varpi_i)$. Designing each RIO control as in Theorem 2, we have the following result.

Theorem 3. Consider the closed-loop system consisting of the plant (2.21), RIO control (2.26), and human force input $\mathfrak{v}$. Suppose the human chooses $\mathfrak{v}(t)$ such that $\mathfrak{z}_d(t)$ in (2.22) is a solution of the closed-loop system. Let positive scalars $\delta_i, \varpi_i \in \mathbb{R}$ be given such that

$$0 < \frac{\omega_d^2 - \varpi_i^2}{\omega_i^2 - \varpi_i^2} < \frac{\rho\omega_i^2}{\delta_i}, \tag{2.27}$$

Then, for each $\mu \in \mathbb{R}^n$ such that $\mu_i > 1$ with sufficiently small $\mu_i - 1$, there exists an $h \in \mathbb{R}^n$ with sufficiently small $\|h\|$ such that a T-periodic solution $x_{d_i}(t) \in \mathbb{R}$ to

$$x_{d_i} = b_i(s)(\mu_i \psi(x_{d_i}) + h_i z_{d_i}), \quad z_d = E^{-1}\mathsf{z}_d \tag{2.28}$$

exists and $\mathsf{z}_d(t)$ is a stable solution of the closed-loop system, where the remaining RIO parameter $g \in \mathbb{R}^n$ is chosen as

$$g_i = \frac{\delta_i(\varpi_i^2 - \omega_d^2)}{4h_i\varpi_i\kappa(x_{d_i})}.$$

Proof. With the modal decomposition of the plant and the RIO control applied to each mode separately, the closed-loop system can be viewed as a collection of n independent subsystems, each of which consists of (2.25) and (2.26b). The result then follows directly from Theorem 2 under the open-loop human control $\alpha = \beta = 0$. □

The benefit of the RIO control is to reduce the human burden and stabilize the intended oscillation z_d. The stability property is as described in Theorem 3. Let us discuss how the human burden can be reduced. As in the single-DOF case result in the previous section, the control input in the steady state approaches the linear damping compensation $u_i = \delta_i \dot{z}_i$ when the parameters h_i and μ_i are chosen so that $|h_i|$ and $\mu_i - 1$ are sufficiently small. Thus, the control law approaches

$$\mathfrak{u} = \Delta\dot{\mathsf{z}}, \quad \Delta := ME\nabla E^{\mathsf{T}}M, \quad \nabla := \mathrm{diag}(\delta_1, \ldots, \delta_n)$$

in the limit, where it is noted that $E^{\mathsf{T}}ME = I$. Under the assistive RIO control with the damping compensation, the human force input should be

$$\boldsymbol{\nu}_\Delta = M\ddot{\mathsf{z}}_d + (D - \Delta)\dot{\mathsf{z}}_d + K\mathsf{z}_d.$$

When compared with the human input without assistive control, $\boldsymbol{\nu}_o$ in (2.23), the oscillation amplitude of each entry of $\boldsymbol{\nu}_\Delta$ is not necessarily smaller than that of $\boldsymbol{\nu}_o$. However, it can readily be verified that

$$\dot{\mathsf{z}}_d^{\mathsf{T}}\boldsymbol{\nu}_o - \dot{\mathsf{z}}_d^{\mathsf{T}}\boldsymbol{\nu}_\Delta = \dot{\mathsf{z}}_d^{\mathsf{T}}\Delta\mathsf{z}_d \geq 0$$

holds. This means that the power that needs to be supplied by the human to maintain z_d can be reduced by the assistive control.

2.6 Numerical Example

Let us consider the situation where a human and an RIO controller are collaborating to drive a simple mechanical system described by (2.1) to achieve a desired oscillation z_d in (2.2). The system parameters (m, d, k) for the plant are set as $m = 1$, $d = 10$ and $k = 1$, while the desired oscillation is $z_d = \sin 2t$. The nominal human control is open loop in this example, i.e. $(\alpha, \beta) = (0, 0)$. In the design process, I assume the accurate information about the system parameters (m, d, k), frequency of the human intended oscillation ω_d, and human control parameters (α, β) are all known. Once an RIO controller is designed, I will verify stability of z_d and effectiveness of human effort reduction for the nominal case. In addition, I will examine robustness of these properties against perturbations in the mechanical damping d, intended frequency ω_d, and human parameters (α, β).

The control design proceeds as follows. Noting that $\omega_n = \sqrt{k/m} = 1$ and $\omega_d = 2$, the stability region for (ϖ, r) is given by Fig. 2.3 (left). For maximum reduction of human effort, I choose $\delta = d = 10$, fixing $r := d/\delta = 1$. Let us choose $\varpi = 3$ so that the point $(\log \varpi, \log r) = (0.48, 0)$ lies in region II of Fig. 2.3. Next I calculate the maximum real part of the roots of the characteristic polynomial (2.18) as a function of ζ (Fig. 2.4, top). In accordance with Theorem 2 (and its proof), all the characteristic roots have negative real parts when $\zeta = 0$, which is guaranteed by the choice of (ϖ, r). From the figure, the Hurwitz property is maintained for all $|\zeta| < \varepsilon := 0.06$. Based on this, I choose $\mu = 1.01$, which satisfies $1 < \mu < 1 + \varepsilon$.

To complete the control design, I now simulate the system (2.10) and obtain a T-periodic solution x_d for various values of h. As shown in Lemma 3, x_d can be obtained by looking for a stable or unstable limit cycle of the system (2.10) in the neighborhood of the origin, which can be found by simulating system (2.10) forward or backward in time with an initial state near the origin. It was observed that there is a threshold $\hbar = 0.05$ such that the limit cycle is stable/unstable when $|h|$ is larger/smaller than $\hbar$.

For each h, the periodic signal x_d thus obtained allows us to explicitly compute $|\tau(h)|$, the maximum magnitude of Floquet multiplier of the linear periodic system (2.14), while g

is chosen to satisfy the condition (2.11a). Figure 2.4 (middle) shows $|\tau(h)|$ for various h, and we see that a large range of h yields stable system (2.14) and hence z_d as a stable solution for the nonlinear closed-loop system. Figure 2.4 (bottom) shows the value of $\zeta := 1 - \mu\kappa(x_d)$ as a function of h, where ζ is nearly zero when $h = 0.1$. Thus I choose $h = 0.1$ to ensure proper damping compensation through satisfaction of (2.11b) for the best human effort reduction.

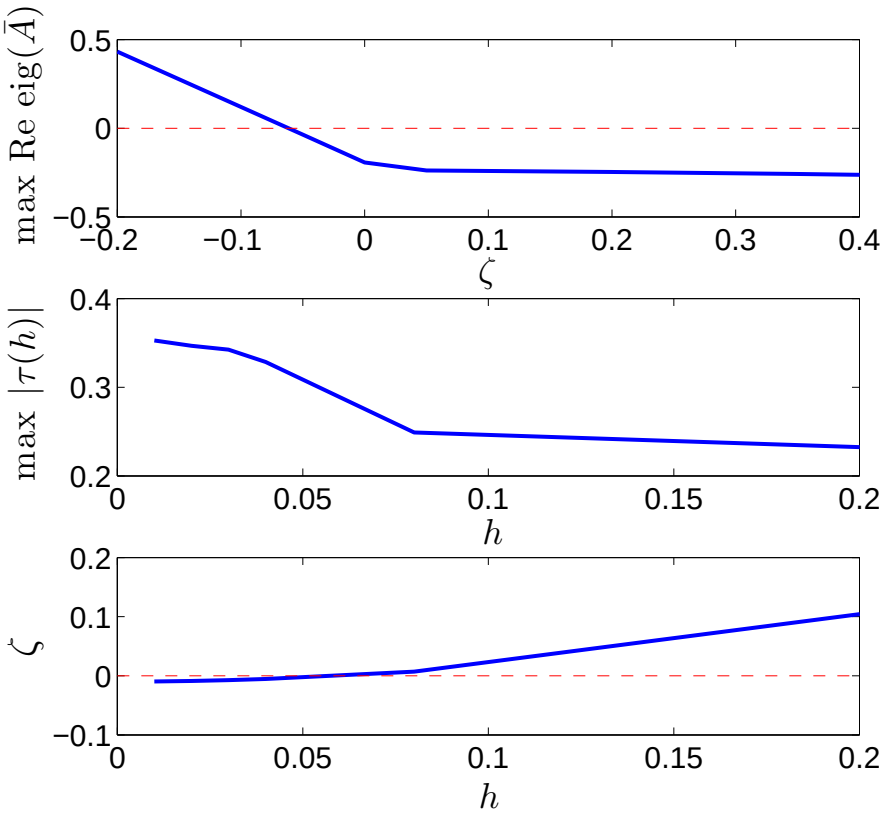

Figure 2.4: Stability and damping compensation analyses

The controller parameters are now fixed to $\delta = 10$, $h = 0.1$, $\mu = 1.01$, and $\varpi = 3$. I evaluate the design by simulating the closed-loop system of (2.1), (2.6), and (2.7). In the simulation, let us consider the situation where the plant and human control operate at their nominal condition for the first 30 s and then switch to a perturbed condition as indicated in Table 2.1. Under the perturbed condition, the models for the plant damping (d) and the human control (α, β) are inaccurate and differ from what I assume during the control design. The human intended oscillation z_d also changes, but the transition takes 15 s. This change is reflected in the human control through a linear interpolation of the feedforward component γ

Table 2.1: Simulation condition

	Duration	d	α	β	z_d
Nominal	$0 < t < 30$	10	0	0	$z_{dn} := \sin(2t)$
Transition	$30 < t < 45$	15	3	0.5	$(1-\sigma)z_{dn} + \sigma z_{dp}$
Perturbed	$45 < t < 80$	15	3	0.5	$z_{dp} := 2\sin(1.2t)$

$\sigma := (t-30)/15$

in (2.4) during the transition similarly to z_d. All through the simulation, the RIO controller remains the same in order to illustrate the adaptivity and robustness of the controller.

The simulation result of the closed-loop system with RIO controller is shown in Fig. 2.5. For comparison, also shown is the simulated behavior of the human-controlled mechanical system without assistive RIO control. The desired oscillation z_d is successfully stabilized for both nominal and perturbed conditions, showing that the controller is capable of tolerating certain uncertainty in the modeling. The robustness is achieved because the stability region in Fig. 2.3 is large enough to contain the perturbed operating point. The human effort is greatly reduced under the nominal condition since the controller has an accurate estimate for the amount of damping ($\delta = d = 10$). After the perturbation in d, this is no longer the case, but some reduction of the human effort is still achieved with stability.

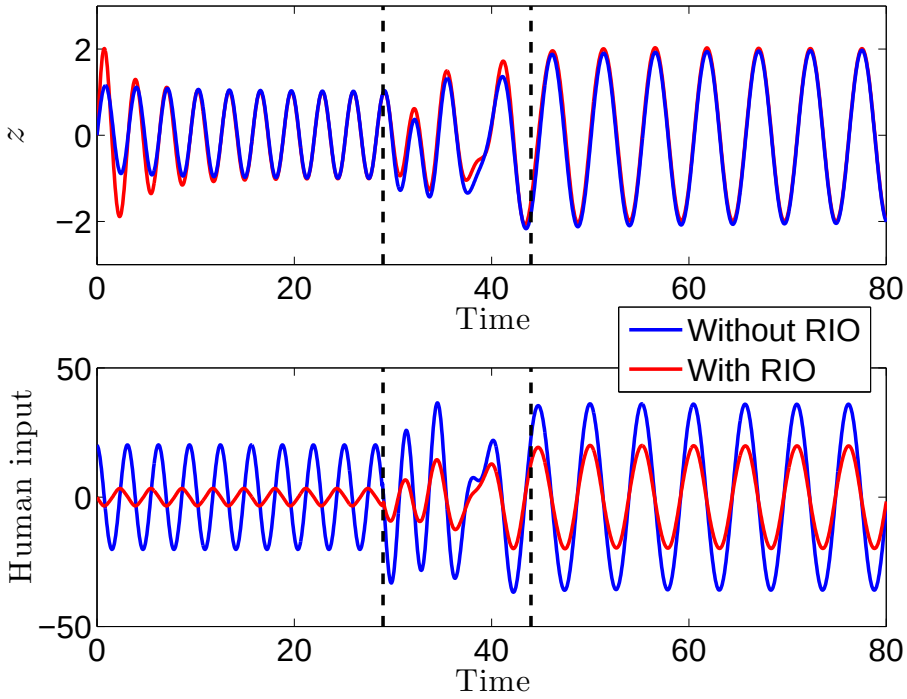

Figure 2.5: Simulated behavior of the closed-loop system

2.7 Discussion

This chapter starts with considering the case where a human and an RIO controller cooperate to drive a one-DOF mechanical system in order to achieve a human-intended oscillation. When focus on oscillatory movement, I can learn from the biological counter part, CPG. Based on structure of CPG, I have proposed an RIO control design method such that the human effort is reduced by a nonlinear damping compensation. It is also shown that the human-intended oscillation is a locally stable trajectory of the closed-loop system. The results of a numerical study have indicated that the selection of control parameters does not require accurate information of the plant system. The result is then extended to multi-DOF systems with the assumption of Rayleigh damping. A numerical example demonstrated that the proposed method maintains robust stability with some human effort reduction even under a condition where the plant and human control are perturbed from the design models. This theoretical result mainly considers the problem in the linear domain, and the result

of extension to multi-DOF system is proven with the assumption of Rayleigh damping. However, in practice, the plant system could be nonlinear and the system damping may not necessarily be Rayleigh damping. To further justify the controller performance, all the unmodeled will be tested via experiments, which will be introduced in chapter 6.

CHAPTER 3

Adaptive Andronov-Hopf Oscillator (AHO) Control

3.1 Overview

In this chapter, I consider a general class of linear mechanical systems with multiple degrees of freedom (DOF), and propose a method for designing a controller to achieve exact entrainment to a selected mode of natural oscillations with a theoretical guarantee for convergence. The design starts with discussing a general method of analyzing the stability of a linear periodic system with certain structure in section 3.2. The controller is designed in section 3.3, I first develop an oscillator that synchronizes with the external sinusoidal input, using the AHO as the basic structure with additional adaptation mechanisms to tune the frequency parameter. In section 3.4, I then modify the adaptive AHO to include a damping estimation mechanism, place it in the feedback loop with a single-DOF mechanical system, and show that the closed-loop system has a stable limit cycle on which the natural oscillation is achieved for the plant variable. Finally in section 3.5, I will extend the result for multi-DOF mechanical systems to achieve exact entrainment to a selected mode of natural oscillations.

Local stability of the natural oscillation orbit is rigorously proven. Our approach is based on linearization around the orbit and Floquet analysis of the resulting linear periodic (LP) system. I consider the limiting case where the adaptation of the AHO parameters is arbitrarily slow, and develop a simple stability condition, using an averaging technique, for the class of perturbed LP systems arising from linearization of a general oscillator with slow adaptation mechanisms. Although convergence is guaranteed only for the limiting case, numerical examples in section 3.6 demonstrate that the target orbit remains stable when the perturbation parameters are large, and thus fast convergence can be achieved.

3.2 Stability Analysis of Periodic Solutions of Perturbed Nonlinear Systems

In this section, I will consider a class of perturbed nonlinear systems and develop a general framework for stability analysis of periodic solutions. I employ a classical approach (e.g. [1]) to separate and average the slow dynamics in the neighborhood of the periodic orbit, and provide a new condition for exponential stability of the orbit in the limiting case. The technical tool developed here will be used in later analyses.

Let us first introduce two notions of stability.

Definition 2. *Consider a dynamical system* $\dot{\mathfrak{x}} = \mathfrak{f}(t, \mathfrak{x})$ *and a solution* $\mathfrak{x} = \xi$*. The trajectory* ξ *is said to be stable if*

$$\lim_{t\to\infty} \|\mathfrak{x}(t) - \xi(t)\| = 0$$

holds whenever $\|\mathfrak{x}(0) - \xi(0)\|$ *is sufficiently small. The trajectory* ξ *is said to be orbitally stable if*

$$\lim_{t\to\infty} \|\mathfrak{x}(t) - \xi(t+c)\| = 0$$

holds for some $c \in \mathbb{R}$ *whenever* $\|\mathfrak{x}(0) - \xi(t_o)\|$ *is sufficiently small for some* $t_o \in \mathbb{R}$*.*

Clearly, for a solution of a dynamical system, stability implies orbital stability. It is well known that a periodic solution cannot be orbitally stable unless the system is nonlinear, and cannot be stable unless the system is time-varying.

Consider a nonlinear system

$$\begin{aligned} \dot{x} &= \mathsf{f}(x, y, t) + \varepsilon \mathsf{h}(x, y, t) \\ \dot{y} &= \varepsilon \mathsf{g}(x, y, t) \end{aligned} \tag{3.1}$$

where (x, y) are the states, $\varepsilon \in \mathbb{R}$ is a perturbation parameter, and functions $\mathsf{f}, \mathsf{g}, \mathsf{h}$ are periodic in t with period $T \geq 0$ (the system is time invariant when $T = 0$). I consider the case where $\varepsilon > 0$ is small, and y slowly changes its value over time. The variable x with fast dynamics and y with slow dynamics are mutually coupled. Suppose the system has a

T-periodic solution (x_o, y_o). The linearization of the system (3.1) around the solution yields a linear periodic system

$$\begin{bmatrix} \dot{\tilde{x}} \\ \dot{\tilde{y}} \end{bmatrix} = \begin{bmatrix} A_1(t) + \varepsilon B_1(t) & A_2(t) + \varepsilon B_2(t) \\ \varepsilon C_1(t) & \varepsilon C_2(t) \end{bmatrix} \begin{bmatrix} \tilde{x} \\ \tilde{y} \end{bmatrix}, \tag{3.2}$$

where

$$\tilde{x} := x - x_o, \quad \tilde{y} := y - y_o,$$
$$A_1(t) = \frac{\partial \mathsf{f}}{\partial x}, \quad B_1(t) = \frac{\partial \mathsf{h}}{\partial x}, \quad C_1(t) = \frac{\partial \mathsf{g}}{\partial x},$$
$$A_2(t) = \frac{\partial \mathsf{f}}{\partial y}, \quad B_2(t) = \frac{\partial \mathsf{h}}{\partial y}, \quad C_2(t) = \frac{\partial \mathsf{g}}{\partial y},$$

with the partial derivatives evaluated at (x_o, y_o, t). Note that all the coefficient matrices are T-periodic.

The solution (x_o, y_o) is stable if the linear periodic system (3.2) is stable. However, stability of the linear system is not required for orbital stability of (x_o, y_o). In fact, (3.2) can never be stable if the original nonlinear system (3.1) is time-invariant and the solution is not constant since $(\tilde{x}, \tilde{y}) = (\dot{x}_o, \dot{y}_o)$ is a solution of the linear system not converging to the origin. In this case, the non-convergent mode can be isolated by a coordinate transformation and then orbital stability of (x_o, y_o) is implied by stability of the remaining part of the system. This idea was used in [30] for a coupled oscillator problem, and will also be used later in this chapter for the natural entrainment problem. The reduced system turns out to have the same form as (3.2). Thus, for both stability and orbital stability of periodic solutions, a fundamental problem is the stability analysis of the linear periodic system of the form (3.2).

A general method for analyzing stability of linear periodic systems is to use the Floquent multiplier. Solution (x_o, y_o) is stable when all the Floquet multipliers are inside the unit circle, and is orbitally stable when all the Floquet multipliers are inside the unit circle except one multiplier at one [10]. While computing the Floquet multipliers is straightforward, the analysis is numerical and the method is not suitable for analytical development of design conditions for guaranteed stability. Here I propose an alternative method for stability analysis exploiting the structure of the linear periodic system.

A simple stability condition is obtained if the two variables $(\tilde{x}, \tilde{y})$ in (3.2) are decoupled. Let us introduce a linear transformation

$$\begin{bmatrix} w \\ \tilde{y} \end{bmatrix} = \begin{bmatrix} I & -\mathcal{L}_\varepsilon(t) \\ 0 & I \end{bmatrix} \begin{bmatrix} \tilde{x} \\ \tilde{y} \end{bmatrix} \tag{3.3}$$

where $\mathcal{L}_\varepsilon(t)$ is a matrix-valued differentiable function of time, depending on the perturbation parameter ε. Let us choose $\mathcal{L}_\varepsilon(t)$ such that

$$\dot{\mathcal{L}}_\varepsilon(t) = A_1(t)\mathcal{L}_\varepsilon(t) + A_2(t) + \varepsilon G(t, \mathcal{L}_\varepsilon(t)), \tag{3.4}$$

where

$$G(t, X) := B_2(t) + B_1(t)X - XC_2(t) - XC_1(t)X. \tag{3.5}$$

Then the system can be described as

$$\begin{bmatrix} \dot{w} \\ \dot{\tilde{y}} \end{bmatrix} = \begin{bmatrix} \mathcal{A}_1(t) & 0 \\ \varepsilon C_1(t) & \varepsilon(C_2(t) + C_1(t)\mathcal{L}_\varepsilon(t)) \end{bmatrix} \begin{bmatrix} w \\ \tilde{y} \end{bmatrix} \tag{3.6}$$

where the (1,2) block of the coefficient matrix is made equal to zero by the choice of $\mathcal{L}_\varepsilon(t)$, and

$$\mathcal{A}_1(t) := A_1(t) + \varepsilon(B_1(t) - \mathcal{L}_\varepsilon(t)C_1(t)).$$

Now the original linear periodic system (3.2) is transformed into system (3.6), where the fast dynamics w is decoupled from the slow dynamics $\tilde{y}$. With the help of the separation, I can examine stability of the original system (3.2) by analyzing the two subsystems associated with w and $\tilde{y}$. Furthermore, when $|\varepsilon|$ is sufficiently small, we may approximate $\mathcal{A}_1$ by A_1, and $\mathcal{L}_\varepsilon$ by $\mathcal{L}_o$ satisfying

$$\dot{\mathcal{L}}_o(t) = A_1(t)\mathcal{L}_o(t) + A_2(t). \tag{3.7}$$

This idea leads to the following result.

Lemma 1. *Consider the linear T-periodic system* (3.2)*, where all the coefficient matrices are continuous and bounded functions of time. Suppose there exists a solution $\mathcal{L}_o(t)$ to* (3.7) *that is T-periodic or constant, and define*

$$\mathcal{B} := \int_0^T \big(C_2(t) + C_1(t)\mathcal{L}_o(t)\big)dt. \tag{3.8}$$

If the system $\dot{x} = A_1(t)x$ is stable and $\mathcal{B}$ is Hurwitz, then there exists $\bar{\varepsilon}$ such that system (3.2) is exponentially stable for all $\varepsilon \in (0, \bar{\varepsilon})$.

Proof. For each $\varepsilon > 0$, let $\mathcal{L}_\varepsilon(t)$ be the solution to (3.4) with initial condition $\mathcal{L}_\varepsilon(0) = \mathcal{L}_o(0)$, and define $\Delta_\varepsilon(t)$ by

$$\mathcal{L}_\varepsilon(t) = \mathcal{L}_o(t) + \varepsilon\Delta_\varepsilon(t). \tag{3.9}$$

By Lemma 5 in the appendix, there exists $\bar{\varepsilon}_1 > 0$ such that $\mathcal{L}_\varepsilon$ and Δ_ε with $\varepsilon \in (0, \bar{\varepsilon}_1)$ are bounded and continuously differentiable when $\dot{x} = A_1(t)x$ is stable. Then, through the Lyapunov transformation introduced in (3.3), two systems (3.2) and (3.6) are equivalent when $\varepsilon \in (0, \bar{\varepsilon}_1)$. The stability of system (3.6) depends on two separate systems

$$\dot{z} = \Big(A_1(t) + \varepsilon(B_1(t) - \mathcal{L}_\varepsilon(t)C_1(t))\Big)z, \tag{3.10}$$

$$\dot{y} = \varepsilon\Big(C_2(t) + C_1(t)\mathcal{L}_\varepsilon(t)\Big)y. \tag{3.11}$$

Based on Lemma 6 in the appendix, there exists $\bar{\varepsilon}_2$ such that system (3.10) is exponentially stable for all $\varepsilon \in (0, \bar{\varepsilon}_2)$ due to stability of $A_1(t)$ and boundedness of the perturbation term multiplied by ε. The system (3.11) can be rewritten as

$$\dot{y} = \varepsilon\Big(C_2(t) + C_1(t)\mathcal{L}_o(t) + \varepsilon C_1(t)\Delta_\varepsilon(t)\Big)y. \tag{3.12}$$

By Lemma 7, there exists $\bar{\varepsilon}_3 > 0$ such that system (3.12) is stable for all $\varepsilon \in (0, \bar{\varepsilon}_3)$ since $\mathcal{B}$ in (3.8) is Hurwitz and C_1 and Δ_ε are bounded. □

Lemma 1 will play a crucial role in our main results to prove stability for an adaptive oscillator and orbital stability for natural entrainment problems.

3.3 Adaptive Oscillator

3.3.1 Problem Formulation

Now let us consider the problem of designing an oscillator that synchronizes to an external periodic signal in an adaptive manner. In particular, the system to be designed comprises a

nonlinear oscillator and an adaptation mechanism that dynamically modifies oscillator parameters based on the periodic input. The trajectory of the adaptive oscillator will converge locally to a periodic orbit on which one of the oscillator variables is synchronized with the periodic input, and the adaptation variables are constant with values at the frequency and amplitude of the input. A formal statement of the problem is the following.

Problem 2. *Let $z(t)$ be a T-periodic sinusoidal signal*

$$z(t) = \alpha \sin(\omega t) \tag{3.13}$$

where $\alpha, \omega \in \mathbb{R}$ are unknown amplitude and frequency, and $T := 2\pi/\omega$. Design an adaptive nonlinear oscillator

$$\begin{aligned} \dot{x} &= f(x, y, z) \\ \dot{y} &= g(x, y, z) \\ q &= h(x) \end{aligned} \tag{3.14}$$

where $(x, y) \in \mathbb{R}^n \times \mathbb{R}^m$ is the state vector, and $q \in \mathbb{R}$ is the output signal, to satisfy the following specifications:

(i) There exists a stable solution (x, y) to (3.14) such that

$$x(t) = x(t+T), \quad y(t) \equiv \begin{bmatrix} \omega \\ \alpha \end{bmatrix}, \quad q(t) = z(t).$$

(ii) The oscillator dynamics f, g, and h are independent of the signal parameters (ω, α).

3.3.2 Approach

Our approach to solve Problem 2 is to exploit the structure of the Andronov-Hopf oscillator with additional adaptation mechanisms. The AHO is a simple planar nonlinear oscillator, in which every nontrivial trajectory converges to a single limit cycle. The orbit in the state space is circular, and the time courses of the state variables are sinusoidal. The amplitude and frequency of the oscillation are directly specified by certain model parameters. More

specifically, AHO is described as

$$\begin{bmatrix} \dot{x}_1 \\ \dot{x}_2 \end{bmatrix} = \begin{bmatrix} \sigma(x_1, x_2) & \omega \\ -\omega & \sigma(x_1, x_2) \end{bmatrix} \begin{bmatrix} x_1 \\ x_2 \end{bmatrix}, \tag{3.15}$$

$$\sigma(x_1, x_2) := \mu(\alpha^2 - x_1^2 - x_2^2)$$

where $x_i(t) \in \mathbb{R}$ for $i = 1, 2$ are the states, α and ω are the amplitude and frequency parameters, respectively, and $\mu > 0$ specifies the convergence rate. When σ is zero, the AHO is a linear (undamped) oscillator. The nonlinear function σ provides positive/negative damping when the oscillation amplitude $\sqrt{x_1^2 + x_2^2}$ is larger/smaller than α, allowing for convergence of the amplitude to α.

Precise analysis is rather simple. Introducing the polar coordinates

$$\begin{bmatrix} x_1 \\ x_2 \end{bmatrix} = \begin{bmatrix} r \sin\theta \\ r \cos\theta \end{bmatrix}, \tag{3.16}$$

system (3.15) is expressed as

$$\dot{r} = \mu(\alpha^2 - r^2)r, \quad \dot{\theta} = \omega.$$

It is then easy to see that the amplitude $r(t)$ will converge to $\pm\alpha$ unless $r(0) = 0$, and the phase $\theta(t)$ is given by $\theta(t) = \omega t + \theta(0)$. Thus, the sinusoidal trajectory

$$\begin{bmatrix} x_1 \\ x_2 \end{bmatrix} = \begin{bmatrix} \alpha \sin\omega t \\ \alpha \cos\omega t \end{bmatrix}$$

is an orbitally stable limit cycle of the system (3.15).

I design an adaptive oscillator using the AHO as the starting point. Since ω and α are unknown in Problem 2, I replace (ω, α) in (3.15) with (y_1, y_2) as the variables to be adjusted so that they converge to the frequency and amplitude of z. A natural choice for the output is $q := x_1$, and I drive the AHO by the error $z - x_1$ to achieve synchronization $q = z$. Overall, I add the following adaptation mechanism to the dynamics of Andronov-Hopf oscillator:

$$\begin{bmatrix} \dot{x}_1 \\ \dot{x}_2 \end{bmatrix} = \begin{bmatrix} \sigma & y_1 \\ -y_1 & \sigma \end{bmatrix} \begin{bmatrix} x_1 \\ x_2 \end{bmatrix} + \gamma \begin{bmatrix} z - x_1 \\ 0 \end{bmatrix} \tag{3.17a}$$

$$\dot{y}_1 = \eta x_2(z - x_1), \tag{3.17b}$$

$$\dot{y}_2 = \kappa\Big(z^2 + x_2^2 - y_2^2\Big) \tag{3.17c}$$

$$\sigma := \mu(y_2^2 - x_1^2 - x_2^2), \tag{3.17d}$$

where $\gamma, \eta, \kappa, \mu \in \mathbb{R}$ are positive constants, and (x_1, x_2, y_1, y_2) are the states of the oscillator. It is designed such that $x_1(t)$ synchronizes with the signal $z(t)$, while (y_1, y_2) converges to (ω, α). The parameters μ and γ specify the convergence rates of the oscillation amplitude and synchronization, and η and κ specify the rates of adaptation of frequency and amplitude.

The idea behind the adaptation mechanism is as follows. It is easy to verify that, if $y_1(t) \equiv \omega$ and $\mu = 0$ in (3.17a), then the linear system driven by the error signal converges to a sinusoidal trajectory on which $x_1 = z$. It turns out that the convergence property is maintained when the nonlinearity in the AHO becomes active (i.e., $\mu > 0$), provided $y_2(t) \equiv \alpha$. The mechanism in (3.17c) increases/decreases the estimated amplitude y_2 when the actual amplitude $\sqrt{z^2 + x_2^2}$ is larger/smaller than the current estimate y_2. Finally, the mechanism in (3.17b) increases/decreases the estimated frequency y_1 when the phase of x_1 is behind/advance with respect to z. In particular, with x in (3.16), we can see

$$x_2(z - x_1) \cong -(\alpha \cos \omega t)^2 \varphi + O(\varphi^2), \quad \varphi := \theta - \omega t,$$

provided the amplitude is correct; $r = \alpha$. Thus, assuming the phase difference $|\varphi|$ is small, $\dot{y}_1$ is positive/negative when z is ahead/behind of x_1, which causes an increase/decrease of y_1 and acceleration/deceleration of x_1. Eventually, z and x_1 will have no phase difference and synchronize. These intuitive ideas are rigorously verified to work in the next subsection.

3.3.3 Result

The following theorem provides a formal statement of a sufficient condition for synchronization of the adaptive oscillator.

Theorem 4. *Consider the adaptive oscillator* (3.17) *is connected with a sinusoidal signal* (3.13). *Suppose* $\gamma, \eta, \kappa \in \mathbb{R}$ *are positive and* $\mu \in \mathbb{R}$ *is nonnegative. Then there exists* $\bar{\varepsilon}$ *such*

that the state trajectory

$$(x_1, x_2, y_1, y_2) = (\alpha \sin(\omega t), \alpha \cos(\omega t), \omega, \alpha) \tag{3.18}$$

is stable whenever $\eta, \kappa, \mu \in \mathbb{R}$ *are smaller than* $\bar{\varepsilon}$.

Proof. It is straightforward to verify that the signal in (3.18) is a solution of the system. Let the small parameters be expressed as

$$\begin{bmatrix} \eta & \kappa & \mu \end{bmatrix} = \varepsilon \begin{bmatrix} \tilde{\eta} & \tilde{\kappa}/4 & \tilde{\mu}/4 \end{bmatrix}$$

with small $\varepsilon > 0$. Introducing the perturbation variables

$$\begin{aligned} \tilde{x}_1 &:= x_1 - \alpha s, \quad \tilde{y}_1 := y_1 - \omega, \quad s := \sin(\omega t), \\ \tilde{x}_2 &:= x_2 - \alpha c, \quad \tilde{y}_2 := y_2 - \alpha, \quad c := \cos(\omega t), \end{aligned}$$

the linearized system is given by

$$\dot{\tilde{x}} = \begin{bmatrix} A_1 + \varepsilon B_1 & A_2 + \varepsilon B_2 \\ \varepsilon C_1 & \varepsilon C_2 \end{bmatrix} \tilde{x},$$

where

$$\begin{bmatrix} A_1 & A_2 \\ C_1 & C_2 \end{bmatrix} := \left[\begin{array}{cc|cc} -\gamma & \omega & \alpha c & 0 \\ -\omega & 0 & -\alpha s & 0 \\ \hline -\tilde{\eta}\alpha c & 0 & 0 & 0 \\ 0 & \tilde{\kappa}\alpha c & 0 & -\tilde{\kappa}\alpha \end{array}\right],$$

$$\begin{bmatrix} B_1 & B_2 \end{bmatrix} := -\tilde{\mu}\alpha^2 \left[\begin{array}{cc|cc} s^2 & sc & 0 & -s \\ sc & c^2 & 0 & -c \end{array}\right].$$

It is easy to verify that A_1 is Hurwitz, and the periodic solution $\mathcal{L}_o$ to

$$\dot{\mathcal{L}}_o = A_1 \mathcal{L}_o + A_2$$

exists and is given by

$$\mathcal{L}_o = \Re[\hat{\mathcal{L}}_o e^{j\omega t}],$$
$$\hat{\mathcal{L}}_o := (j\omega I - A_1)^{-1}\hat{A}_2 = \frac{\alpha}{\omega\gamma}\begin{bmatrix} 2\omega & 0 \\ \gamma + 2j\omega & 0 \end{bmatrix}$$
$$\hat{A}_2 = \begin{bmatrix} \alpha & 0 \\ \alpha j & 0 \end{bmatrix}.$$

Noting that

$$\mathcal{B} = \frac{1}{T}\int_0^T \Big(C_1\mathcal{L}_o + C_2\Big)dt = \frac{1}{2}\Re\Big(\hat{C}_1\hat{\mathcal{L}}_o\Big) + C_2$$
$$= \begin{bmatrix} -\alpha^2\tilde{\eta}/\gamma & 0 \\ \alpha^2\tilde{\kappa}/(2\omega) & -\alpha\tilde{\kappa} \end{bmatrix}, \quad \hat{C}_1 := \alpha\begin{bmatrix} -\tilde{\eta} & 0 \\ 0 & \tilde{\kappa} \end{bmatrix},$$

and $\mathcal{B}$ is Hurwitz, I now conclude the result. □

Theorem 4 provides an approach to design the oscillator dynamics to adaptively synchronize with an external sinusoidal signal. Synchronization is asymptotically achieved as long as the adaptation of the frequency and amplitude variables is sufficiently slow. Moreover, the system is designed to sustain, after the convergence, the oscillation in a stable and autonomous manner without the input (i.e., $\gamma = 0$), and therefore the process can be seen as learning of a training periodic signal by a nonlinear oscillator. For practical purposes, the convergence rate can be made fast by adjusting the adaptation parameters η, κ and μ. A numerical example in Section 3.6 illustrates this point in comparison with an existing method. Noting that $\mu = 0$ is a valid choice for the design, the nonlinearity σ is not essential for the convergence property of the adaptive oscillator. However, it will play a crucial role when I extend the result to consider a feedback control problem in the next section.

3.4 Adaptive Natural Entrainment

3.4.1 Problem Formulation

Let us now consider a single degree-of-freedom mechanical system with unknown parameters and develop a method for designing a feedback controller to achieve the natural oscillation of the system. The control architecture is based on the adaptive oscillator described in the previous section. The single-DOF result provides a comprehensive explanation of the idea for closing the loop and embedding a stable limit cycle in the state space, and sets a stage for multi-DOF extension in the next section.

Let a mechanical system be given by

$$m\ddot{z} + d\dot{z} + kz = u, \tag{3.19}$$

where $m, d, k \in \mathbb{R}$ are positive parameters representing the mass, damping and stiffness, $u(t) \in \mathbb{R}$ is the force input from an actuator, and $z(t) \in \mathbb{R}$ is the resulting displacement. The natural oscillation of the system is defined as

$$z_n(t) = \alpha \sin(\omega_n t), \quad \omega_n := \sqrt{k/m}, \tag{3.20}$$

where ω_n is the undamped natural frequency of the system, and $\alpha \in \mathbb{R}$ is the amplitude of z_n. Let $T := 2\pi/\omega_n$ be the natural period.

I aim to design a feedback controller that achieves local convergence of $z(t)$ to $z_n(t + c)$ in the steady state, where the oscillation amplitude α is assigned by the controller while the constant c depends on the initial state of the closed-loop system. In addition, I would like the controller to be adaptive in the sense that the controller meets the objective with no information of the system parameters m, d and k. A formal statement of the design problem is as follows.

Problem 3. *Let a mechanical system in* (3.19) *and a positive scalar* $\alpha \in \mathbb{R}$ *be given, and*

consider the natural oscillation z_n defined in (3.20)*. Design a feedback controller of the form*

$$\dot{x} = f(x, y, z)$$

$$\dot{y} = g(x, y, z)$$

$$u = h(x)$$

where $(x, y) \in \mathbb{R}^n \times \mathbb{R}^m$ is the state vector, to achieve the natural oscillation with amplitude α in the steady state. In particular, the design specifications are the following:

(i) There exists an orbitally stable solution $(x, y, z, \dot{z})$ of the closed-loop system such that

$$x(t) = x(t + T), \quad y(t) \equiv \begin{bmatrix} \omega_n \\ d \end{bmatrix}, \quad z = z_n.$$

(ii) Functions f, g and h specifying the controller are independent of the system parameters m, d, and k.

This is an adaptive natural entrainment problem where a controller is sought to adaptively achieve entrainment to the natural oscillation. The adaptation variable y should estimate all the unknown system parameters necessary for the natural entrainment, and it turns out that estimation of the natural frequency ω_n and the damping coefficient d is sufficient for the purpose as explained in the next section.

3.4.2 Approach

The basic idea for solving Problem 3 is the following. When the control objective is met, the natural oscillation $z = z_n$ is achieved for (3.19). This necessitates $u = d\dot{z}_n$ in the steady state. To make this happen, the first step is to drive the AHO by mechanical variable z and add an adaptation mechanism so that the parameter ω is adjusted in real time and converge to the natural frequency ω_n of the mechanical system when $z = z_n$. The second step is to add another mechanism to estimate the mechanical damping d, and close the loop by setting the control input u to compensate for the damping.

These two steps are accomplished by placing the adaptive oscillator (3.17) in the feedback loop, with modifications to estimate d and generate u. In particular, I consider the following

AHO based feedback controller

$$\begin{bmatrix} \dot{x}_1 \\ \dot{x}_2 \end{bmatrix} = \begin{bmatrix} \sigma & y_1 \\ -y_1 & \sigma \end{bmatrix} \begin{bmatrix} x_1 \\ x_2 \end{bmatrix} + \gamma \begin{bmatrix} z - x_1 \\ 0 \end{bmatrix} \tag{3.21a}$$

$$\dot{y}_1 = \eta x_2 (z - x_1), \tag{3.21b}$$

$$\dot{y}_2 = \kappa\Big(\alpha^2 - z^2 - x_2^2\Big) \tag{3.21c}$$

$$u = x_2 y_1 y_2, \quad \sigma := \mu(\alpha^2 - x_1^2 - x_2^2), \tag{3.21d}$$

where $\gamma, \eta, \kappa, \mu \in \mathbb{R}$ are positive constants, and $x_1(t)$ through $y_2(t)$ are the states of the controller. The controller (3.21d) turns out to solve Problem 3, achieving entrainment to the natural oscillation of (3.19). The controller is designed so that x_1 and x_2 synchronize with the plant states z and $\dot{z}/\omega_n$, respectively, while y_1 and y_2 estimate the natural frequency ω_n and damping coefficient d, respectively. The parameters γ and μ specify the rates of convergence for the amplitude and synchronization, and η and κ specify the rates of adaptation for frequency and damping, respectively. The underlying mechanism can be roughly explained as follows.

First, (3.21a) and (3.21b) form an adaptive oscillator with a frequency estimator similarly to the previous development. If $z(t)$ oscillates sinusoidally with frequency ω_n and amplitude α, (3.21a) stably generates sinusoidal signals $(x_1, x_2) = (\alpha \sin(\omega_n t), \alpha \cos(\omega_n t))$ so that $x_1 = z$, while (3.21b) makes y_1 converge to the natural frequency ω_n. In this case, the control input in (3.21d) is $u = y_2 \dot{z}$. Based on (3.21c), the variable y_2 estimates the damping coefficient and converges to d by the following mechanism. If y_2 is larger/smaller than d, then system (3.19) under the control input has negative/positive damping, leading to larger/smaller amplitude of oscillation. If the amplitude becomes larger/smaller than α, the dynamics of (3.21c) decrease/increase the estimated damping y_2. Hence y_2 is regulated around the value d. In this case, the control input is $u = d\dot{z}$. From (3.19), I see that z satisfies $m\ddot{z} + kz = 0$ and therefore oscillates with natural frequency ω_n.

3.4.3 Result

The following theorem presents a formal statement of the result and gives a sufficient condition for entrainment to the natural oscillation.

Theorem 5. *Consider mechanical system* (3.19) *and the feedback controller given by* (3.21)*. Suppose the plant parameters m, d, k and controller parameters $\mu, \gamma, \eta, \kappa \in \mathbb{R}$ are positive constants. Then*

$$\begin{aligned} &col(z, \dot{z}, x_1, x_2, y_1, y_2) \\ &= col(z_n, \dot{z}_n, \alpha \sin \omega_n t, \alpha \cos \omega_n t, \omega_n, d) \end{aligned} \tag{3.22}$$

is a solution of the closed-loop system. Moreover, there exists $\bar{\varepsilon} > 0$ such that the solution is orbitally stable whenever γ, η, and κ are smaller than $\bar{\varepsilon}$.

Proof. It is easily verified that (3.22) is a solution of the closed-loop system. Let normalized controller parameters be defined by

$$\varepsilon \begin{bmatrix} \tilde{\gamma} & \tilde{\eta} & \tilde{\kappa} \end{bmatrix} := \begin{bmatrix} \gamma & \eta\alpha^2 & 2\kappa\alpha^2\omega_1 \end{bmatrix}, \quad \tilde{\mu} := 2\mu\alpha^2.$$

Orbital stability will be proven for the case where $\tilde{\gamma}$, $\tilde{\eta}$, $\tilde{\kappa}$, and $\tilde{\mu}$ are arbitrary positive constants and $\varepsilon > 0$ is sufficiently small. Using the polar coordinates and error variables

$$\begin{aligned} x_1 &= r \sin\theta, \quad e_1 = z_n - x_1, \\ x_2 &= r \cos\theta, \quad e_2 = \dot{z}_n - \omega_n x_2, \end{aligned}$$

define a new state vector (θ, ξ) with

$$\xi := \mathrm{col}(r, e_1, e_2, \alpha y_1, \alpha\omega_n y_2).$$

The trajectory (3.22) can then be given by

$$\theta = \omega_n t, \quad \xi = \mathrm{col}(\alpha, 0, 0, \alpha\omega_n, \alpha\omega_n d). \tag{3.23}$$

Linearizing the closed-loop system around the solution (3.23), the resulting system is

$$\begin{bmatrix} \dot{\tilde{\theta}} \\ \dot{\tilde{\xi}} \end{bmatrix} = \begin{bmatrix} 0 & b \\ 0 & \Sigma \end{bmatrix} \begin{bmatrix} \tilde{\theta} \\ \tilde{\xi} \end{bmatrix}, \quad \tilde{\xi} = \mathrm{col}(\tilde{r}, e_1, e_2, \alpha\tilde{y}_1, \alpha\omega_n\tilde{y}_2)$$

where the variables with tilde are the perturbations from (3.23), e.g., $\tilde{r} := r - \alpha$, and

$$b = \begin{bmatrix} 0 & \gamma c & 0 & 1 & 0 \end{bmatrix} / \alpha$$

$$\Sigma = \begin{bmatrix} A_1 + \varepsilon B_1 & A_2 \\ \varepsilon C_1 & 0 \end{bmatrix}, \qquad \begin{aligned} s &:= \sin \omega_n t, \\ c &:= \cos \omega_n t, \end{aligned}$$

$$\begin{bmatrix} A_1 \\ C_1 \end{bmatrix} := \left[\begin{array}{ccc} -\tilde{\mu} & 0 & 0 \\ \tilde{\mu} s & 0 & 1 \\ \tilde{\mu}\omega_n c & -\omega_n^2 & -d \\ \hline 0 & \tilde{\eta} c & 0 \\ -\tilde{\kappa} & -\tilde{\kappa} s & 0 \end{array}\right],$$

$$\begin{bmatrix} B_1 & A_2 \end{bmatrix} := \left[\begin{array}{ccc|cc} 0 & \tilde{\gamma} s & 0 & 0 & 0 \\ 0 & -\tilde{\gamma} & 0 & -c & 0 \\ 0 & 0 & 0 & \omega_n s + dc & c \end{array}\right],$$

Thus, solution (3.22) is orbitally stable if and only if the system $\dot{\tilde{\xi}} = \Sigma \tilde{\xi}$ is stable. I use Lemma 1 to prove the stability.

Noting that A_1 is block triangular, it is easy to see that it is Hurwitz. To show that $\mathcal{B}$ is Hurwitz as well, note that (3.7) is a stable linear time-invariant system driven by a sinusoidal input, and the steady state solution is easily obtained as

$$\mathcal{L}_o = \frac{1}{d\omega_n} \begin{bmatrix} 0 & 0 \\ -2\omega_n c & s \\ * & * \end{bmatrix},$$

where $*$ denotes irrelavant entries. We can then calculate $\mathcal{B}$ as

$$\mathcal{B} = \int_0^T C_1 \mathcal{L}_o dt = -\frac{T}{2} \begin{bmatrix} \tilde{\eta}/d & 0 \\ 0 & \tilde{\kappa}/(\omega_n d) \end{bmatrix},$$

which is clearly Hurwitz. □

Theorem 5 provides a systematic method for designing an AHO-based controller to achieve entrainment to the natural oscillation of a single-DOF mechanical system. Selecting the control parameters do not require information from the plant system such as (m, d, k).

3.5 Extension to Multi-DOF Systems

3.5.1 Problem Formulation

In this section, I consider an extension of the result in the previous section to multi-DOF mechanical systems. Let the mechanical system be given by

$$M\ddot{q} + D\dot{q} + Kq = w \tag{3.24}$$

where $q, w \in \mathbb{R}^n$ are generalized coordinates and force inputs, and $M, D, K \in \mathbb{R}^{n\times n}$ are system parameters representing the mass, damping and stiffness. I assume that M, D, and K are positive definite.

Consider a natural mode of oscillation

$$q_d(t) = \alpha e_1 \sin \omega_1 t \tag{3.25}$$

defined by the amplitude parameter $\alpha \in \mathbb{R}$ and a pair of generalized eigenvector $e_1 \in \mathbb{R}^n$ and eigenvalue $\lambda_1 \in \mathbb{R}$ satisfying

$$(\lambda_1 M - K)e_1 = 0, \quad e_1^{\mathrm{T}} M e_1 = 1,$$

where $\omega_1 := \sqrt{\lambda_1}$ is a natural frequency, and e_1 is the associated mode shape, with the second equation normalizing the magnitude of e_1. Since M and K are real symmetric positive definite, both e_1 and λ_1 are real, and $\lambda_1 > 0$.

The objective is to achieve entrainment to the arbitrarily chosen mode of natural oscillation in (3.25) by a nonlinear feedback controller without full knowledge of the mechanical parameters. In particular, I assume that the system parameters are unknown except for e_1 and M. While M can be estimated fairly accurately in practice, the knowledge of e_1 may not be fully justified but is required in the result that follows.

Assuming the knowledge of (e_1, M), I can formulate a control design problem in the modal coordinates. Define matrices $E \in \mathbb{R}^{n\times n}$ and $E_2 \in \mathbb{R}^{n\times(n-1)}$ by

$$E := \begin{bmatrix} e_1 & E_2 \end{bmatrix}, \quad e_1^{\mathrm{T}} M E_2 = 0, \quad E_2^{\mathrm{T}} M E_2 = I.$$

Through the coordinate transformation

$$q = Ez, \quad w = MEu$$

the original system can then be transformed into

$$\ddot{z} + \nabla \dot{z} + \Lambda z = u, \tag{3.26}$$

where

$$\nabla := E^{\intercal} D E \quad \Lambda := \mathrm{diag}(\omega_1^2, \Omega), \quad \Omega := E_2^{\intercal} K E_2,$$

and I also partition ∇ into

$$\nabla = \begin{bmatrix} d & \delta^{\intercal} \\ \delta & \Delta \end{bmatrix},$$

where $d \in \mathbb{R}$, $\delta \in \mathbb{R}^{n-1}$ and $\Delta \in \mathbb{R}^{(n-1)\times(n-1)}$. The natural oscillation of z corresponding to (3.25) is

$$z_d(t) = \mathrm{col}(\alpha \sin \omega_1 t, 0). \tag{3.27}$$

Now, the problem is reduced to the design of a controller that generates control input u using the sensory information of z.

Our goal is to design a controller that can achieve orbital stability of $z = z_d$, i.e., the convergence of $z(t)$ to $z_d(t + c)$ in the steady state, where the constant c depends on the initial state of the closed-loop system. I seek an adaptive controller that meets the objective with no information of the system parameters Δ and Λ. The formal statement of the design problem is given as follows.

Problem 4. *Let a mechanical system in* (3.26) *with positive definite* (∇, Λ)*, and a positive scalar* $\alpha \in \mathbb{R}$ *be given, and consider the natural oscillation* z_d *defined in* (3.27)*. Design a feedback controller of the form*

$$\dot{x} = f(x, y, z)$$

$$\dot{y} = g(x, y, z)$$

$$u = h(x)$$

where $(x, y) \in \mathbb{R}^n \times \mathbb{R}^m$ *is the state vector, to achieve the natural oscillation with amplitude* α *in the steady state. In particular, the design specifications are the following:*

(i) There exists an orbitally stable solution $(x, y, z, \dot{z})$ of the closed-loop system such that

$$x(t) = x(t+T), \quad y(t) \equiv \begin{bmatrix} \omega_1 \\ d \\ \delta \end{bmatrix}, \quad z = z_d.$$

(ii) Functions f, g and h specifying the controller are independent of the system parameters ∇ and Λ.

3.5.2 Approach

The idea for the control design is a direct extension of the single-DOF case in the previous section. The natural oscillation $z = z_d$ is a solution of (3.26) if and only if the controller output in the steady state compensates for the damping as

$$u = \nabla \dot{z}_d(t) = \begin{bmatrix} d \\ \delta \end{bmatrix} \alpha\omega_1 \cos \omega_1 t.$$

Since ∇ and Λ are unknown, the controller should be capable of estimating d, δ and ω_1. I thus propose the following controller as an extension of (3.21d):

$$\begin{bmatrix} \dot{x}_1 \\ \dot{x}_2 \end{bmatrix} = \begin{bmatrix} \sigma & y_1 \\ -y_1 & \sigma \end{bmatrix} \begin{bmatrix} x_1 \\ x_2 \end{bmatrix} + \gamma \begin{bmatrix} z_1 - x_1 \\ 0 \end{bmatrix} \tag{3.28a}$$

$$\dot{y}_1 = \eta x_2 (z_1 - x_1) \tag{3.28b}$$

$$\dot{y}_2 = \kappa(\alpha^2 - z_1^2 - x_2^2) \tag{3.28c}$$

$$\dot{y}_3 = -\zeta z_2 x_1, \tag{3.28d}$$

$$u = \begin{bmatrix} y_2 \\ y_3 \end{bmatrix} y_1 x_2, \quad \sigma = \mu(\alpha^2 - x_1^2 - x_2^2), \tag{3.28e}$$

where $\gamma, \eta, \kappa, \zeta, \mu \in \mathbb{R}$ are positive constants, $z_1(t) \in \mathbb{R}$ and $z_2(t) \in \mathbb{R}^{n-1}$ are defined by $z = \mathrm{col}(z_1, z_2)$, and $x_i(t), y_i(t) \in \mathbb{R}$ are scalar variables for $i = 1, 2$ and $y_3(t) \in \mathbb{R}^{n-1}$. Equations (3.28a)–(3.28c) and the first entry of u in (3.28e) are identical to (3.21a)–(3.21c) when z_1 is replaced by z. Hence, variables (y_1, y_2) estimate (ω_1, d), and (x_1, x_2) locally

converges to the orbit $(\alpha \sin \omega_1 t, \alpha \cos \omega_1 t)$, provided $z_2 = 0$. The rationale for the remaining part of the controller is explained below.

The additional variable $y_3(t)$ in (3.28d) is introduced as an estimate for δ. To see how it works, consider the situation where the trajectory is on the target orbit, i.e. $y_1 = \omega_1$, $x_1 = z_1 = \alpha \sin \omega_1 t$, and $x_2 = \alpha \cos \omega_1 t$, except for nonzero errors in $y_3 - \delta$ and z_2. The z_2 dynamics can be described as

$$\ddot{z}_2 + \Delta \dot{z}_2 + \Omega z_2 = (y_3 - \delta)\dot{x}_1. \tag{3.29}$$

If ζ is sufficiently small, y_3 can be regarded as constant and z_2 is a sinusoid. Then the dynamics of $\dot{y}_3$ in (3.28d) is approximated as

$$\dot{y}_3 \approx -\frac{\zeta}{T} \int_0^T z_2 x_1 dt = -\frac{\zeta}{\omega_1^2 T} \int_0^T \dot{z}_2 \dot{x}_1 dt, \tag{3.30}$$

where the latter equality holds since z_2 and x_1 are sinusoids of frequency ω_1. Multiplying (3.29) by $\dot{z}_2^{\mathsf{T}}$ from left, taking the average over the cycle, and using (3.30), I have

$$\begin{aligned} 0 < \int_0^T \dot{z}_2^{\mathsf{T}} \Delta \dot{z}_2 dt &= (y_3 - \delta)^{\mathsf{T}} \int_0^T \dot{z}_2 \dot{x}_1 dt \\ &\approx -\frac{\omega_1^2 T}{2\zeta} \frac{d}{dt} \Big(\|y_3 - \delta\|^2 \Big). \end{aligned}$$

Thus the derivative of $\|y_3 - \delta\|^2$ is negative, making y_3 converge to δ. When $y_3 = \delta$, the second entry of u in (3.28e) decouples z_2 from z_1, achieving convergence of z_2 to zero due to the inherent stability of the mechanical system.

3.5.3 Result

The following theorem gives a sufficient condition for entrainment to the desired natural oscillation.

Theorem 6. *Consider mechanical system* (3.26) *and the feedback controller given by* (3.28). *Suppose* ∇ *and* Λ *are symmetric positive definite, and* $\mu, \gamma, \eta, \kappa, \zeta \in \mathbb{R}$ *are positive constants. Then*

$$\begin{aligned} &col(z, \dot{z}, x_1, x_2, y_1, y_2, y_3) \\ &= col(z_d, \dot{z}_d, \alpha \sin \omega_1 t, \alpha \cos \omega_1 t, \omega_1, d, \delta) \end{aligned} \tag{3.31}$$

is a solution of the closed-loop system. Moreover, there exists $\bar{\varepsilon} > 0$ such that the solution is orbitally stable whenever γ, η, κ and ζ are smaller than $\bar{\varepsilon}$.

Proof. The framework for the proof is roughly the same as the single-DOF case, with some additional complication due to the extra degrees of freedom. With the normalized controller parameters

$$\varepsilon \begin{bmatrix} \tilde{\gamma} & \tilde{\eta} & \tilde{\kappa} & \tilde{\zeta} \end{bmatrix} := \begin{bmatrix} \gamma & \eta\alpha^2 & 2\kappa\alpha^2\omega_1 & \zeta\alpha^2\omega_1 \end{bmatrix},$$
$$\tilde{\mu} := 2\mu\alpha^2,$$

I prove orbital stability for the case where $\tilde{\gamma}$, $\tilde{\eta}$, $\tilde{\kappa}$, $\tilde{\zeta}$ and $\tilde{\mu}$ are arbitrary positive constants and $\varepsilon > 0$ is sufficiently small. Let us introduce a coordinate transformation and a new state vector (θ, ξ) where

$$\xi := \mathrm{col}(r, e_1, z_2, e_2, \dot{z}_2, \alpha y_1, \alpha\omega_1 y_2, \alpha\omega_1 y_3).$$

$$x_1 = r\sin\theta, \quad e_1 = z_1 - x_1,$$
$$x_2 = r\cos\theta, \quad e_2 = \dot{z}_1 - \omega_1 x_2,$$

The trajectory (3.31) in the new coordinates is given by

$$\begin{aligned} \theta &= \omega_1 t \\ \xi &= \mathrm{col}(\alpha, 0, 0, 0, 0, \alpha\omega_1, \alpha\omega_1 d, \alpha\omega_1\delta). \end{aligned} \tag{3.32}$$

Linearization around the solution (3.32) yields

$$\begin{bmatrix} \dot{\tilde{\theta}} \\ \dot{\tilde{\xi}} \end{bmatrix} = \begin{bmatrix} 0 & b \\ 0 & \Sigma \end{bmatrix} \begin{bmatrix} \tilde{\theta} \\ \tilde{\xi} \end{bmatrix},$$
$$\tilde{\xi} = \mathrm{col}(\tilde{r}, e_1, z_2, e_2, \dot{z}_2, \alpha\tilde{y}_1, \alpha\omega_1\tilde{y}_2, \alpha\omega_1\tilde{y}_3)$$

where the variables with tilde are the perturbations from (3.32), e.g., $\tilde{y}_1 := y_1 - \omega_1$, and

$$b = \begin{bmatrix} 0 & \gamma c & 0 & 0 & 0 & 1 & 0 & 0 \end{bmatrix} / \alpha$$

$$\Sigma = \begin{bmatrix} A_1 + \varepsilon B_1 & A_2 \\ \varepsilon C_1 & 0 \end{bmatrix}, \qquad \begin{aligned} s &:= \sin\omega_1 t, \\ c &:= \cos\omega_1 t, \end{aligned}$$

$$\left[\begin{array}{c} A_1 \\ C_1 \end{array}\right] := \left[\begin{array}{ccccc} -\tilde{\mu} & 0 & 0 & 0 & 0 \\ \tilde{\mu}s & 0 & 0 & 1 & 0 \\ 0 & 0 & 0 & 0 & I \\ \tilde{\mu}\omega_1 c & -\omega_1^2 & 0 & -d & -\delta^{\mathsf{T}} \\ 0 & 0 & -\Omega & -\delta & -\Delta \\ \hline 0 & \tilde{\eta}c & 0 & 0 & 0 \\ -\tilde{\kappa} & -\tilde{\kappa}s & 0 & 0 & 0 \\ 0 & 0 & -\tilde{\zeta}sI & 0 & 0 \end{array}\right],$$

$$\left[\begin{array}{cc} B_1 & A_2 \end{array}\right] := \left[\begin{array}{ccccc|ccc} 0 & \tilde{\gamma}s & 0 & 0 & 0 & 0 & 0 & 0 \\ 0 & -\tilde{\gamma} & 0 & 0 & 0 & -c & 0 & 0 \\ 0 & 0 & 0 & 0 & 0 & 0 & 0 & 0 \\ 0 & 0 & 0 & 0 & 0 & \omega_1 s + dc & c & 0 \\ 0 & 0 & 0 & 0 & 0 & \delta c & 0 & cI \end{array}\right],$$

Thus, solution (3.31) is orbitally stable if and only if the system $\dot{\tilde{\xi}} = \Sigma\tilde{\xi}$ is stable.

From Lemma 1, orbital stability is shown if the dynamics of A_1 and $\mathcal{B}$ are both stable. First note that $A_1(t)$ has a block-triangular structure with a negative number on the first diagonal entry and the second diagonal block is constant and Hurwitz due to stability of plant (3.26). Thus the LP system with $A_1(t)$ is stable. Next note that the periodic solution to (3.7) has the form

$$\mathcal{L}_o = \begin{bmatrix} 0 \\ M_1 \\ M_2 \end{bmatrix} s + \begin{bmatrix} 0 \\ N_1 \\ N_2 \end{bmatrix} c. \tag{3.33}$$

Let A_2 and C_1 be expressed as

$$A_2 = \begin{bmatrix} 0 \\ 0 \\ P \end{bmatrix} s + \begin{bmatrix} 0 \\ Q_1 \\ Q_2 \end{bmatrix} c, \quad \begin{bmatrix} P \\ Q_1 \\ Q_2 \end{bmatrix} := \left[\begin{array}{ccc} \omega_1 & 0 & 0 \\ 0 & 0 & 0 \\ \hline -1 & 0 & 0 \\ 0 & 0 & 0 \\ \hline d & 1 & 0 \\ \delta & 0 & I \end{array}\right],$$

$$C_1 = \begin{bmatrix} R_1 & 0 & 0 \end{bmatrix} + \begin{bmatrix} 0 & R_2 & 0 \end{bmatrix} s + \begin{bmatrix} 0 & R_3 & 0 \end{bmatrix} c,$$

$$R_1 := \begin{bmatrix} 0 \\ -\tilde{\kappa} \\ 0 \end{bmatrix}, \quad R_2 := \begin{bmatrix} 0 & 0 \\ -\tilde{\kappa} & 0 \\ 0 & -\tilde{\zeta} I \end{bmatrix}, \quad R_3 := \begin{bmatrix} \tilde{\eta} & 0 \\ 0 & 0 \\ 0 & 0 \end{bmatrix}.$$

Substituting (3.33) into (3.7), setting the coefficients of s and c to zero, and eliminating M_2 and N_2, I obtain

$$\begin{bmatrix} M_1 \\ N_1 \end{bmatrix} = V^{-1} W,$$

where

$$V := \begin{bmatrix} \omega_1 \nabla & \Lambda - \omega_1^2 I \\ \omega_1^2 I - \Lambda & \omega_1 \nabla \end{bmatrix}, \quad W := \begin{bmatrix} \nabla Q_1 + Q_2 \\ \omega_1 Q_1 - P \end{bmatrix}.$$

Here, it is noted that V is invertible because $V + V^{\mathsf{T}} > 0$ due to $\nabla > 0$. Then I can calculate $\mathcal{B}$ as

$$\mathcal{B} = \int_0^T C_1 \mathcal{L}_o dt = \frac{T}{2} \cdot U V^{-1} W, \quad U := \begin{bmatrix} R_2 & R_3 \end{bmatrix}.$$

I first show that $\mathcal{B}$ is nonsingular. Suppose, for contradiction, that there exists a nonzero vector v in the null space of $\mathcal{B}$. Then, defining $w := V^{-1} W v$, I have

$$U V^{-1} W v = 0 \quad \Rightarrow \quad U w = 0, \quad V w = W v.$$

Since the left $(n+1) \times (n+1)$ block of U is square nonsingular and the remaining columns are zero, w has the form $w = \mathrm{col}(0, w_2)$ with $w_2 \in \mathbb{R}^{n-1}$. The lower $n-1$ rows of $Vw = Wv$

then gives $\nabla w_2 = 0$, implying $w = 0$ and $Wv = 0$. Since W has full column rank, I conclude $v = 0$. By contradiction, $\mathcal{B}$ must be nonsingular.

An arbitrary eigenvalue λ of $(2/T)\mathcal{B}$ is nonzero and satisfies the characteristic equation

$$\det V \det(\lambda I - UV^{-1}W) = \det(\lambda V - WU) = 0,$$

where I used determinant formulas. Noting that

$$WU = \mathrm{diag}(\tilde{\kappa}, \tilde{\zeta} I, 2\omega_1 \tilde{\eta}, 0) \geq 0,$$

it follows from Lemma 8 that the real part of $\lambda \in \mathbb{C}$ is negative. Thus $\mathcal{B}$ is hurwitz and I conclude the result. □

Theorem 6 shows that the orbital stability of the natural oscillation is guaranteed for the closed-loop system whenever the adaptation of the frequency and damping variables y_i is sufficiently slow. The controller is independent of the plant parameters except for the mode shape e_1 and the mass matrix M, and can be obtained without fine tuning of the design parameters.

3.6 Numerical Examples

3.6.1 Adaptive Oscillator

This section illustrates how our adaptive oscillator works, in comparison with the one presented in [40]. The former is given by (3.17) and its convergence property is guaranteed as in Theorem 4. The latter is given by an Andronov-Hopf oscillator with a Hebbian learning mechanism:

$$\begin{bmatrix} \dot{x}_1 \\ \dot{x}_2 \end{bmatrix} = \begin{bmatrix} 1 - r^2 & \omega_{\mathrm{est}} \\ -\omega_{\mathrm{est}} & 1 - r^2 \end{bmatrix} \begin{bmatrix} x_1 \\ x_2 \end{bmatrix} + \varepsilon \begin{bmatrix} 0 \\ z \end{bmatrix} \tag{3.34a}$$

$$\dot{\omega}_{\mathrm{est}} = -\varepsilon z x_1 / \sqrt{r}, \quad r := x_1^2 + x_2^2, \tag{3.34b}$$

and it was explained using perturbation argument [40] that ω_{est} globally (and approximately) converges to a frequency component of periodic input z when parameter $\varepsilon > 0$ is small.

For the numerical study, I use the input $z(t) = \cos(30t)$ for both oscillators. The system parameters and initial states are set as

$$\mu = 1, \quad \gamma = 10, \quad \eta = 50, \quad \kappa = 2,$$

$$x(0) = \mathrm{col}(0, 1), \quad y(0) = \mathrm{col}(40, 2),$$

for our adaptive oscillator (3.17) and

$$\varepsilon = 0.4, \quad 0.6, \quad 0.8, \quad 1, \quad \text{or} \quad 100,$$

$$x(0) = \mathrm{col}(0, 1), \quad \omega_{\mathrm{est}}(0) = 40,$$

for the Hebbian learning oscillator (3.34). The input z and initial states are taken from [40] and are used for both here, except that the initial estimate of the amplitude $y_2(0)$ is needed for (3.17) and is set twice as large as the true value.

Figure 3.1 shows the input z and response x_1, as well as the estimated frequency y_1 and amplitude y_2, for the adaptive oscillator in (3.17). We see that x_1 synchronizes with z within several cycles, while the estimated frequency and amplitude converge to their true values. For comparison, Fig. 3.2 shows the estimated frequency using the Hebbian learning approach in [40]. For small values of ε, the learning process takes a long time as seen in Fig. 3.2 (right), which is reproduced from the ε values in [40]. With a larger value of ε, their method could achieve faster convergence as seen in Fig. 3.2 (left), but there is a trade-off between convergence rate and steady-state error in the method of [40]. The larger the parameter ε, the faster the convergence, but the larger the error in the steady state. In contrast, such trade-off does not exist in our method since the adaptation mechanism is designed so that the error is zero at convergence.

3.6.2 Single-DOF Natural Entrainment

Let me now present an example of feedback control for natural entrainment. Consider the single-DOF mechanical system in (3.19) with parameter values switching from one set to another:

$$\begin{aligned} (m, d, k) &= (1, 2, 4) \quad \text{when } t < 30, \\ &= (1, 5, 16) \quad \text{when } t \geq 30. \end{aligned}$$

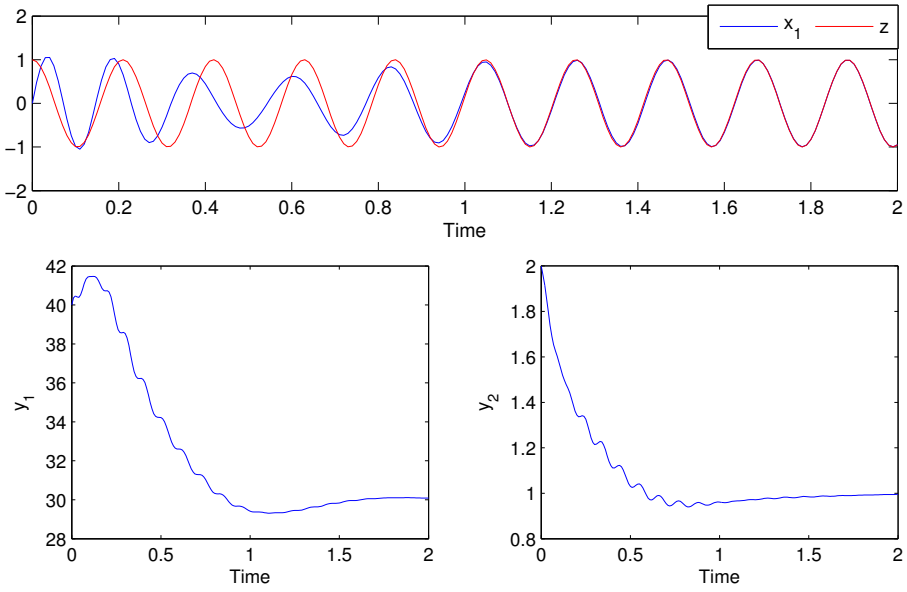

Figure 3.1: Adaptive Andronov-Hopf Oscillator

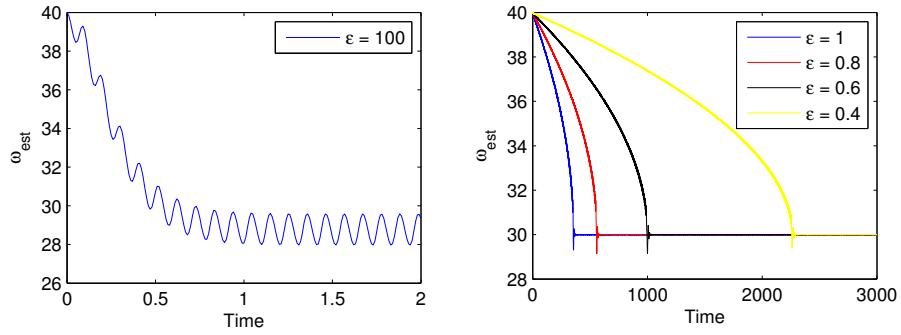

Figure 3.2: Andronov-Hopf Oscillator with Hebbian Learning

Note that the frequency of natural oscillation $z_n(t)$ in (3.20) is switched from $\omega_n = 2$ to 4. I design a feedback controller in (3.21) so that the frequency of mechanical oscillation is automatically tuned into the current natural frequency. The desired oscillation amplitude is fixed as $\alpha = 1$ at all time. The controller parameters are set as

$$\mu = 2, \quad \eta = 3, \quad \gamma = \kappa = 1.$$

The result in Fig. 3.3 shows that mechanical variable $z(t)$ eventually synchronizes with x_1 in the steady state, and both of them converge to a sinusoidal signal with the natural frequency ω_n and amplitude $\alpha = 1$. Furthermore, estimated frequency y_1 converges to the

natural frequency ω_n, and estimated damping y_2 converges to the true value d, respectively. Although Theorem 5 only guarantees local orbital stability when the control gains are sufficiently small, our numerical experience suggests that the domain of attraction for the natural oscillation remains fairly large when the control gains are made larger for faster convergence.

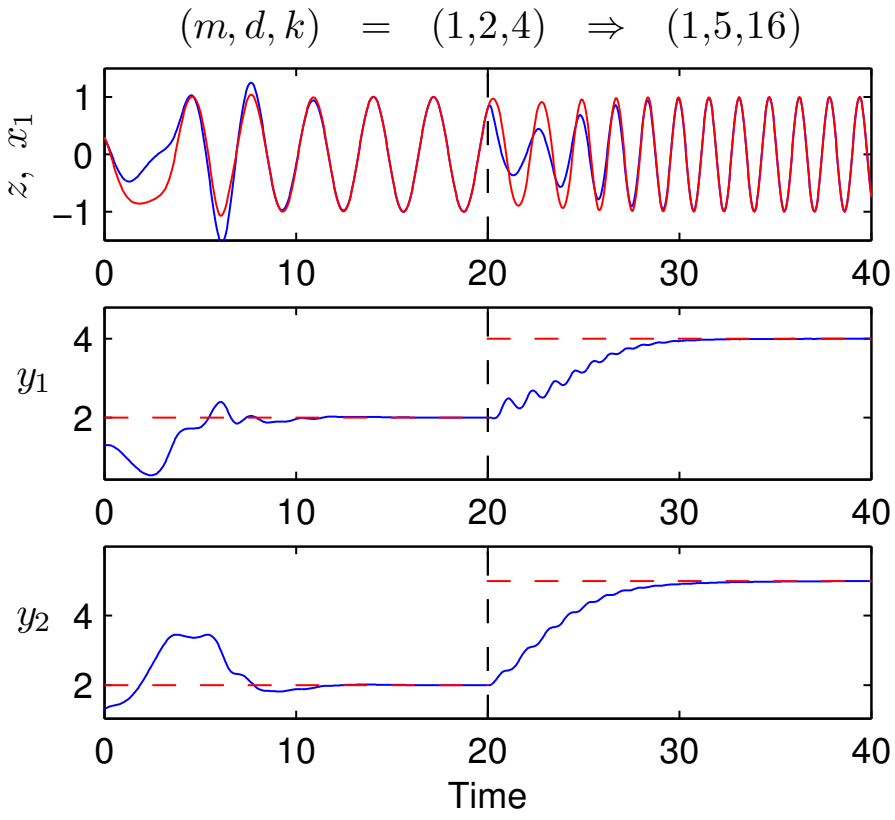

Figure 3.3: Single-DOF AHO Resonance Controller. Top row: z (blue), x_1 (red)

3.6.3 Multi-DOF Natural Entrainment

For the multi-DOF case, I consider system (3.26) with

$$\nabla = \begin{bmatrix} 2 & 1 & 1 \\ 1 & 9 & 5 \\ 1 & 5 & 3 \end{bmatrix}, \quad \Lambda = \begin{bmatrix} 9 & 0 & 0 \\ 0 & 4 & 6 \\ 0 & 6 & 16 \end{bmatrix},$$

where the targeted natural frequency is $\omega_1 = 3$, which is the square root of the $(1,1)$ entry of Λ. The desired oscillation amplitude is arbitrarily set as $\alpha = 1$, and the controller parameters

are chosen as

$$\mu = 2, \quad \gamma = \eta = \kappa = \zeta = 1.$$

The system was simulated for various values of the initial state, but reported below is the result for the case where all the 12 state variables ($z, \dot{z} \in \mathbb{R}^3$, $x \in \mathbb{R}^2$, $y \in \mathbb{R}^4$) of the closed-loop system are set to 1 at $t = 0$.

Figure 3.4 shows that z_1 converges to a sinusoidal signal with amplitude $\alpha = 1$ and frequency $\omega_1 = 3$ rad/s as desired. Meanwhile, the other two modes $z_2 \in \mathbb{R}^2$ are successfully converging to zero. Thus, the targeted natural oscillation is achieved. The mechanisms underlying the natural entrainment are visible in other plots. The AHO variable x_1 eventually synchronizes with z_1, while the adaptation variables y_1 and y_2 quickly converge to the natural frequency $\omega_1 = 3$ and damping coefficient $d = 2$. It takes a long time for the damping estimate y_3 to converge to $\delta = [1, 1]^\intercal$ (e.g. $t = 280$ to reach within 5% error). Although the convergence to the natural oscillation does not seem very sensitive to the slow convergence of y_3, this example suggests that it may be worthwhile to search an improved adaptation mechanism for y_3.

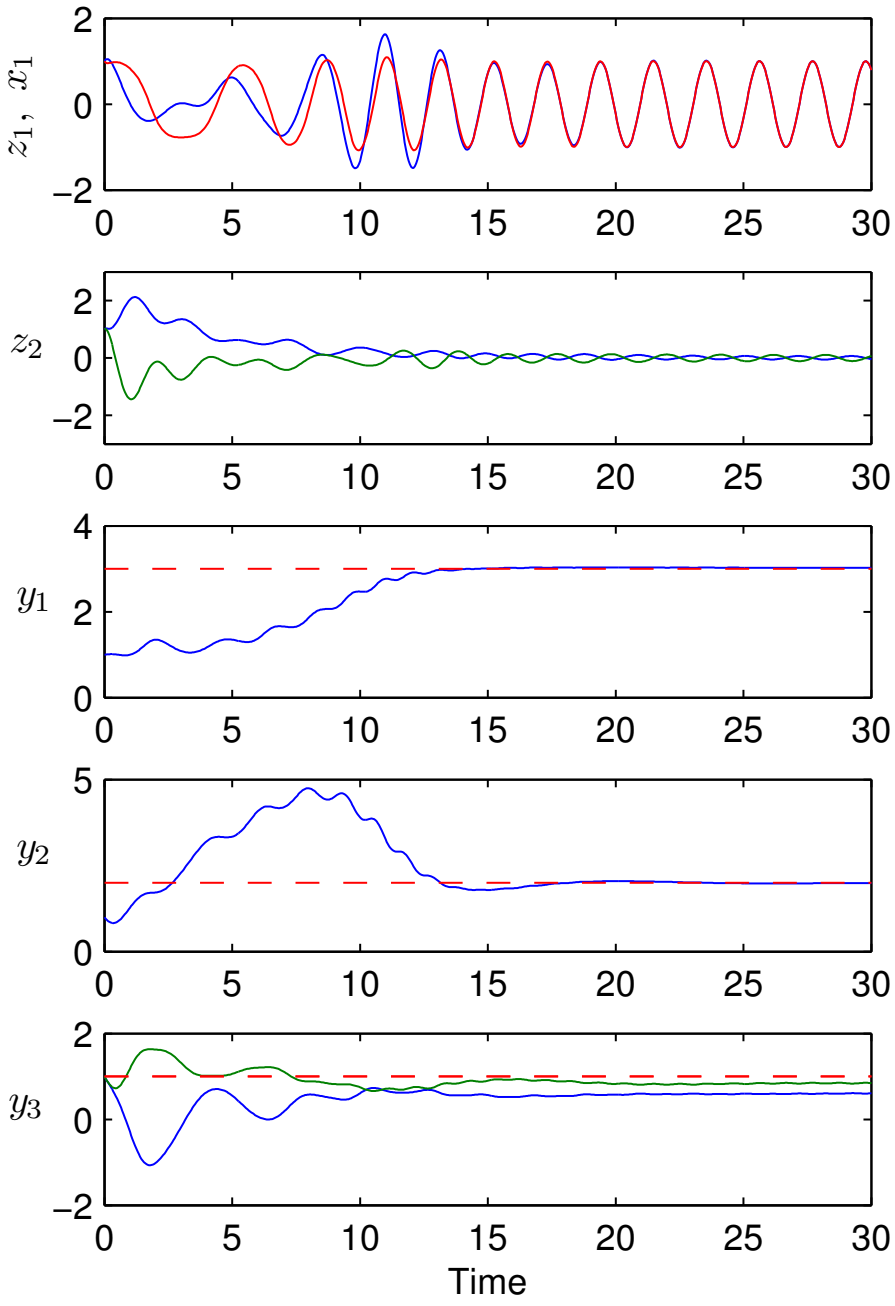

Figure 3.4: Multi-DOF AHO Resonance Controller. Top row: z_1 (blue), x_1 (red)

3.7 Discussion

This chapter considers a fundamental design problem, how to trigger an unknown system natural oscillation in an adaptive manner. To this end, I have formulated and solved problems

of designing adaptive oscillators using the structure of the Andronov-Hopf oscillator (AHO) for multiple goals. I started with developing an adaptive oscillator that synchronizes with an external periodic signal and explicitly estimates the amplitude and frequency of the signal. I then proposed a method for designing a feedback controller to embed an orbitally stable limit cycle in the closed-loop system, on which a natural mode of oscillations is achieved. As usual, the design proceeds from single-DOF problem to a multi-DOF case. Several numerical examples were provided and they demonstrated that the proposed methods were effective with fast and smooth convergence. Further development of this problem could be bi-fold. Since the current theory guarantees the local stability of the closed-loop system, more effort could be made to enlarge the region of contraction of the limit cycle. In addition, current stage of this results merely consider the problem in an ideal environment. Further consideration of a noisy environment would be beneficial for the real-world application.

CHAPTER 4

Experiment Platform

4.1 Overview

In this chapter, a robotic arm hardware platform is prepared for the validation of the assistive control strategy. As mentioned before, understanding the relation, between the input force/torque generated by human and the position/velocity feedback through visual, is critical for this project. Hence, this platform will serve two objectives of human motor identification and assistive control validation. The experiment process is explained and described in section 4.2, the design requirements are also delivered here. Based on the design requirement, the mechanical part of the robotic arm is designed in section 4.3, followed by the electrical components selection such as sensors and motors introduced. The way to make the system adaptive to operate as single-DOF system is also shown here. A control scheme for virtual mechanical impedance system is described in section 4.4 for both single-DOF and 2-DOF systems. This virtual mechanical impedance systems behave much like a theoretical mass-spring-damping system, so that the control can be tested against a theoretically ideal environment.

4.2 Experiment Design and Requirement

The overall design goal is to build a robotic arm that is able to simulate a human arm behavior in the horizontal plane. During the experiment, the human will perform a tracking task. In other words, the human will try to move his/her hand through a reference trajectory on a horizontal plane. Consequently, the robotic arm should be able cooperate with human

and I thus aim to build a robotic arm whose end tip could posses two degree of freedom in the horizontal plane.

The idea of the experiment can be illustrated by Fig. 4.1. A human can grab the end-tip of the robotic arm and tries to move the end tip along a reference trajectory. A device is attached beneath the end tip, which will be merged into viscous fluid to create various damping loads. It emulates a situation where a human and a robot grab a common tool to stir viscous fluids. The robotic arm will be driven by servo motors to rotate around its shoulder joint and elbow joint in a horizontal plane. The rotational angles, as well as angular velocities of the motors are measured by encoders. A force sensor is fixed at the end-tip of the robotic arm with a handle attached to it. A human grabs the handle and apply torque through the handle, while the measured force and angular positions data are collected by the sensors and fed back to the computer. The computer will generate appropriate control command signals to the motors and records the sensor measurements. The experiment scheme can be illustrated by Fig. 4.1.

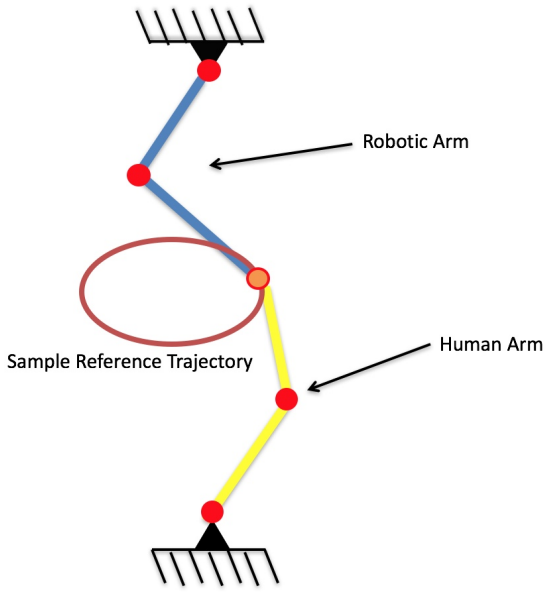

Figure 4.1: 2-DOF Experiment diagram

The experiment is actually planned to proceed from single-DOF first and then 2-DOF. Similar to the 2-DOF experiment, the single-DOF experiment can be illustrated by Fig. 4.2.

The only different feature of this single-DOF scenario is that the reference trajectory can only be a curve.

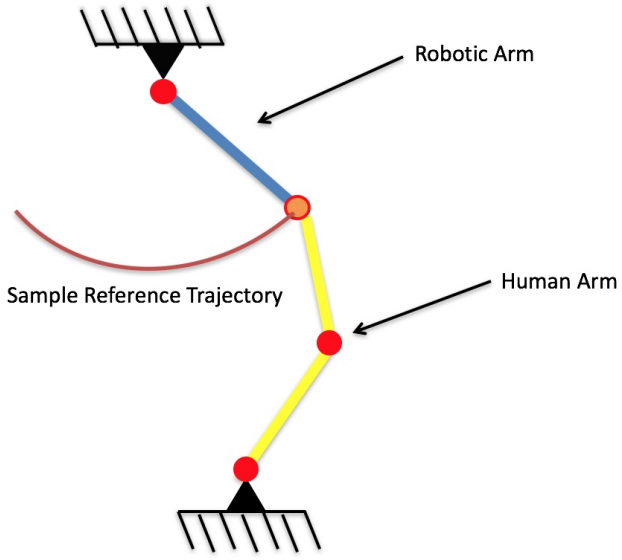

Figure 4.2: Single-DOF experiment diagram

However, in the mechanical design part, the 2-DOF case is first considered and the arm is designed accordingly. A slight modification or redesign is then made. By removing several parts of the robotic arm, the remaining part will be suited for a single-DOF experiment. Therefore, the robotic arm will be later designed according to these scenarios.

4.3 Robotic Arm Design

A simple design scheme is first proposed as shown in a diagram Fig. 4.3, that motor 1 is fixed to a base and link 1 is attached to motor 1. Then motor 2 can be installed on the other end of link 1 and the link 2 is attached to motor 2. However, this simple design could cause several problems. First of all, in order to support motor 2 and link 2, link 1 has to be extremely strong, which consequently increases its inertial. As a result, the combination of the two links inertial and the inertial caused by motor 2 largely raised up the requirement of the motor 1 capability, making the motor size and the cost well beyond reality.

An improved design plan is then proposed that a four-linkage structure could help reduce

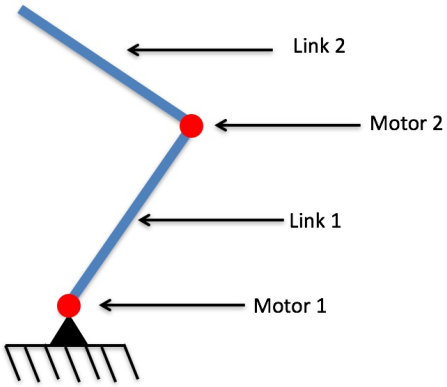

Figure 4.3: Two-linkage structure

the required motor capability. As shown in diagram Fig. 4.4(left), the the two motors are overlapped at the base position, minimizing the inertial caused by motor. Motor 1 will move the whole linkage system, while motor 2 changes the angle between link 1 and link 2, thus changing the shape of the quadrilateral.

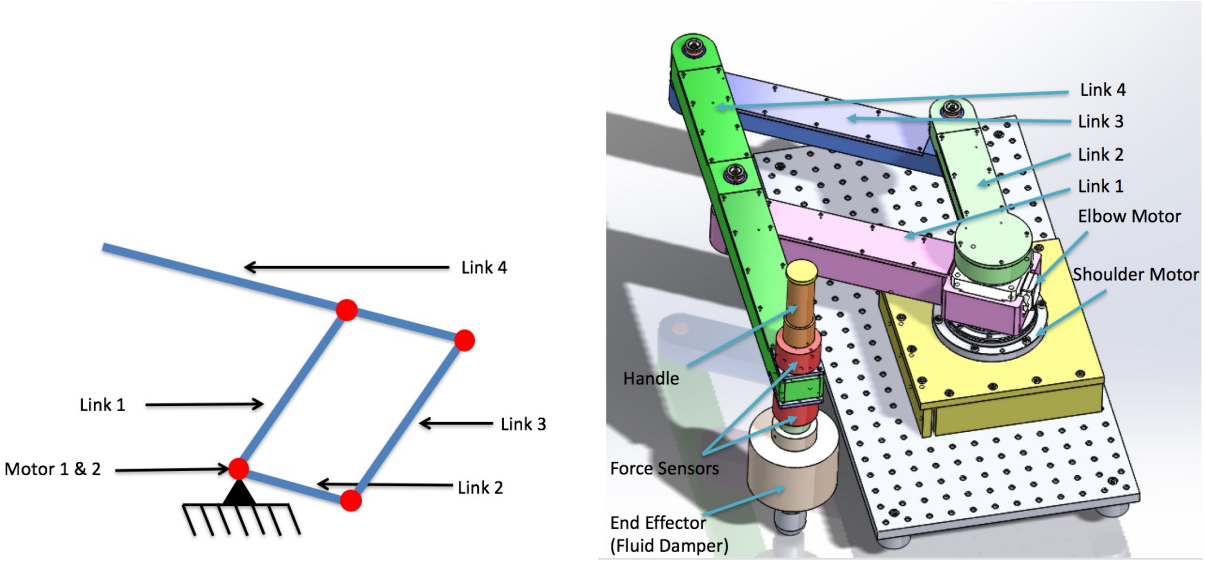

Figure 4.4: A four-linkage structure

Now that the robotic arm basic structure was determined, a detailed plan for the robotic arm is specified now. Objective of this part is to determine the size of the robotic arm based on that of a human arm. Towards this end, firstly, link 1 was chosen to be 0.3m, which is

about the same length of a human upper arm, so as well for link 3. I chose link 2 to be 0.2m and link 4 is 0.5m total. All the linkages should be shelled so that their masses and inertia is much reduced, as well as the cost. The cross-section of the link is chosen as follows. Both the width and height are 50 mm and the thickness is 5 mm, as shown in Fig. 4.5.

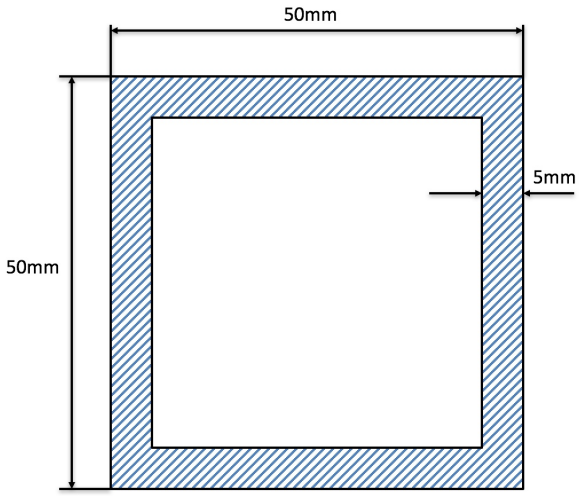

Figure 4.5: Link cross-section

The maximum shear force that can applied to the link can be calculated as

$$F_{max} = \sigma_{0.2} W_z = 369N$$

where

$$W_z = \frac{0.05^4/12 - 0.04^4/12}{0.05/2} = 1.23 \cdot 10^{-5}$$

and the yield stress for aluminum is $\sigma_{0.2} = 15MPa$.

The overall mass of the linkages system can be approximated as

$$m = (0.05^2 - 0.04^2) \cdot 1.5 \cdot 2.7 \cdot 10^3 = 3.645kg.$$

It can be seen that, the link is strong enough to handle the force applied by human, since a normal human can barely generate 369N force with one arm. Moreover, the overall weight of the arm is not too high, thus the cost of the material will be reasonable.

To create additional damping load, a cylinder-like object is attached beneath the arm end-tip. In the experiment, this part is merged inside the viscous fluid. The 3-D model of the overall designed system is shown in Fig. 4.4 (right).

Given the determined four-linkage structure, the hardware components would be determined before the actual sizes of the robotic arm were chosen. Suppose a human is lifting a 10 kg dumbbell with 0.6 m full arm length, then the torque required would be 58 N·m, I considered motor 1 should be capable of doing the same and chose its maximum torque to be 58 N·m. Meanwhile, motor 2 was selected in order to able to lift a 6 kg dumbbell with a 0.3m lower arm, thus the maximum torque was chosen as 18 N·m. In order to collect the human input data, a two-dimensional force cell was selected. The main hardware devices are chosen as follows:

Controller: Speedgoat Performance real-time target machine

Motor 1: Harmonic Drive FHA-17C-100

Motor 2: Harmonic Drive FHA-14C-50

Force Sensor: Futek MBA400.

The Speedgoat target machine is a real-time controller that is able to well cooperate with Matlab/Simulink. The target machine is connected to a computer that runs Matlab/Simulink through a serial bus and the computer is called as "host machine". Simulink models are designed at the "host machine" end and then transmitted and built into the target machine. The host machine is able to start/stop the running of the model, as well as read/change the model parameters while the model is running. Along with an appropriate I/O port accessory, the target machine is able to read sensor signals and send command signal to the motors. The overall actual system is shown in Fig. 4.6.

As mentioned above, the experiment is planned to take place step by step and the experiment would start with a single-DOF system first. Hence, the robotic arm is made possible to operate with only one link as a single-DOF system by removing other linkages, for that purpose. Similarly, the single-DOF system was designed for a situation where a human cooperate to stir viscous fluids simply along a curve. The sole link is driven by a servo motor to rotate around its shoulder joint or origin in a horizontal plane. The rotational angle of the motor is still measured by an encoder. A force sensor is as well fixed at the end-tip of the robotic arm with a handle attached to it. A human is again asked to grab the handle

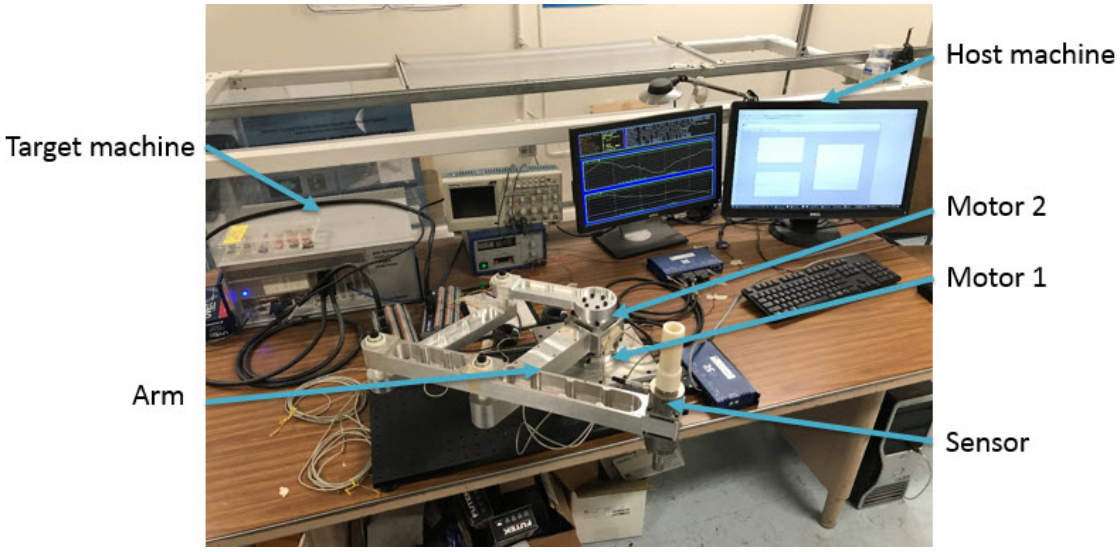

Figure 4.6: The actual experiment platform

and apply torque through the handle, while the measured force and angular position data are collected by the sensors and fed back to the computer. The computer generates an appropriate control command signal to the motor and records the sensor measurements. This single-DOF experimental test rig is shown in Fig. 4.7.

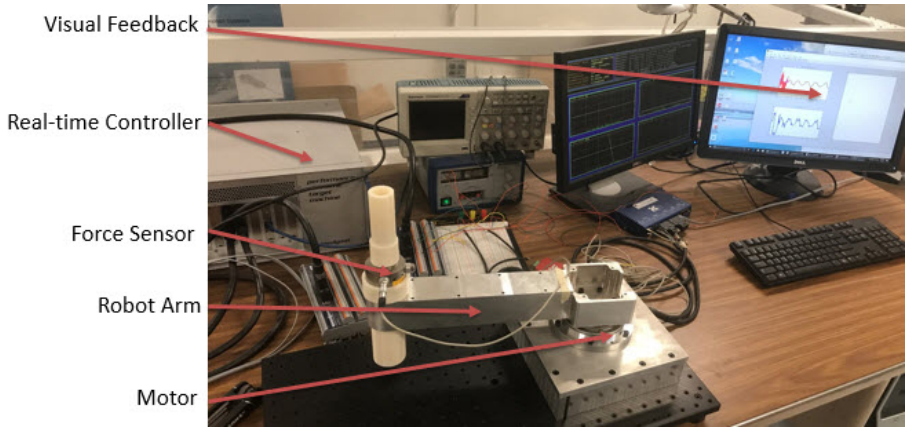

Figure 4.7: Single-DOF Experimental test rig

4.4 Virtual Mechanical Impedance System

In this part, a control scheme is proposed to regulate the physical system to behave almost exactly as a mass-spring-damping system, where the mass, stiffness and damping coefficient can be chosen arbitrarily. The idea of such control application is to exploit a reference model programmed inside the software generating reference velocity signal and to use a high-gain PI control to eliminate the error between actual velocity and reference velocity. With such system, the control algorithm can be tested against the theoretical environment initially, before it is tested against practical environment. In addition, human motor control model identification will be performed under this control implementation, because the system mass, damping and stiffness can be set and known.

4.4.1 Single-DOF Virtual Mechanical Impedance System

For the single-DOF system, during the experiment, a human holds the end tip of the robot arm and applies torque on the handle to make the arm move back and forth. The torque applied by the human is measured by a force sensor and the arm angle is measured by an encoder. The dynamics from human torque input v to the arm rotating angle $z = \theta$ are set via a minor feedback loop to match a single-DOF mass-damping-stiffness system as shown in Fig. 4.8.

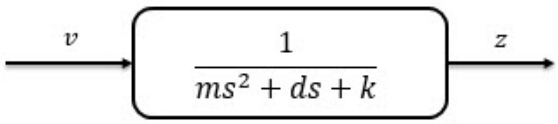

Figure 4.8: Robot Arm Plant Model

In the transfer function, m, d, k are virtual system mass, damping and stiffness parameters, assigned by the software. The system block diagram is shown in Fig. 4.9, where $G(s)$ represents the physical dynamics of arm-gear-motor system, $K(s)$ is a PID controller, $Q(s)$ represents the electrical dynamics from the PID output to the actual torque τ generated by the motor, and v is the human torque input. The velocity command is calculated as the

velocity output of the virtual system $M(s) := s/(ms^2 + ds + k)$ when the input v is applied. Here, the parameters (m, d, k) of the virtual mechanical system are set to arbitrary desired values. The motor velocity is regulated by the high-gain PID controller $K(s)$ to track the reference command velocity signal. Ideally, the velocity $\dot{\theta}$ matches the command so that the overall dynamics from v to $\dot{\theta}$ have the desired mechanical impedance $(ms + d + k/s)$. From Fig. 4.9, we see that the arm-gear-motor system $G(s)$ receives both τ and v as inputs, and this v could act as a disturbance for the PID control system. However, the transfer function from v to the model matching error e is given by $(M - G)/(1 + GKQ)$, and the high gain control $K(s)$ will achieve the desired mechanical impedance.

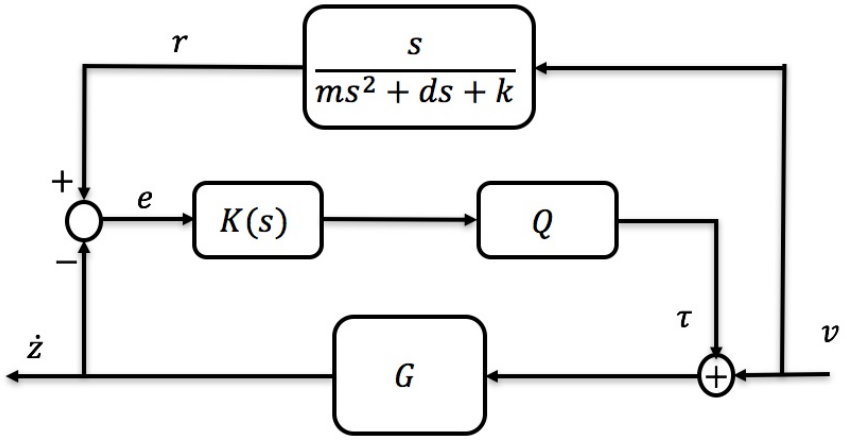

Figure 4.9: Virtually programmed system

4.4.2 2-DOF Virtual Mechanical Impedance System

Similar to the single-DOF case, a 2-DOF reference model is programmed to generate reference angular velocities for shoulder and elbow motors. However, the 2-DOF reference model is more complicated and is a nonlinear system. A two-linkage model is considered here as shown in Fig. 4.10 and the equations of motions is derived first.

In Fig. 4.10, (x_i, y_i) indicates the position of the centers of mass, l_i means the half length of one link, (h_{xi}, h_{yi}) indicates the interacting forces between the base and link 1, link 1 and link 2, u_0 and u_1 are the torque generated by the actuators locates at the joint, which in

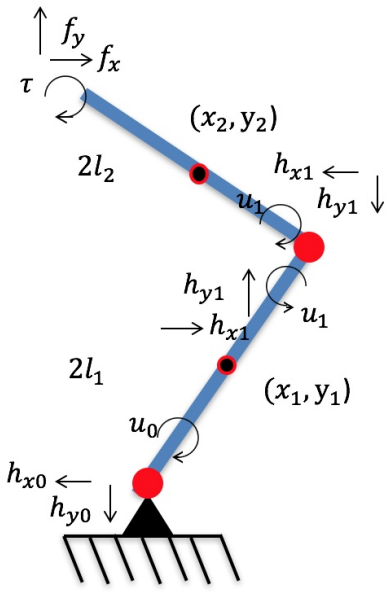

Figure 4.10: 2-linkage reference model diagram

our model, are zero. Based on Newton second law, dynamics of this virtual system can be described as

$$J_1\ddot{\theta}_1 = u_1 - u_0 - (h_{x1} + h_{x0})l_1 sin\theta_1 + (h_{y1} + h_{y0})l_1 cos\theta_1$$

$$m_1\ddot{x}_1 = h_{x1} - h_{x0}$$

$$m_1\ddot{y}_1 = h_{y1} - h_{y0}$$

$$J_2\ddot{\theta}_2 = \tau - u_1 - (f_x + h_{x1})l_2 sin\theta_2 + (f_y + h_{y1})l_2 cos\theta_2$$

$$m_2\ddot{x}_2 = f_x - h_{x1}$$

$$m_2\ddot{y}_2 = f_y - h_{y1}$$

where τ, f_x and f_y are interacting forces and torque with the environment.

Meanwhile, the kinematics of this virtual system is described by the following equations

$$x_1 = l_1 cos\theta_1$$

$$y_1 = l_1 sin\theta_1$$

$$x_2 - x_1 = l_1 cos\theta_1 + l_2 cos\theta_2$$

$$y_2 - y_1 = l_1 sin\theta_1 + l_2 sin\theta_2$$

By letting

$$E = \begin{bmatrix} 1 & 0 \\ -1 & 1 \end{bmatrix}, \quad S_\theta = \begin{bmatrix} \sin\theta_1 & 0 \\ 0 & \sin\theta_2 \end{bmatrix}, \quad C_\theta = \begin{bmatrix} \cos\theta_1 & 0 \\ 0 & \cos\theta_2 \end{bmatrix}, \text{ and } L = \begin{bmatrix} l_1 & 0 \\ 0 & l_2 \end{bmatrix},$$

the above kinematic equations are equivalent to

$$E\ddot{x} = -E^{-1}L(C_\theta\dot{\theta}^2 + S_\theta\ddot{\theta}) \tag{4.1a}$$

$$E\ddot{y} = E^{-1}L(-S_\theta\dot{\theta}^2 + C_\theta\ddot{\theta}) \tag{4.1b}$$

Now, the equations of dynamics and kinematics can be combined to derive the full equations of motion.

Let $M = \begin{bmatrix} m_1 & 0 \\ 0 & m_2 \end{bmatrix}$, then it can be obtained

$$M\ddot{x} = -E^T \begin{bmatrix} h_{x0} \\ h_{x1} \end{bmatrix} + \begin{bmatrix} 0 \\ f_x \end{bmatrix} \tag{4.2a}$$

$$M\ddot{y} = -E^T \begin{bmatrix} h_{y0} \\ h_{y1} \end{bmatrix} + \begin{bmatrix} 0 \\ f_y \end{bmatrix} \tag{4.2b}$$

Combining (4.1) and (4.2),

$$-E^{-2}L(C_\theta\dot{\theta}^2 + S_\theta\ddot{\theta}) = -M^{-1}E^T \begin{bmatrix} h_{x0} \\ h_{x1} \end{bmatrix} + M^{-1} \begin{bmatrix} 0 \\ f_x \end{bmatrix}$$

$$E^{-2}L(-S_\theta\dot{\theta}^2 + C_\theta\ddot{\theta}) = -M^{-1}E^T \begin{bmatrix} h_{y0} \\ h_{y1} \end{bmatrix} + M^{-1} \begin{bmatrix} 0 \\ f_y \end{bmatrix}$$

Thus, the interacting forces between links can be derived as

$$\begin{bmatrix} h_{x0} \\ h_{x1} \end{bmatrix} = E^{-T}ME^{-2}L(C_\theta\dot{\theta}^2 + S_\theta\ddot{\theta}) + E^{-T} \begin{bmatrix} 0 \\ f_x \end{bmatrix} \tag{4.3a}$$

$$\begin{bmatrix} h_{y0} \\ h_{y1} \end{bmatrix} = -E^{-T}ME^{-2}L(-S_\theta\dot{\theta}^2 + C_\theta\ddot{\theta}) + E^{-T} \begin{bmatrix} 0 \\ f_y \end{bmatrix}. \tag{4.3b}$$

Let the inertial matrix be $J = \begin{bmatrix} J_1 & 0 \\ 0 & J_2 \end{bmatrix}$, then the dynamics equation can be also expressed as

$$J\ddot{\theta} = \begin{bmatrix} -1 & 1 \\ 0 & -1 \end{bmatrix} \begin{bmatrix} u_0 \\ u_1 \end{bmatrix} + \begin{bmatrix} 0 \\ \tau \end{bmatrix} - LS_\theta(E^{-T} \begin{bmatrix} h_{x0} \\ h_{x1} \end{bmatrix} + \begin{bmatrix} 0 \\ f_x \end{bmatrix}) + LC_\theta(E^{-T} \begin{bmatrix} h_{y0} \\ h_{y1} \end{bmatrix} + \begin{bmatrix} 0 \\ f_y \end{bmatrix}) \quad (4.4)$$

By substituting (4.3) into (4.4),

$$\mathcal{J}\ddot{\theta} + \mathcal{D}\dot{\theta}^2 = Bu + \begin{bmatrix} 0 \\ \tau \end{bmatrix} + \mathcal{B}f \quad (4.5)$$

where

$$B = \begin{bmatrix} -1 & 1 \\ 0 & -1 \end{bmatrix}, \quad u = \begin{bmatrix} u_0 \\ u_1 \end{bmatrix}, \quad f = \begin{bmatrix} f_x \\ f_y \end{bmatrix}$$

$$\mathcal{J} = J + S_\theta \Lambda S_\theta + C_\theta \Lambda C_\theta$$

$$\mathcal{D} = S_\theta \Lambda C_\theta - C_\theta \Lambda S_\theta$$

$$\Lambda = LE^{-2T}ME^{-2}L$$

$$\mathcal{B} = 2L \begin{bmatrix} -\sin\theta_1 & \cos\theta_1 \\ -\sin\theta_2 & \cos\theta_2 \end{bmatrix}.$$

Now, assuming there exists resistive force at the tip, whose magnitude is proportional to the magnitude of the tip velocity and whose direction is in the opposite direction of the tip velocity. The tip velocity can be represented as

$$\begin{bmatrix} \dot{x}_t \\ \dot{y}_t \end{bmatrix} = \begin{bmatrix} -2l_1 \sin(\theta_1)\dot{\theta}_1 - 2l_2 \sin(\theta_2)\dot{\theta}_2 \\ 2l_1 \cos(\theta_1)\dot{\theta}_1 + 2l_2 \cos(\theta_2)\dot{\theta}_2 \end{bmatrix}. \quad (4.6)$$

Suppose the friction coefficient is μ, then the resistive force is

$$\begin{bmatrix} f_x \\ f_y \end{bmatrix} = -\mu \begin{bmatrix} \dot{x}_t \\ \dot{y}_t \end{bmatrix} = -\mu \mathcal{B}^\intercal \dot{\theta} \quad (4.7)$$

By substituting (4.7) into (4.5), also letting $u = \tau = 0$, we can obtain the equations of motion

$$\mathcal{J}\ddot{\theta} + \mathcal{D}\dot{\theta}^2 + D\dot{\theta} = \mathcal{B}f \tag{4.8}$$

where

$$D = \mu\mathcal{B}\mathcal{B}^{\intercal}.$$

Therefore, I derive the equations of motion of this virtual system as shown in (4.8) and they are programmed into the software to generate a reference angular velocities for both links. Additional high-gain PI control law is deployed to ensure the actual angular velocities tracking.

Recall that, in the 1-DOF case, a virtual model described as $\frac{1}{m^2+ds+k}$ is programmed inside the software as a reference angular velocity generator. This time, the 2-DOF virtual model derived above is programmed inside the software and a two-dimensional high gain PI controller is employed to regulate the behaviour of this 2-DOF system. The system control scheme can be seen as a block diagram in Fig. 4.11, which is similar to the one of the single-DOF case. However, in this 2-DOF experiment, the blocks $K(s)$, Q and G are now 2 by 2 and represent two-dimensional PI controller, two motor dynamics and four-linkage practical system (2-DOF). The signals $\dot{z}$, e, r, τ and v are two dimensional vectors.

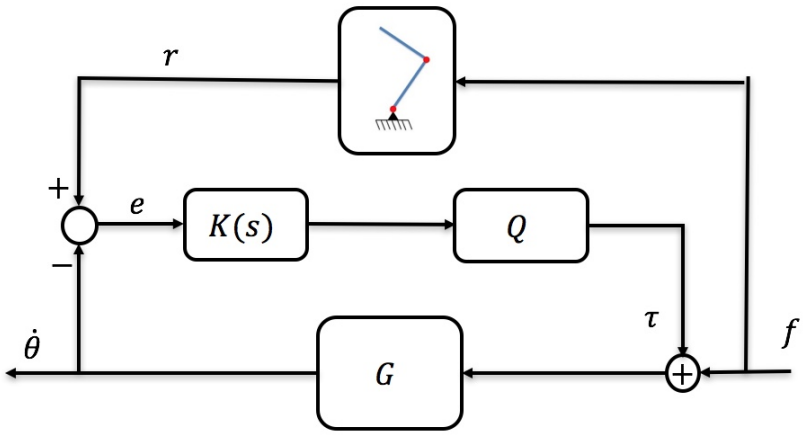

Figure 4.11: Virtual 2-DOF system

4.5 Discussion

The design process of the a hardware platform is described in this part. Consider the objectives of assistive control validation and human motor control model identification, the experiment is first designed. Accordingly, a 2-DOF robotic arm with four links is designed and detailed to satisfy the experimental requirement. Appropriate sensors and motors are also chosen based on the experiment needs. The robotic arm design is as well adaptive to reduction to a single-DOF arm system for corresponding experiments. To create an ideal environment that encounter the proposed theory, a virtual mechanical impedance system control scheme is illustrated. The idea is to enforce the actual system to behave almost same as the programmed reference model, with the help of a high-gain PI control.

CHAPTER 5

Human motor control

5.1 Overview

Understanding the relation between the force/torque a human would apply and the position/velocity feedback he/she receives, can be beneficial for assistive robotic devices design. When discussing the RIO controlled system stability, I proposed a hybrid human motor control model, which is a combination of feedforward and feedback models. In this chapter, I will conduct several experiments to first identify the parameters and then validate the model. The validation of the model will compare how close the control model caused trajectory and human caused trajectory. The experiment is first conduct in single-DOF and then extended to 2-DOF case. The experiment process of single-DOF is first described in section 5.2, where a human subject receives visual feedback and the applied force/torque is measured and recorded. Then a least-squared minimization problem is formulated for the purpose of identifying parameters. In the last part of section 5.2, human and control model each operates the robotic arm system and the generated trajectories are recorded. I define a correlation function to conclude the closeness of these two trajectories. In section 5.3, the 2-DOF human motor control identification experiment is discussed, which shares similar process and analysis method with single-DOF case.

5.2 Single-DOF Human Motor Control Modeling

The experiment has been described in the previous chapter and let us re-address it now. The intended operation of the system can be explained using the diagram shown in Fig. 5.1. A

human grabs the handle at the end of the robotic arm. The arm angle is visually shown on the computer screen as a blue circle. A reference position of the arm is also shown on the screen as a red star. While the red star goes back and forth to indicate sinusoidal oscillation of the reference arm angle z_d, the human is asked to apply force so that the actual arm angle z follows the reference position (i.e. the blue circle tracks the red star). The force sensor measurement will then indicate the human effort required for the periodic operation.

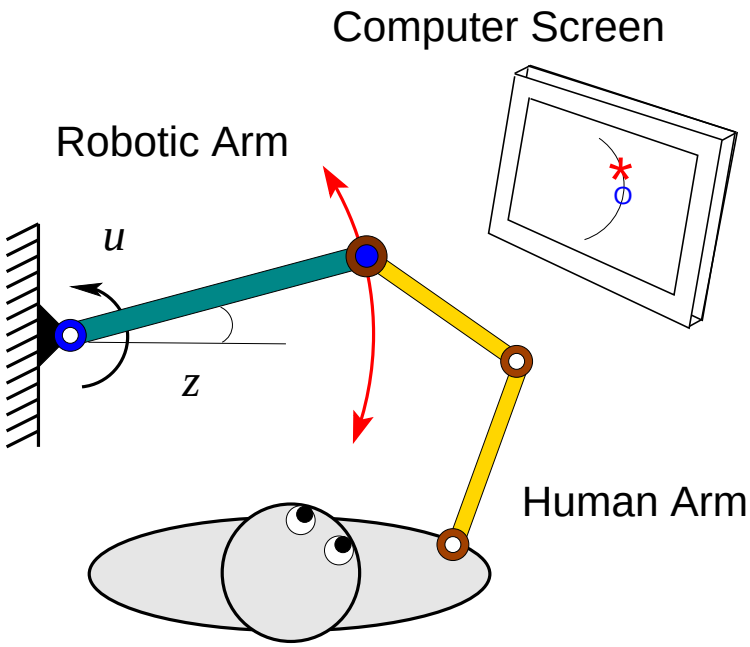

Figure 5.1: Schematic of human-robot experiment

5.2.1 Framework and approach

In this experiment, the virtual mechanical impedance system control scheme is employed. When human reach out to an object and move it along a desired trajectory, human would use certain control strategy to achieve the movement. For the single-DOF mechanical system described by (2.1) with $u(t) = 0$, a model for the human motor control may be given by

$$v(t) = \hat{m}\ddot{z}_d + \hat{d}\dot{z}_d + \hat{k}z_d + \alpha(\dot{z} - \dot{z}_d) + \beta(z - z_d), \tag{5.1}$$

where $z_d(t)$ is the desired trajectory, $(\hat{m}, \hat{d}, \hat{k})$ are the mass, damping, and stiffness parameters assumed by the human, and (α, β) are the feedback gains to generate corrective forces

/torques. This mathematical model is consistent with the literature on human motor control, where the human is often found to employ both feedforward and feedback strategies. The feedforward action is captured by the term of the control model $\hat{m}\ddot{z}_d + \hat{d}\dot{z}_d + \hat{k}z_d$, which is the human estimated force appropriate for achieving the motion $z_d(t)$ nd can be refined through experience. The feedback action is captured by the term $\alpha(\dot{z}_d - \dot{z}) + \beta(z_d - z)$, which adjusts the applied force in accordance with the error between the desired and actual trajectories. The feedforward/feedback model in (5.1) was assumed for the human motor control when we developed the assistive CPG control theory. The objective here is to identify the parameters $(\hat{m}, \hat{d}, \hat{k})$ and (α, β) and validate the human motor control model (5.1).

The actual and desired end-tip positions, $z(t)$ and $z_d(t)$, are shown on a computer screen, and the human is asked to track the desired trajectory by moving the arm.

During the experiment, the time histories of the variables $z(t)$, $z_d(t)$, and $v(t)$ are recorded at time instants $t = t_i$ for $i = 1, \ldots, n$ where n is the number of data points collected. The data is fit by the human motor control model (5.1) through the least square optimization:

$$\min_x \|b - Ax\| \tag{5.2}$$

where

$$\begin{aligned}
&b = \text{col}(v(t_1), v(t_2), ..., v(t_n)),\\
&x = \text{col}(\hat{m}, \hat{d}, \hat{k}, \alpha, \beta),\\
&A = \text{col}(a(t_1), a(t_2), ..., a(t_n)),\\
&a(t) = \begin{bmatrix} \ddot{z}_d(t) & \dot{z}_d(t) & z_d(t) & \dot{z}(t) - \dot{z}_d(t) & z(t) - z_d(t) \end{bmatrix}.
\end{aligned}$$

To assess the importance of the feedforward and feedback terms, we also consider the feedforward controller

$$v_{ff} = \hat{m}\ddot{z}_d + \hat{d}\dot{z}_d + \hat{k}z_d, \tag{5.3}$$

and feedback controller

$$v_{fb} = \alpha(\dot{z} - \dot{z}_d) + \beta(z - z_d). \tag{5.4}$$

The corresponding optimization problems can be formulated as (5.2) with

$$x = \text{col}(\hat{m}, \hat{d}, \hat{k}), \quad a(t) = \begin{bmatrix} \ddot{z}_d(t) & \dot{z}_d(t) & z_d(t) \end{bmatrix}.$$

for the feedforward model and

$$x = \mathrm{col}(\alpha, \beta), \quad a(t) = \begin{bmatrix} \dot{z}(t) - \dot{z}_d(t) & z(t) - z_d(t) \end{bmatrix}.$$

for the feedback model.

The accuracy of the mixed feedforward/feedback model (5.1) is evaluated by applying it as the controller to the system and comparing the resulting motion with the recorded motion under the human control. In particular, for a fixed reference position $z_d(t)$, the human drives the system to track it, and the resulting motion is denoted as $z(t)$. For the same reference position $z_d(t)$, the model (5.1) drives the system to track it, and the resulting motion is denoted by $z_m(t)$. In this case, $v(t)$ generated by (5.1) drives the reference model $s/(ms^2 + ds + k)$ in Fig. 4.9, but does not add to τ since no physical force $v(t)$ is applied directly to the arm. The correlation between z and z_m is calculated as follows:

$$r_m = \frac{\sum_{k=1}^{n} z(t_k) z_m(t_k)}{\sqrt{(\sum_{k=1}^{n} z^2(t_k))(\sum_{k=1}^{n} z_m^2(t_k))}}.$$

The correlation r_m will be 1, if z_m matches z perfectly, and hence closeness of r_m to 1 indicates accuracy of the human control model (5.1). Similarly, feedforward controller (5.3) and feedback controller (5.4) are evaluated by the correlations r_{ff} and r_{fb}, where z_{ff} and z_{fb} are the measured angles during the experiments in which the system is driven by $z_d(t)$ under the control (5.3) and (5.4), respectively.

5.2.2 Experimental result and discussion

During the experiment, we assigned different values to m and d virtually in the software using minor feedback control (velocity mode), while the stiffness was set to $k = 0$. The desired oscillation is

$$z_d(t) = \frac{\pi}{3} \sin(\frac{2\pi}{9} t). \tag{5.5}$$

For each m and d values, the experiment was conducted for 15 times and 50 seconds for each run. The measurements of the force sensor and encoder were collected as frequently as possible within the hardware limitation, so the sampling period $(t_{i+1} - t_i)$ was not fixed

constant. However, this does not affect the formulation of the optimization problems that identify the model parameters.

The result of the parameter identification for the 3 human control models, (5.1), (5.3) and (5.4), are shown in Table 5.1, where $\hat{k}$ was set to zero during the optimization. For the mixed model (5.1), the feedforward parameters $(\hat{m}, \hat{d})$ are very close to the actual mass and damping values (m, d), the rate feedback gain α is slightly less than the damping d to mostly compensate for the damping load while maintaining stability, and the position feedback gain β is negative so that stiffness is added for achieving the oscillation task. The closed-loop system is given by

$$m\ddot{z} + (d - \alpha)\dot{z} - \beta z = \hat{m}\ddot{z}_d + (\hat{d} - \alpha)\dot{z}_d - \beta z_d.$$

It is observed that the human control parameters are chosen so that the dynamics on the left hand side have the undamped natural frequency and the resonance frequency are around 1 rad/s, which is fairly close to the driving frequency $2\pi/9 = 0.7$ of the reference signal $z_d(t)$.

Table 5.1: Human Control Model Parameter

m = 2					
	d	5	10	15	18
Mixed Model	$\hat{m}$	2.01	2.38	2.33	2.49
	$\hat{d}$	4.95	10.10	14.93	17.86
	α	4.72	8.52	14.72	17.89
	β	-4.02	-1.02	-4.84	-3.87
Feedforward	$\hat{m}$	1.98	1.60	1.69	1.19
	$\hat{d}$	5.08	9.79	15.31	18.16
Feedback	α	5.39	5.04	17.77	18.26
	β	-6.70	-1.46	-15.64	-25.46
m = 5					
	d	5	10	15	18
Mixed Model	$\hat{m}$	5.05	5.51	5.37	5.46
	$\hat{d}$	4.62	10.13	14.85	18.00
	α	3.95	7.20	14.19	16.69
	β	-7.81	-7.58	-7.21	-6.54
Feedforward	$\hat{m}$	4.81	5.01	4.28	4.15
	$\hat{d}$	5.19	10.44	15.44	18.57
Feedback	α	1.64	4.22	13.58	16.71
	β	-15.16	-17.82	-26.08	.25.23

Another set of experiments were first conducted to validate the obtained human control models. In particular, for each system parameter value of (m, d), the following four experiments were conducted with the common $z_d(t)$ in (5.5), where $u = 0$ in system (2.1):

- A human applies v to system (2.1).
- The mixed model controller (5.1) applies v to system (2.1).
- The feedforward controller (5.3) applies v to system (2.1).

- The feedback controller (5.4) applies v to system (2.1).

Then during each experiment, $z(t)$, $z_d(t)$, and $v(t)$ are measured and the data of $z(t)$ are used to compute the correlations r_m, r_{ff}, and r_{fb}. The results of the correlation analysis are summarized in Tables 5.2 and 5.3. In the tables, $*$ indicates that the controller failed to stabilize the system and the resulting correlations were negative. For the results in Table 5.2, the initial condition was set to $z(0) = \dot{z}(0) = 0$ which matches with the initial value of the desired oscillation $z_d(0) = \dot{z}_d(0) = 0$, while for Table 5.3, the initial condition was $z(0) = \pi/4$ and $\dot{z}(0) = 0$, which is away from the initial value of the desired oscillation $z_d(t)$.

Table 5.2: Model Validation: $z(0) = z_d(0)$

	m = 2			
d	5	10	15	18
r_m	0.8411	0.9457	0.8067	0.6328
r_{ff}	0.9473	0.9659	0.9685	0.9740
r_{fb}	$*$	-0.8317	$*$	$*$
	m = 5			
d	5	10	15	18
r_m	0.9498	0.9728	0.9150	0.9011
r_{ff}	0.7412	0.8683	0.9717	0.9383
r_{fb}	0.9476	0.9291	0.5990	0.8466

Table 5.3: Model Validation: $z(0) \neq z_d(0)$

	m = 2			
d	5	10	15	18
r_m	0.8476	0.9496	0.8887	0.9374
r_{ff}	0.8448	0.7204	0.7065	0.6846
r_{fb}	0.6383	-0.7845	0.4260	0.4497
	m = 5			
d	5	10	15	18
r_m	0.9292	0.9886	0.9384	0.9446
r_{ff}	0.9701	0.8659	0.7653	0.7489
r_{fb}	0.958	0.9148	0.8259	0.8298

In general, the mixed human motor control model (5.1) shows good correlation. In cases where the initial state is aligned with the desired trajectory z_d (Table 5.2), the feedforward control model (5.3) achieves high correlations. However, in cases where the initial state differs from the desired trajectory (Table 5.3), the feedforward control model (5.3) exhibits lower correlations than those of the mixed control model (5.1). Regardless of the initial conditions, the feedback control model gives the worst performance. Thus, feedforward action seems essential in the human motor control, while feedback action would also be included for corrective behavior.

5.3 2-DOF Human Motor Control Modeling

The 2-DOF experiment process is similar to the single-DOF case. A human subject is asked to hold the handle locates at the end-tip of the robotic arm. The actual position of the end-tip is shown on the screen as a blue circle. The reference position of the end-tip is also shown on the screen as a red star. On the screen, the red star moves along a predefined orbit. The reference position is recorded as z_d, based on which the reference robotic arm joint angles are obtained via inverse kinematic transformation. The human subject moves the robotic arm end-tip to control the blue circle on the screen, while trying to match the blue circle and red star. The actual position is recorded as z, and the actual joint angles are obtained as well via inverse kinematics. The force sensor measures the force applied by the human in both horizontal and perpendicular directions. The 2-DOF virtual mechanical impedance system control scheme is implemented into the system.

5.3.1 Frame and Approach

Let us first derive the inverse kinematics of the robotic arm, so that based on which we can find out the joint angles according to an end-tip position. As shown in Fig. 5.2, the end-tip position is (x, y) and the joints angles to be determined are θ_1 and θ_2. The following calculation can solve this problem.

$$
\begin{aligned}
l &= \sqrt{x^2 + y^2} \\
\gamma &= \arccos \frac{l^2 + l_1^2 - l_2^2}{2 l_1 l} \\
\theta_1 &= arcan \frac{y}{x} - \gamma \\
\theta_2 &= arctan \frac{y - l_1 \sin \theta_1}{x - l_1 \cos \theta_1}
\end{aligned}
$$

We should also be interested in what the joint angular velocities are, with respect to the

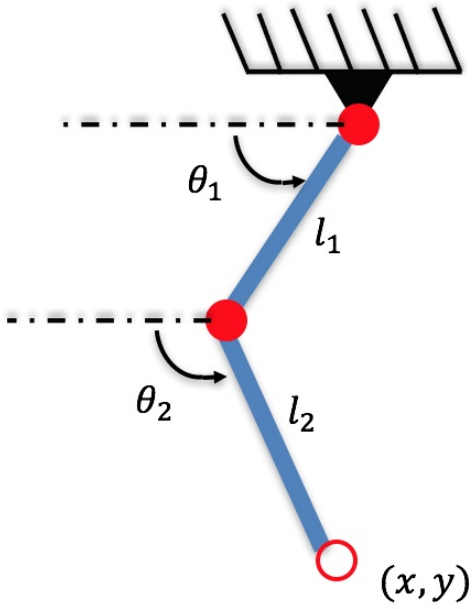

Figure 5.2: 2-DOF inverse kinematics

end-tip moving velocity $(\dot{x}, \dot{y})$. Based on the relation

$$\begin{bmatrix} x \\ y \end{bmatrix} = \begin{bmatrix} l_1 \cos\theta_1 + l_2 \cos\theta_2 \\ l_1 \sin\theta_1 + l_2 \cos\theta_2 \end{bmatrix},$$

we can further take derivation to obtain

$$\begin{bmatrix} \dot{x} \\ \dot{y} \end{bmatrix} = \begin{bmatrix} -l_1 \sin\theta_1 & -l_2 \sin\theta_2 \\ l1 \cos\theta_1 & l_2 \cos\theta_2 \end{bmatrix} \begin{bmatrix} \dot{\theta}_1 \\ dot\theta_2 \end{bmatrix}$$

Suppose we have the information of (x, y) and $(\dot{x}, \dot{y})$ and (θ_1, θ_2) has been obtained via the previous calculation. The $(\dot{\theta}_1, \dot{\theta}_2)$ can be concluded as

$$\begin{bmatrix} \dot{\theta}_1 \\ \dot{\theta}_2 \end{bmatrix} = \begin{bmatrix} -l_1 \sin\theta_1 & -l_2 \sin\theta_2 \\ l1 \cos\theta_1 & l_2 \cos\theta_2 \end{bmatrix}^{-1} \begin{bmatrix} \dot{x} \\ \dot{y} \end{bmatrix}$$

assuming the matrix

$$\begin{bmatrix} -l_1 \sin\theta_1 & -l_2 \sin\theta_2 \\ l1 \cos\theta_1 & l_2 \cos\theta_2 \end{bmatrix}$$

is invertible.

In addition, we can keep taking derivatives to obtain a relation

$$\begin{bmatrix} \ddot{x} \\ \ddot{y} \end{bmatrix} = -l_1 \begin{bmatrix} \cos\theta_1\dot{\theta}_1^2 + \sin\theta_1\ddot{\theta}_1 \\ -\sin\theta_1\dot{\theta}_1^2 + \cos\theta_1\ddot{\theta}_1 \end{bmatrix} + l_2 \begin{bmatrix} \cos\theta_2\dot{\theta}_2^2 + \sin\theta_2\ddot{\theta}_2 \\ -\sin\theta_2\dot{\theta}_2^2 + \cos\theta_2\ddot{\theta}_2 \end{bmatrix}.$$

Hence, given (x, y), $(\dot{x}, \dot{y})$ and $(\ddot{x}, \ddot{y})$, suppose (θ_1, θ_2) and $(\dot{\theta}_1, \dot{\theta}_2)$ have been calculated, then we we further find out $(\ddot{\theta}_1, \ddot{\theta}_2)$ as follows

$$\begin{bmatrix} \ddot{\theta}_1 \\ \ddot{\theta}_2 \end{bmatrix} = \begin{bmatrix} -l_1\sin\theta_1 & -l_2\sin\theta_2 \\ l1\cos\theta_1 & l_2\cos\theta_2 \end{bmatrix}^{-1} \Big(\begin{bmatrix} \ddot{x} \\ \ddot{y} \end{bmatrix} + \begin{bmatrix} l_1\cos\theta_1 & -l_2\cos\theta_2 \\ -l_1\sin\theta_1 & l_2\sin\theta_2 \end{bmatrix} \begin{bmatrix} \dot{\theta}_1^2 \\ \dot{\theta}_2^2 \end{bmatrix} \Big).$$

The human subject watches the computer screen for actual robotic arm end tip position and the desired position and moves the robotic arm end tip. The time history of desired and actual positions z_d, z, velocities $\dot{z}_d$, $\dot{z}$ and accelerations$\ddot{z}_d$, $\ddot{z}$ are recorded and transferred to $(\ddot{\theta}_d, \dot{\theta}_d, \theta_d)$ and $(\ddot{\theta}, \dot{\theta}, \theta)$. Again the proposed human motor control is composed of feedforward and feedback parts, such as

$$\mathcal{B}f(t) = \mathcal{J}\ddot{\theta}_d + \mathcal{D}\dot{\theta}_d^2 + D\dot{\theta}_d + K_\alpha(\dot{\theta} - \dot{\theta}_d) + K_\beta(\theta - \theta_d).$$

During the experiments, the time histories of the variables $\theta(t)$, $\dot{\theta}(t)$ and $f(t)$ are collected at time instants $t = t_i$ for $i = 1, ..., n$ where n is the number of data points collected. The feedback coefficients K_α and K_β are found through a least square optimization problem:

$$\min_x ||b - Ax|| \tag{5.6}$$

where

$$
\begin{aligned}
b &= \mathrm{col}(b_1, b_2, ..., b_n) \\
b_i &= \mathcal{B}f(t_i) - \mathcal{J}\ddot{\theta}(t_i) - \mathcal{D}\dot{\theta}(t_i)^2 - D\dot{\theta}(t_i) \\
f(t_i) &= \mathrm{col}(f_x(t_i), f_y(t_i)) \\
A &= (col)(A_1, A_2, ..., A_3) \\
A_i &= [A_{il},\ A_{ir}] \\
A_{il} &= \begin{bmatrix} \dot{\theta}_1(t_i) - \dot{\theta}_{1d}(t_i) & \dot{\theta}_2(t_i) - \dot{\theta}_{2d}(t_i) & 0 \\ 0 & \dot{\theta}_1(t_i) - \dot{\theta}_{1d}(t_i) & \dot{\theta}_2(t_i) - \dot{\theta}_{2d}(t_i) \end{bmatrix} \\
A_{ir} &= \begin{bmatrix} \theta_1(t_i) - \theta_{1d}(t_i) & \theta_2(t_i) - \theta_{2d}(t_i) & 0 \\ 0 & \theta_1(t_i) - \theta_{1d}(t_i) & \theta_2(t_i) - \theta_{2d}(t_i) \end{bmatrix}.
\end{aligned}
$$

The feedback coefficients can be re-constructed from x as

$$
K_\alpha = \begin{bmatrix} x_1 & x_2 \\ x_2 & x_3 \end{bmatrix}, \quad K_\beta = \begin{bmatrix} x_4 & x_5 \\ x_5 & x_6 \end{bmatrix}.
$$

Note here, $\mathcal{J}, \mathcal{D}, D$ are all nonlinear matrices with respect to θ_1, θ_2, thus they cannot be identified by a least square problem. In the analysis, I would mainly focus on the feedback part and assume the human is able to generate the perfect feedforward signal.

5.3.2 Result and Discussion

The shape of the desired trajectory is a circle with radius $r = 0.1$m. The reference point travels on this orbit at a constant speed with a period of $T = 10$s. The results of the identifications of K_α and K_β are shown in Table 5.4. It can be seen that K_α are all positive definite while K_β are all negative position.

Table 5.4: 2-DOF Human Motor Control Feedback Coefficients

damping μ	10	20	30
K_α	$\begin{bmatrix} 2.36 & -0.79 \\ -0.79 & 3.28 \end{bmatrix}$	$\begin{bmatrix} 2.56 & -0.89 \\ -0.89 & 4.44 \end{bmatrix}$	$\begin{bmatrix} 3.06 & -1.21 \\ -1.21 & 5.42 \end{bmatrix}$
K_β	$\begin{bmatrix} -2.20 & 0.032 \\ 0.032 & -2.10 \end{bmatrix}$	$\begin{bmatrix} -2.70 & -0.050 \\ -0.050 & -2.53 \end{bmatrix}$	$\begin{bmatrix} -3.15 & -0.18 \\ -0.18 & -2.86 \end{bmatrix}$
damping μ	40	50	
K_α	$\begin{bmatrix} 3.50 & -1.56 \\ -1.56 & 5.82 \end{bmatrix}$	$\begin{bmatrix} 3.84 & -1.62 \\ -1.62 & 7.12 \end{bmatrix}$	
K_β	$\begin{bmatrix} -3.53 & -0.23 \\ -0.23 & 3.29 \end{bmatrix}$	$\begin{bmatrix} -4.05 & -0.42 \\ -0.42 & -3.51 \end{bmatrix}$	

The nonlinear nature of the model complicates the analysis, but linearization of system (4.8) around a reference point can be done to obtain a linear system has the mass-spring-damping form

$$\mathbf{M}\ddot{\theta} + \mathbf{D}\dot{\theta} + \mathbf{K}\theta = \mathcal{B}f(t).$$

Then we can verify the values of

$$\mathbf{D} - K_\alpha \quad \text{and} \quad \mathbf{K} - K_\beta.$$

In this case, $\mathbf{K} = 0$, so $\mathbf{K} - K_\beta > 0$ all the time, this confirms parts of the stability condition when using RIO control. However, calculations indicate that $\mathbf{D} - K_\alpha$ is not guaranteed to be positive definite, which is desired by stability condition. The problem could be caused by the accuracy of linearization to represent the nonlinear system. In other words, here I choose the center of the orbit as the reference point to conduct linearization and the radius of the orbit may be not small enough, so that the linear system cannot describe the original nonlinear system behavior. Another cause may be the assumption that human has already been able to generate the perfect feedforward signal.

An alternative way of conduct 2-DOF system and build a 2-DOF reference model is shown

in Fig. 5.3. The force applied by the human can be measured as f_x and f_y. According to the initial position, the software can generate a set of velocity signal as $\dot{x}_r$ and $\dot{y}_r$. This set of reference velocity can be assigned to the end-tip of the 2-DOF robotic system via inverse kinematics and high gain PI control. Such that, when a human holds the handle and tries movement, he/she feels the behavior of the 2-DOF system as shown in Fig. 5.3.

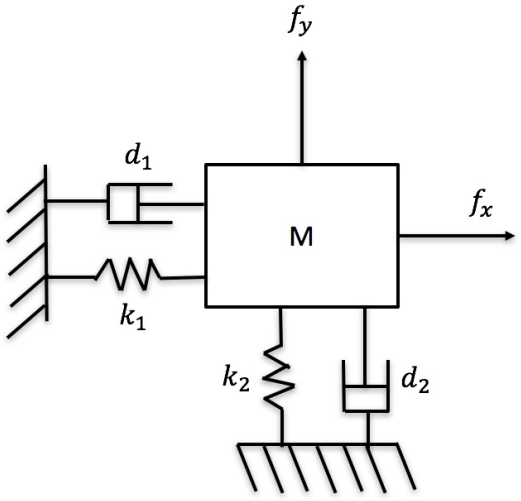

Figure 5.3: Alternative 2-DOF reference model

This reference model is much simpler and more close to the theoretical development environment that we described when analyzing the closed-loop system. Probably this linear system should be studied first before proceeding to the nonlinear model. I expect with this pure linear model, the stability condition will be satisfied. And the previous path from linear single-DOF system directly to nonlinear 2-DOF system could be a too big step.

5.4 Discussion

A combined feedforward and feedback human motor control model is proposed previously for the purpose of RIO assistive control design. The motor control model is of independent interest for understanding how a human controls his/her motion, and for developing devices that interact with humans. The experiments and analysis proceed from single-DOF

system to 2-DOF system and the virtual mechanical impedance system control schemes are exploited respectively. For the single-DOF case, the model parameters were identified using experimental measurements of human generated torque, robotic arm position (angle), and its reference command. The model was validated by a separate set of experimental data, obtained under multiple initial conditions. It was found that the feedforward action is important for human motor control, but the feedback action is also used to cancel the damping effect and set the natural frequency slightly above the operating frequency. The results show that the proposed human control model is able to capture necessary information of human motor control behaviour. The identified model parameter values confirmed that the RIO controller can be designed to satisfy the stability condition.

For the multi-DOF case, the inverse kinematics is first derived to transfer end-tip position, velocity and acceleration to joints angles, angular velocities and accelerations. However, the nonlinear nature of the plant system causes much difficulty and only the feedback coefficients can be identified by solving a least-square problem. An alternative reference model that can be programmed into the software is proposed to eliminate any nonlinearity and the situation will be much closer to an ideally theoretical test environment. It is expect that with such linear 2-DOF model, the results will be encounter the single-DOF results. Afterwards, the nonlinear model can be studied again.

CHAPTER 6

Assistive Robotic Arm

6.1 Overview

In this chapter, we validate the proposed control strategy using the prototyped robotic arm to assist human to perform oscillatory movement tasks within the horizontal plane. This experiment is repeated with and without an assistive CPG-based controller. The controller is designed to drive the arm through the servo motor so that the human effort is reduced while achieving the same or better tracking performance. The controller uses only the encoder measurement of the robot arm angle as sensory feedback, and the force sensor measurement is used only for evaluation of the human effort. The controller is deemed effective if the human effort is smaller with the controller than without it, while achieving the same or better tracking performance. The experiments are conducted under two loading conditions: a virtual load that electronically emulates a mass-damper system, and a physical load to stir high viscosity fluid by an effector attached at the arm end. As usual, the process starts with single-DOF and then expands to 2-DOF system. This chapter is organized as follows. Starting with a single-DOF system, in section 6.2, the control problem is formulated and the controller parameters are chosen. In section 6.3, the experiment is conducted with a virtual load set by the computer, while the arm tries to help human subject with an oscillatory movement. In section 6.4, a physical load is attached to the system. Extension to 2-DOF system experiments and analysis is discussed in section 6.5.

6.2 Problem formulation and approach

Now that the human motor control model is verified, we design an assistive CPG controller for the robotic arm and experimentally validate its performance. The controller should drive the robotic arm to provide assistance when human tries to maintain a rhythmic movement of the robotic arm. That is, with the CPG control, the human should be able to maintain the same oscillation with less effort than required without the CPG control.

The robotic arm system can be approximately described by (2.1) where $v(t)$ is the toque applied by the human and $u(t)$ is the toque applied by the assistive controller. The RIO controller parameters were designed based on the steps in Section 2.4 and the desired damping compensation was set to be $\delta = 10$. As a result, the parameters were selected as

$$h = 0.1, \quad \mu = 1.001, \quad \omega_0 = 10, \quad g = 225.$$

A human subject is asked to perform the same task as described in Section 6.3, under various loading conditions with and without the assistive control. The human applied torques were recorded and compared to evaluate the effort reduction. The actual trajectory of the end-tip was compared with the desired trajectory to evaluate the performance of the human control. A human would be able to achieve good tracking for a plant with passive dynamics (i.e. without the assistive control), and a similar performance is expected if the assistive CPG control does not add dynamics that are felt as unnatural by the human. Theoretically, our controller is guaranteed to achieve stability of the targeted trajectory, provided the human motor control is of the form (5.1) with $d > \alpha$ and $k > \beta$. We expect that the stability property makes the human feel easy to control the plant.

6.3 Virtual load experiment

As in the case of the human control modeling, the virtual load was set as the mechanical impedance specified by (m, d, k) through the minor feedback in the virtual mechanical impedance system as described in Section 4.4.1. With the RIO control, the system in Fig. 4.9 has an additional outer loop that goes from z (generated by multiplying $1/s$ to $\dot{z}$) through

the RIO to its output u which is added to v before entering the reference model block $M(s)$. The block diagram is shown in Fig. 6.1, where the block labeled by "RIO" denotes the nonlinear mapping from z to u defined by (2.7). Note that v is added to τ, but u does not affect this part since this v is the physical human force directly applied to the arm.

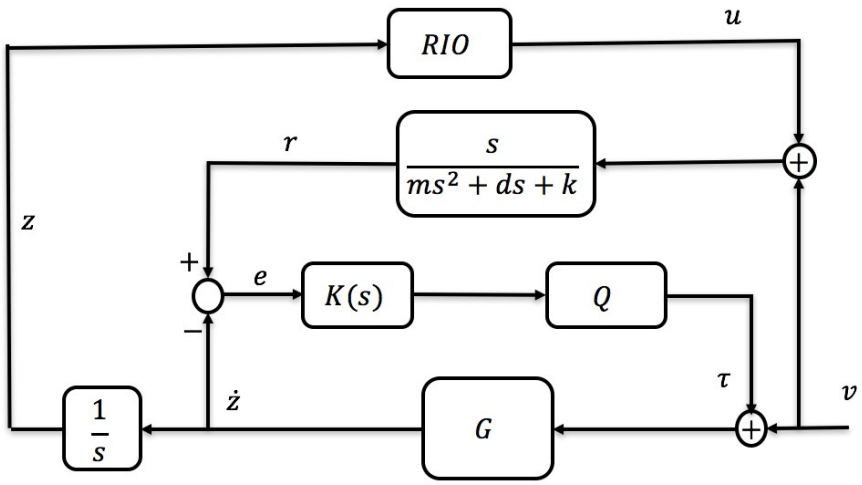

Figure 6.1: Virtual load system with RIO control

We fixed $k = 0$ and varied system parameters m and d to test the assistive effect of the RIO control. The desired oscillation was set as (5.5). The experimental result is shown in Fig. 6.2. The average error defined as

$$\text{average error} = \frac{\sum_{k=1}^{n} \|z(t_k) - z_d(t_k)\|_2^2}{\sum_{k=1}^{n} \|z_d(t_k)\|_2^2}$$

indicates the amount of errors in tracking the reference trajectory $z_d(t)$. The average effort defined as

$$\text{average effort} = \frac{\sum_{k=1}^{n} \|v(t_k)\|_2^2}{n}$$

indicates the amount of human effort in achieving the trajectory tracking. Each dot represents one episode of experiment with running time 60 seconds. The actual collected data points are not evenly distributed in time and thus interpolated into a new sequence with equal time step $t_{k+1} - t_k = 0.1$ second. In this process, the data points during the first and last 1 second are omitted because of the interpolation. Therefore, the number of the resulting sampling points, n, is slightly less than 600.

It can be seen from Fig. 6.2 that the average effort is clearly smaller with the RIO control than without it. The effort reduction is larger when the damping load is larger, but is roughly the same for $m = 2$ and 5 under the same damping load. This is exactly what is expected since the RIO control is designed to compensate for the damping effect. We see that the average error for tracking is larger with heavier mass, but is insensitive to the damping. With the RIO control, the average error tends to be slightly smaller than without it.

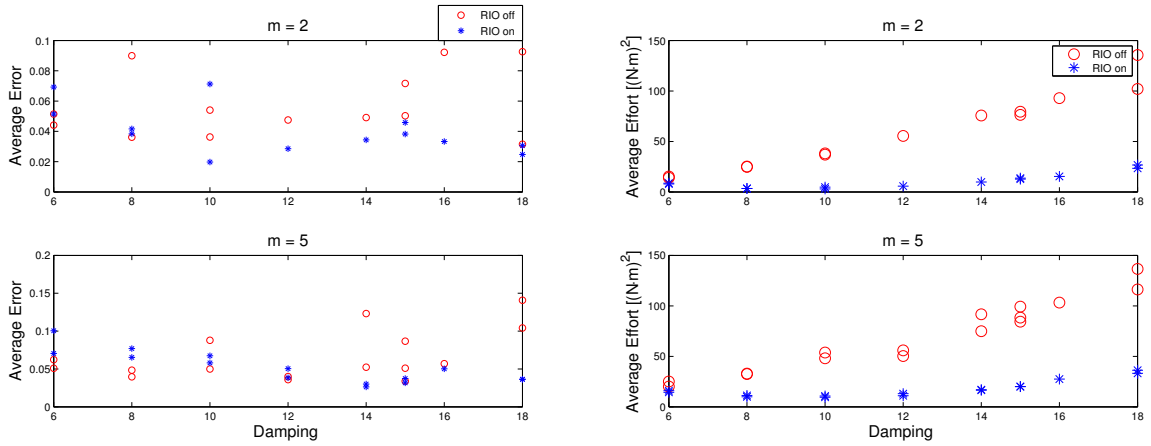

Figure 6.2: Comparisons of human effort and tracking error

6.4 Physical load experiment

In the previous section, the mechanical impedance of the plant was set by minor feedback with high gain PID control, using the electrical signal of human torque measurement as the input to the system. Here, we consider combining the virtual mechanical impedance with a physical load to test robustness of the RIO control against complex loading dynamics that are difficult to emulate.

For this experiment, a cylindrical end-tip effector is attached to the end-tip of the robotic arm and is submerged into a mixed viscous fluid, which serves as the physical load of the system. A picture of the system is shown in Fig. 6.3. The fluid is made by adding food thickeners to water, increasing the viscosity and density. Since the intended arm motion is

rather slow (e.g. oscillation period 4 s with peak-to-peak amplitude 23 cm), the resistive hydrodynamic force is expected to dominate over the reactive force or the added mass effect.

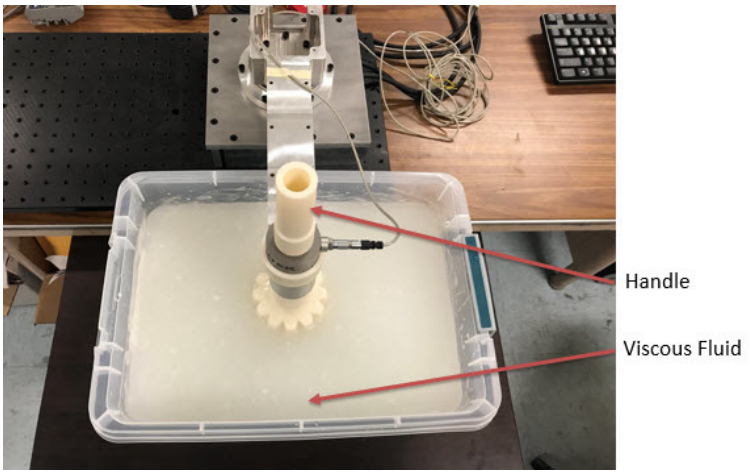

Figure 6.3: Physical Load

When the physical load is attached to the robotic arm, the system is described by the diagram in Fig. 6.4, where G represents the robot-arm mechanical dynamics, D represents the physical load, and the block labeled as "RIO" is the nonlinear mapping of the RIO controller in (2.7) from z to u. We set up the system so that physical human toque v directly acts on the robotic arm, and the human force measurement is used only for monitoring the human effort (not for affecting the servo motor torque). The torque control mode is used for the servo motor, where the output torque τ is (approximately) proportional to the command signal w. The electrical dynamics from w to τ are represented by E in the figure, and is modeled by $E_m(s)$. The control command signal is from the RIO controller, followed by the inverse dynamics $E_m(s)^{-1}$ that approximately cancels E so that $\tau \cong u$.

6.4.1 System Identification

The model of E, G and D are obtained by multiple system identification tests with ARX model described in [31]. We start with identifying the combined EG dynamics, where a chip signal was fed to E while the output of G was measured and recorded. The chirp signal frequency ascended from $2\pi/50$ rad/s to 50 rad/s. The block diagram of this test

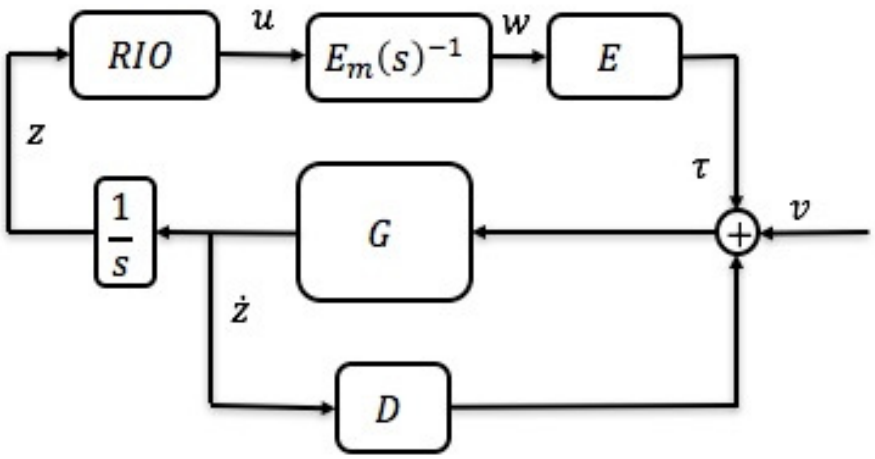

Figure 6.4: Robotic arm driven by human torque v and RIO control u

experiment is shown in Fig. 6.5 and a transfer function model $G_m(s)E_m(s)$ was obtained with the assumption that the transfer function is of 6th order, where

$$G_m(s)E_m(s) = \frac{0.1343s^6 + 11.69s^5 + 911.6s^4 + 2.817e04s^3 + 6.008e05s^2 + 7.332e06s + 3.627e07}{s^6 + 86.17s^5 + 7280s^4 + 2.068e05s^3 + 4.695e06s^2 + 5.39e07s + 2.751e08}. \tag{6.1}$$

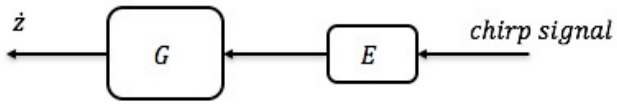

Figure 6.5: Open-loop System Identification

We then close the loop by connecting a controller $L(s) = 0.045$ that took output of G as feedback and generated control signal for E. By manually applying an input torque signal to this system, we rotated the robotic arm and recorded the applied torque $v(t)$ as shown in Fig. 6.7 and output angular velocity $\dot{z}(t)$. The block diagram of this case is shown in Fig. 6.6 and a transfer function model

$$\begin{aligned} H(s) &= \frac{G}{1 - L(s)G_m(s)E_m(s)} \\ &= \frac{0.02217s^6 + 1.306s^5 + 148s^4 + 3883s^3 + 1.331e05s^2 + 2.115e06s + 1.614e07}{s^6 + 65.86s^5 + 6439s^4 + 1.882e05s^3 + 5.285e06s^2 + 5.614e07s + 3.677e08} \end{aligned}$$

is obtained, assuming it is of 6th order.

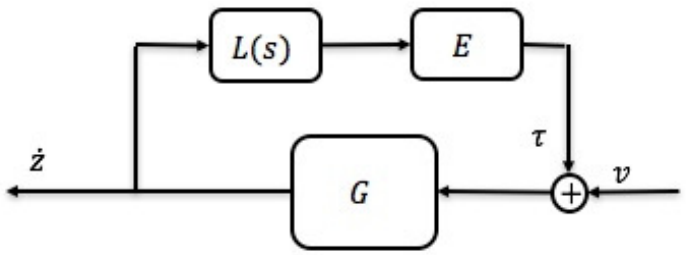

Figure 6.6: Closed-loop System Identification

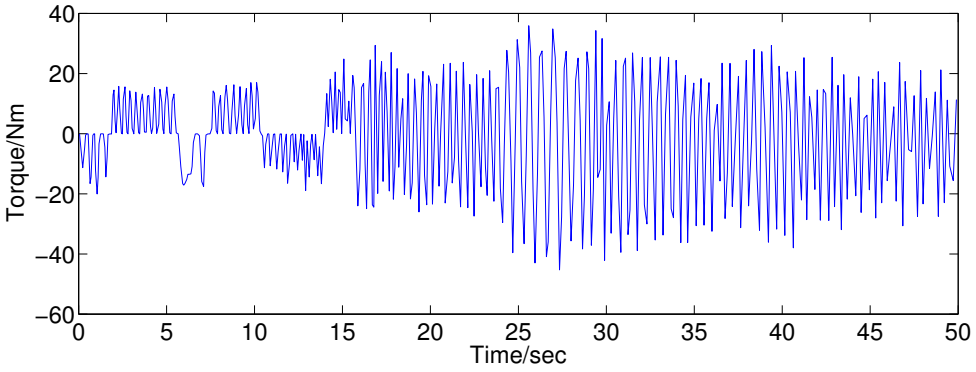

Figure 6.7: Human input torque

We can then compute the transfer function of $E_m(s)$ by

$$E_m(s) = (1 - L(s)E_m(s)G_m(s))H(s),$$

which will be a 12 order transfer function. The first-order approximation is

$$G_m = \frac{0.89}{s + 20}$$

and the comparison between the 12th order transfer function and 1st order transfer function is shown in Fig. 6.8.

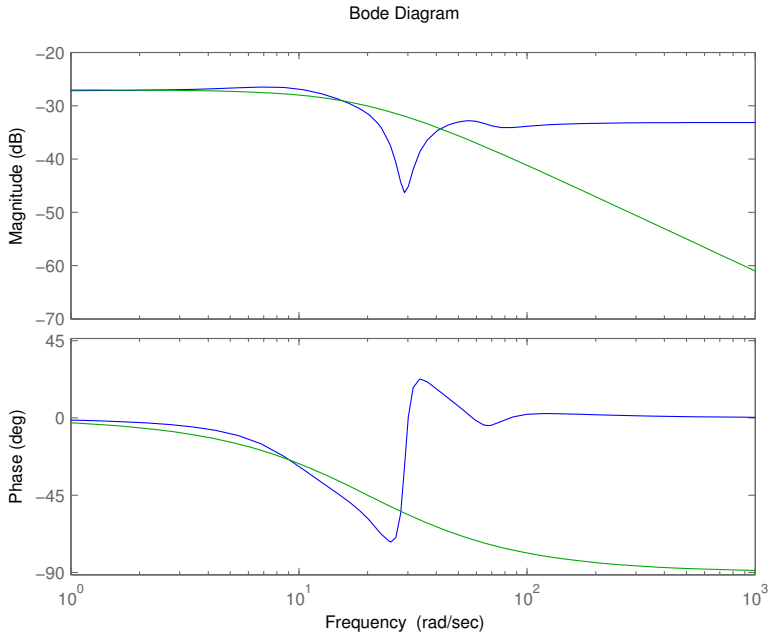

Figure 6.8: Comparison between high order and lower order transfer function of G_m

Then $E_m(s)$ can be calculated by

$$E_m(s) = \frac{E_m(s)G_m(s)}{G_m(s)},$$

and it results in a 18th order transfer function. The bode plot of E_m is shown in Fig. 6.9. At the lower frequency section, E_m can be simplified as a constant value,

$$E_m = 3.125.$$

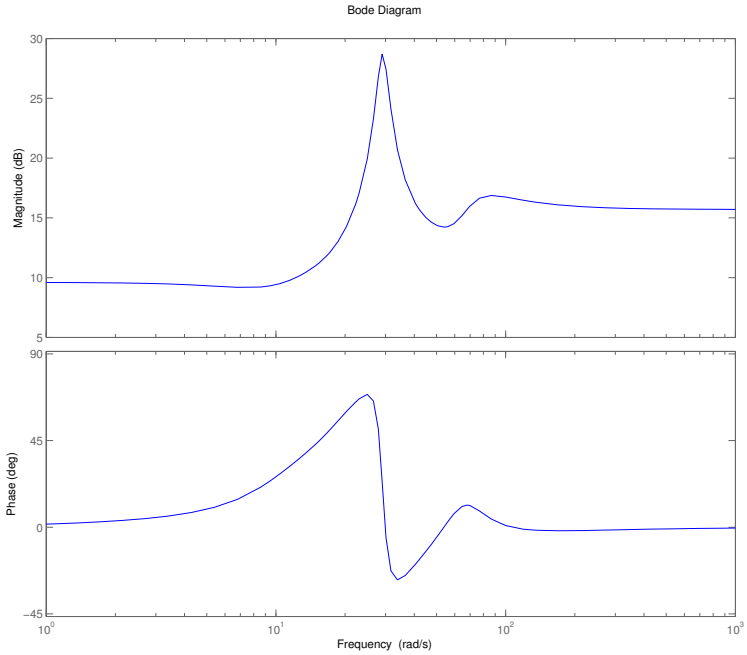

Figure 6.9: Bode plot of $E_m(s)$

Furthermore, we set the inner-loop controller $L(s) = 1$, which should make it more easy for a human to rotate the arm. We repeat the identification process of $H(s)$ with and without attaching the physical load. When the physical loading is attached to the system, the block diagram is shown in Fig. 6.10, where D block represents the physical load. As a result, two more transfer function can be obtained, they are

$$\mathcal{H}_1(s) = \frac{G_m}{1 - LG_mE_m}, \text{with} L(s) = 1; \quad \text{and} \quad \mathcal{H}_2(s) = \frac{\mathcal{H}_1(s)}{1 - \mathcal{H}_1(s)D_m(s)}.$$

Both $\mathcal{H}_1(s)$ and $\mathcal{H}_2(s)$ can be simplified as first order transfer functions that are

$$\mathcal{H}_1(s) = \frac{0.72}{s + 12}, \quad \text{and} \quad \mathcal{H}_2(s) = \frac{0.75}{s + 10}.$$

The comparison between high order transfer functions and simplified low order transfer function are shown in Fig.6.11.

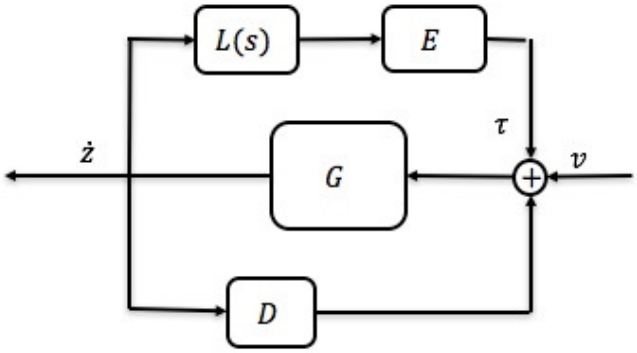

Figure 6.10: Closed-loop System with Physical Load Identification

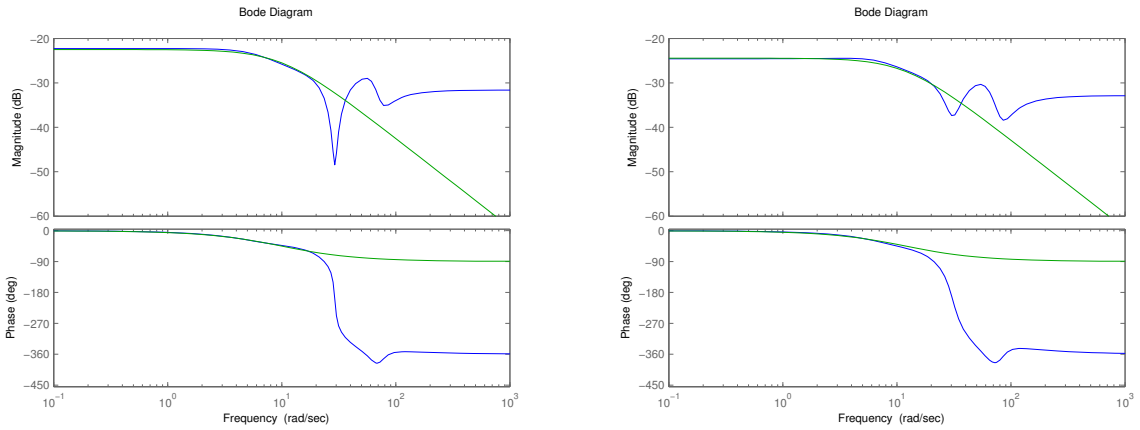

Figure 6.11: Comparison of bode plot $\mathcal{H}_1(s)$(left) and $\mathcal{H}_2(s)$ (right)

Thus the transfer function of $D_m(s)$ could be derived as

$$D_m = \frac{1}{\mathcal{H}_1(s)} - \frac{1}{\mathcal{H}_2(s)} = -(0.00556s + 3.33).$$

6.4.2 Experiment Result

In the experiments, the plant is simply the physical dynamics of the arm-gear-motor system represented by G. The plant may be approximately modeled by (2.1), but there are unmodeled dynamics associated with the viscous load D, gear unit in G, and actuation dynamics E. The RIO controller described in the previous section is tested against these uncertainties.

In the RIO comparison experiment, as before, the human grabs the handle and tries to rotate the robotic arm, with/without the help from RIO controller, to track a desired oscillation, which was given by

$$z_d(t) = \frac{\pi}{8} \sin\left(\frac{\pi}{2}t\right).$$

At this frequency, the damping effect dominates the load; the amplitude of the inertia torque is roughly $m\omega_d^2\alpha_d = 1.1$Nm while that of the damping torque is $d\omega_d\alpha_d = 15.9$ Nm. The RIO control is supposed to reduce the load by $\delta\omega_d\alpha_d = 6.2$ Nm. The experimental measurements are shown in Fig. 6.12. It can be seen that when the RIO control is turned on at $t = 40$s, the human effort is reduced as expected, while the human subject maintains good tracking of the reference trajectory.

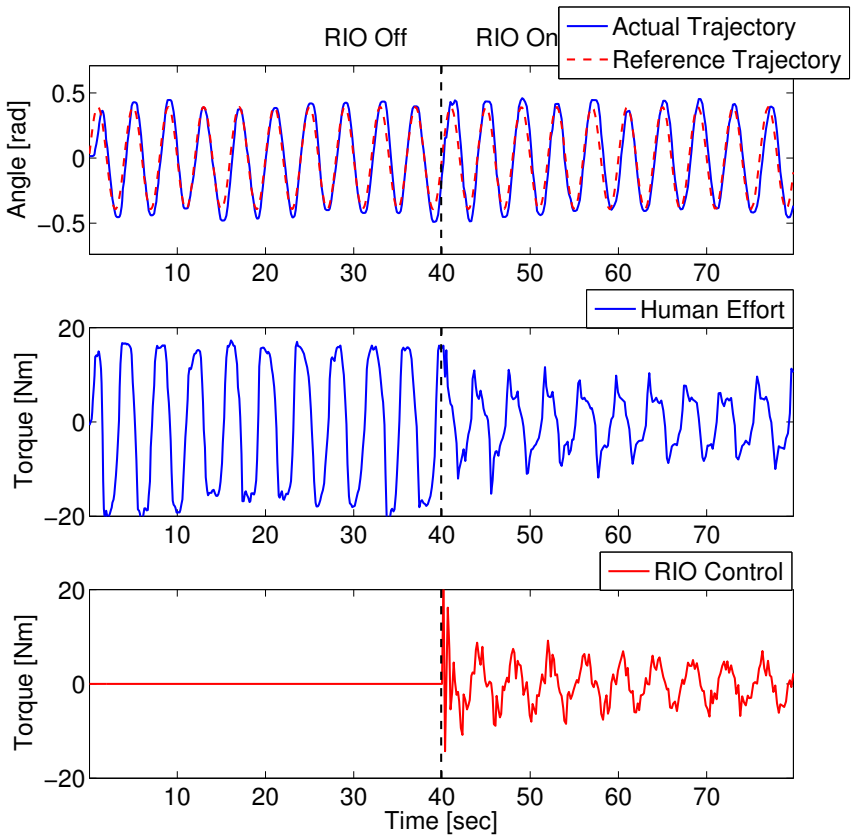

Figure 6.12: Effect of RIO control on human effort reduction

6.5 2-DOF Assistive Control

During this 2-DOF experiment, the human subject looks at the computer screen, which shows the reference and actual position of the robotic arm end-tip. The human is asked to try to match the two points. The implementation of assistive control was first tested with the virtual mechanical impedance system and then with the physical load system.

The 2-DOF assistive control is first implemented with the virtual mechanical impedance system. The control scheme is shown in Fig. 6.13 and this case signals v, τ, e, r, θ, $\dot{\theta}$, e and u are two dimensional. Besides, G represents the four-linkage mechanical system dynamics, Q are the dynamics of the two motors and $K(s)$ is a two-dimensional PI controller. In addition to the 2-DOF virtual mechanical impedance system described in section 4.4.2, an outer loop of 2-D RIO control takes the joint angles θ as feedback signal to generate control input. The 2-dimensional RIO controller is composed of two RIO units. The overall closed loop system can be approximately described as the following equation

$$\mathcal{J}\ddot{\theta} + \mathcal{D}\dot{\theta}^2 + D\dot{\theta} = \mathcal{B}f + u(\theta), \tag{6.2}$$

where $\mathcal{J}, \mathcal{D}, D, \mathcal{B}$ are defined in section 4.4.2 and $u(\theta)$ represents the 2-dimensional RIO controller.

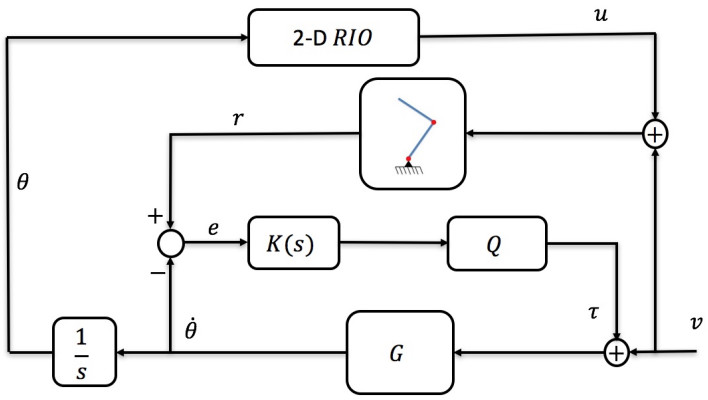

Figure 6.13: 2-DOF Virtual mechanical system with RIO control

Similar to the human motor control model experiment, the nonlinearity of the system causes some difficulties. It is observed that when two RIO units working together, there

exists unexpected oscillatory/shaking movements of the links. It looks like the robotic arm suffers a Parkinson's disease. The undesired shaking disappears when one of the RIO units is switched off. I believe the nonlinear coupling between DOFs actually creates additional communication between the RIO units. In other words, even though each RIO unit is designed independently, they affect each other through the plant system.

An alternative similar to what I proposed in the section 4.4.2 can be exploited here. The simpler 2-DOF reference model can take over to generate reference signal and that case we can test our 2-dimensional RIO control against an ideal environment, which is quite close to the theoretical environment. Afterwards, complexity can be increased gradually and we can revisit the nonlinear system.

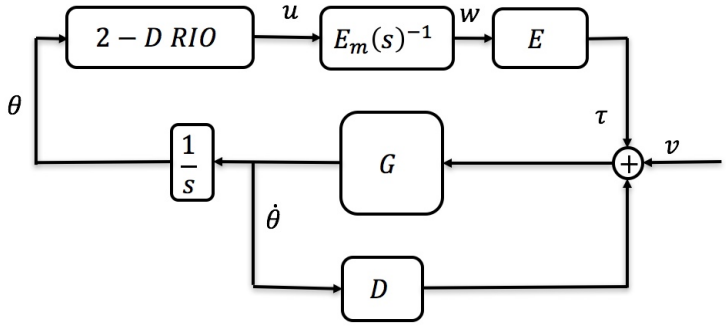

Figure 6.14: 2-DOF Robotic arm driven by human and RIO control

The implementation of 2-dimensional RIO control is also tested against a physical load system. The block diagram is shown in Fig. 6.14. Similarly, signals v, τ, θ, $\dot{\theta}$ and u are two dimensional. Besides, G represents the four-linkage mechanical system dynamics and D represents the physical load. The 2-dimensional RIO controller is as well composed of two RIO units and each RIO unit is designed solely for the corresponding joint and no coupling is added. During the experiment, initially each RIO unit was tested independently while the other unit remains off. For example, when the RIO unit for shoulder motor is on, the RIO unit for elbow motor remains off. Now, only the upper arm link, which is driven by the shoulder motor, is rotated to see the controller performance and if a human can use less effort to rotate that link. Same procedure is conducted while the elbow RIO is on

while the shoulder RIO is off. In both scenario, a human can use less effort to rotate the corresponding link. The fact confronts the expectation since these scenarios are same as single-DOF experiment. Afterward, both RIO control units are switched on altogether to test the cooperation of two RIO units. The human subject feels certain effort reduction while tracking the reference trajectory. However, the human subject also encounter certain difficulty to control the robotic arm properly. The reason is that the damping reduction for each joint in uneven and so as the remaining damping of each joint. To solve such problem, an explicit way is more careful tuning of the RIO controllers. Meanwhile, it could also be helpful to study, besides reducing the system damping, what robotic arm behavior can not only reduce human effort and make the human feel comfortable.

6.6 Discussion

The RIO assistive controller is implemented and experiments are conducted to test its performance. For the single-DOF case, an RIO assistive controller was designed using the theoretical result, and the assistive performance of the control system was tested experimentally. The controller was tested under two conditions - virtual load with various mechanical impedance values set by a minor feedback, and physical load of viscous fluid with uncertain and complex dynamics. The arm-gear-motor system with virtual/physical loads were driven by the RIO controller and human force inputs. Numerous experiments were conducted to verify that, under both loading conditions, the RIO control was capable of reducing the human effort without degrading the tracking performance of the human to follow an oscillatory reference movement.

The experiment process is later extended to a 2-DOF system. The 2-dimensional RIO controller was again tested under two conditions-virtual mechanical impedance system and physical load system. In the case of virtual mechanical impedance system, the robotic arm experiences an unexpected Parkinson's disease-like shaking, caused by the nonlinear coupling of the virtual mechanical impedance system. A simpler model proposed in section 5.3.2 could help largely simplify the complexity. Thus before the nonlinear model, the test

may need to first conducted under the linear 2-DOF case first. As for the physical load case, certain damping reduction can be observed but the human subject feels uncomfortable or difficult to operate the robotic arm. To address such problem or improve the controller performance, further study about how to collaborate robotic arm joint movements to help human feel comfortable, could be quite beneficial. Reducing the system damping may reduce the human effort, but it could be not enough to produce a secure feeling for human.

CHAPTER 7

Conclusion

This research project aims to establish a design method of feedback controller for a general robotic system, where the robotic system should be able to interact with a human to stabilize a rhythmic movement and to reduce the burden on the human by providing assistive force/torque. In biology, animal locomotion periodic movements present behaviour of natural oscillation entrainment to the combined body-environment dynamics. And such movements are under control of central pattern generator (CPG). From the perspective of the assistive robotic systems, helping human with oscillatory movements is analogous to entrainment of animal locomotion movements to the natural oscillation. To this end, a mathematical model of RIO was first investigated to act as an assistive controller of a general mechanical system. The nonlinear closed-loop system was approximated to be a quasi-linear system, and the conditions that the RIO controller can provide assistance were derived accordingly. Following this, the nonlinear closed-loop was then linearized around the reference trajectory and the conditions are found to ensure the stability. A single-DOF system was initially studied and the result is then expended to multi-DOF systems with the assumption that the system damping is Rayleigh damping. Several different types of simulations were created to illustrate different properties of the assistive control, such as stability and human effort reduction.

Another related problem emerged during this project, that was, whether the natural oscillation of a mechanical system can be detected and entrained to, adaptively. Solving such problem not only provides an assistive control design method but should also contribute to robotic locomotion control with compliant mechanism. The answer to the problem was positive. A mathematical model of a type of coupled oscillator, Andronov-Hopf oscillator

was exploited as the main component and additional adaptation mechanism was combined with it. It was successfully proven that, when this appended controller was connected into the control loop, the natural oscillation would be part of the locally stable limit cycle. As before, the single-DOF system was considered to begin with and the result was then modified and expended to multi-DOF systems. Likewise, simulations were generated to show the performance of the controller as well as to investigate the region of attraction.

With the purpose of examining the controller performance in real world, a four-linkage structured robotic arm with two-DOF in horizontal plain, was designed and prototyped for experimental use. Before implementation of the assistive controller, the attention was first paid to the human motor control mechanism. Besides designing control strategy, understanding how human chooses the motor control command would provide a guidance for helping impaired patients to regain certain motor capability, as well as for designing assistive and rehabilitation devices. To explain the visual guided reaching movement mechanism, a hybrid model composed of feedforward and feedback parts was proposed. The control model parameters are identified by fitting the model with the measured human input data, and solving a least-square problem. Afterwards, validation of the proposed model was through comparison experiments. Those experiments were made to exhibit how close the robotic arm behaviours were, between situations when under human operation and when under proposed model control.

Assistive RIO controller was designed according to the proposed design method and the testing was performed under two conditions - virtual load with various mechanical impedance values set by a minor feedback, and physical load of viscous fluid with uncertain and complex dynamics. The arm-gear-motor system with virtual/physical loads were driven by the RIO controller and human force inputs. Numerous experiments were conducted to verify that, under both loading conditions, the RIO control was capable of reducing the human effort without degrading the tracking performance of the human to follow an oscillatory reference movement.

Further development of such research result could proceed in different directions. An direct related and interesting topic could be adaptive/learning network system, that satisfies

human intention. Current result in this research presents an adaptive controller with network format, that can comply with human intention and entrain to the human desired oscillation. This result could be the foundation of studying how a network system could adjust itself to provide desired assistance, satisfying human intention. One application could be in the field of power system. In future development of microgrid or smartgrid, engineers will confront a network system and human intended power request, which will fall in this category. Another exciting application area could be the future autonomous driving vehicles network. Those self-driving vehicles will as well form a network system and all the transportation requests are human intended.

APPENDIX A

ARX model and System Identification

To identify the system models of E, G and P, the ARX model system identification method is exploited and here we review the basic concepts of ARX.

The ARX model can be described as

$$y(t) + \sum_{k=1}^{N} A_k y(t - k\tau) = \sum_{k=0}^{N} B_k u(t - k\tau), \tag{A.1}$$

where N is the order of the system and τ is sampling time. Besides, the linear system (A, B, C, D) can be constructed by

$$A = \begin{bmatrix} -\mathcal{A} & \Sigma \end{bmatrix}, \quad B = \mathcal{B} - \mathcal{A}B_0, \quad C = \begin{bmatrix} I & 0 \end{bmatrix}, \quad D = B_0,$$

where

$$\mathcal{A} = \mathrm{col}(A_1, A_2, ...A_N), \quad \Sigma = \begin{bmatrix} I \\ 0 \end{bmatrix}, \quad \mathcal{B} = \mathrm{col}(B_1, B_2, ...B_N).$$

The discrete-time state space system expression is

$$x(t + \tau) = Ax(t) + Bu(t), \quad y(t) = Cx(t) + Du(t).$$

With a measurements of inputs $u(t_1), u(t_2), ..., u(t_n)$ and outputs $y(t_1), y(t_2), ..., y(t_n)$, as well as sampling time τ, we can formulate a lease-square problem to identify A_i and B_i. Suppose the system is in Nth order,

$$\min_{\mathcal{A},\mathcal{B}} \| Y + \begin{bmatrix} \mathcal{Y} & -\mathcal{U} \end{bmatrix} \begin{bmatrix} \mathcal{A} \\ \mathcal{B} \end{bmatrix} \|$$

where

$$Y = \text{col}(y(t_n), y(t+n-1), ..., y(t_{N+1}))$$

$$\mathcal{Y} = \begin{bmatrix} y(t_{n-1}) & y(t_{n-2}) & ... & y(t_{n-N}) \\ y(t_{n-2}) & y(t_{n-3}) & ... & y(t_{n-1-N}) \\ \vdots & \vdots & \vdots & \vdots \\ y(t_N) & y(t_{N-1}) & ... & y(t_1) \end{bmatrix}$$

$$\mathcal{U} = \begin{bmatrix} u(t_n) & u(t_{n-1}) & ... & u(t_{n-N}) \\ u(t_{n-1}) & u(t_{n-2}) & ... & u(t_{n-1-N}) \\ \vdots & \vdots & \vdots & \vdots \\ u(t_{N+1}) & u(t_N) & ... & u(t_1) \end{bmatrix}.$$

APPENDIX B

Technical Results

Lemma 2. *Consider the linear system*

$$\dot{x} = Ax + Bu, \qquad y = Cx,$$

which may or may not be stable. Let $T > 0$ be given and suppose A has no eigenvalue at $\pm j\omega k$ for any integer k, where $\omega := 2\pi/T$. Then, for an arbitrary T-periodic input $u(t)$, there exists an initial state $x(0)$ that yields T-periodic state $x(t)$ and output $y(t)$. In particular, the T-periodic solution is uniquely given by

$$y(t) = \int_0^T H(\tau)u(\tau + t)d\tau, \quad H(\tau) := C(I - e^{AT})^{-1}e^{A(T-\tau)}B$$

Moreover, the peak values of the input and output are related by

$$||y||_\infty \leq c||u||_\infty, \quad c := \int_0^T ||H(t)||dt.$$

Proof. The general solution is given by

$$x(t) = e^{At}x(0) + \int_0^t e^{A(t-\tau)}Bu(\tau)d\tau.$$

The solution is T-periodic, $x(t) = x(t + T)$, when

$$x(0) = e^{AT}x(0) + \int_0^T e^{A(T-\tau)}Bu(\tau)d\tau,$$

which can be solved for

$$x(0) = (I - e^{AT})^{-1} \int_0^T e^{A(t-\tau)}Bu(\tau)d\tau,$$

where we note that e^{AT} has eigenvalues at $e^{\lambda T}$ with λ being an eigenvalue of A, and hence $I - e^{AT}$ is invertible due to the supposition. Substituting the initial state into the general

formula, we have

$$\begin{aligned} x(t) &= e^{At}(I - e^{AT})^{-1} \int_0^T e^{A(T-\tau)} Bu(\tau) d\tau \\ &\quad + \int_0^t e^{A(t-\tau)} Bu(\tau) d\tau \\ &= (I - e^{AT})^{-1} \int_0^T e^{A(T-\sigma)} Bu(\sigma + t - T) d\tau \end{aligned}$$

The formula for $y(t)$ directly follows from this equation. The bound on the peak-to-peak gain can be seen from

$$\begin{aligned} ||y(t)|| &= || \int_0^T H(\tau) u(\tau + t) d\tau || \\ &\leq \int_0^T ||H(\tau)|| \cdot ||u(\tau + t)|| d\tau \\ &\leq \int_0^T ||H(\tau)|| \cdot ||u||_\infty d\tau = c||u||_\infty. \end{aligned}$$

□

Lemma 3. Consider the harmonically forced nonlinear system

$$x = b(s)(\mu\psi(x) + hz), \quad z(t) = a\sin(\omega t) \tag{B.1}$$

where $x(t) \in \mathbb{R}$ is a scalar variable, $b(s)$ is a strictly proper transfer function, $\mu, h, a, \omega \in \mathbb{R}$ are nonzero constants, and $\psi(x) := \tanh(x)$. Suppose $\omega > 0$ and

$$b_\mu(s) := \frac{b(s)}{1 - \mu b(s)}$$

has no poles on the imaginary axis. Then, for sufficiently small $|h|$, there exists a T-periodic solution $x(t)$ in the neighborhood of the origin, where $T := 2\pi/\omega$. Let such solution be denoted by $x_h(t)$ for each h. There exists a constant γ such that

$$\|x_h\|_\infty \leq \gamma |h|.$$

Moreover, we have

$$\lim_{h \to 0} \frac{1}{h} \Big(\psi'(x_h(t)) - \kappa(x_h(t)) \Big) = 0, \quad \forall t \in \mathbb{R}.$$

Proof. We assume that h is positive without loss of generality since the sign of h can be absorbed into a. All the trajectories of the forced nonlinear system with various values of h can be captured by the autonomous nonlinear system

$$x = b(s)(\mu\psi(x) + \xi), \quad \ddot{\xi} + \omega^2\xi = 0. \tag{B.2}$$

The linearization of the system (B.2) around the origin is given by

$$x = b_\mu(s)\xi, \quad \ddot{\xi} + \omega^2\xi = 0. \tag{B.3}$$

By Lemma 2, the linearized system has a harmonic solution $x(t)$ in the neighborhood of the origin with $\xi(t) = hz(t)$ for sufficiently small h, where its peak value approaches zero as h goes to zero. By a version of the Grobman-Hartman result [4], there exists a (time-preserving) homeomorphism between trajectories in the neighborhoods of the origins of the two systems (B.2) and (B.3). Therefore, we infer that the original nonlinear system (B.1) has a T-periodic solution $x_h(t)$ for sufficiently small h, where its peak value α_h approaches zero as h goes to zero.

Now, let $y_h(t) := x_h(t)/\alpha_h$ and note that the system dynamics (B.1) imply

$$y_h = b_\mu(s)v_h, \quad v_h := \mu\phi_h(y_h) + (h/\alpha_h)z,$$
$$\phi_h(x) := \psi(\alpha_h x)/\alpha_h - x$$

Then, by Lemma 2, there exists $c > 0$, independent of h, such that $||y_h||_\infty \le c||v_h||_\infty$. Since $||y_h||_\infty = 1$ by definition, we have $1 \le c||v_h||_\infty$ for sufficiently small $h > 0$. Note that $||\phi_h(y_h)||_\infty$ approaches zero as $h \to 0$ since $||y_h||_\infty = 1$. Hence, if $h/\alpha_h \to 0$ as $h \to 0$, then $||v_h||_\infty \to 0$ as $h \to 0$, violating the condition $1 \le c||v_h||_\infty$. Therefore, h/α_h cannot approach zero and is bounded away from zero, i.e., there exists $\gamma > 0$ such that $h/\alpha_h \ge 1/\gamma$ for all small $h > 0$.

Finally, by the Taylor series expansion,

$$\psi'(x_h) = \psi'(0) + \psi''(0)x_h + O(h^2) = 1 + O(h^2),$$

where we noted that

$$\psi'(0) = 1, \quad \psi''(0) = 0, \quad ||x_h||_\infty = \alpha_h = O(h).$$

It then follows that

$$\frac{1}{h}\Big(\psi'(x_h(t)) - \frac{1}{T}\int_0^T \psi'(x_h(t)dt\Big)$$
$$= \frac{1}{h}\Big(1 + O(h^2) - \frac{1}{T}\int_0^T \big(1 + O(h^2)\big)dt\Big) \to 0$$

as $h \to 0$.

□

Here we provide several lemmas that are used for the developments in this chapter. The notation $\|\cdot\|$ is used to mean the spectral norm for a matrix and the Euclidean norm for a vector, when the argument is constant. If the argument is a function of time, it denotes the supremum norm, i.e.,

$$\|A\| = \sup_{t\geq 0} \|A(t)\|.$$

for a time-varying matrix $A(t)$.

Lemma 4. *Let matrices $A \in \mathbb{R}^{n\times m}$ and $X_1, X_2 \in \mathbb{R}^{m\times n}$ be given. Suppose $\|A\| \leq \alpha$ and $\|X_i\| \leq \beta$ with $i = 1, 2$ for positive scalars $\alpha, \beta \in \mathbb{R}$. Then*

$$\|X_1AX_1 - X_2AX_2\| \leq 4\alpha\beta\|X_1 - X_2\|.$$

Proof:

$$\begin{aligned}
&\|X_1AX_1 - X_2AX_2\| \\
&= \|(X_1 - X_2)AX_2 + X_2A(X_1 - X_2) + (X_1 - X_2)A(X_1 - X_2)\| \\
&\leq \|X_1 - X_2\|\alpha\beta + \alpha\beta\|X_1 - X_2\| + \|X_1 - X_2\|\alpha\|X_1 - X_2\| \\
&\leq 2\alpha\beta\|X_1 - X_2\| + (\|X_1\| + \|X_2\|)\alpha\|X_1 - X_2\| \\
&= 4\alpha\beta\|X_1 - X_2\|.
\end{aligned}$$

■

Lemma 5 (Boundedness)**.** *Let $A_i(t)$, $B_i(t)$, and $C_i(t)$ with $i = 1, 2$ be matrix-valued functions of $t \in \mathbb{R}$ that are continuous and bounded on $t \geq 0$. Suppose the system*

$$\dot{x} = A_1(t)x \tag{B.4}$$

is asymptotically stable. Let $\mathcal{L}_o(t)$ be a solution of (3.7). For each $\varepsilon > 0$, let $\mathcal{L}_\varepsilon(t)$ be the solution to (3.4) with initial condition $\mathcal{L}_\varepsilon(0) = \mathcal{L}_o(0)$. Then, $\mathcal{L}_o(t)$ is bounded and there exists a positive scalar $\bar{\varepsilon} \in \mathbb{R}$ such that, for each $\varepsilon \in (0, \bar{\varepsilon})$, the function $\mathcal{L}_\varepsilon(t)$ is continuously differentiable and bounded on $t \geq 0$.

Proof. Let $\Psi(t, t_0)$ be the state transition matrix of (B.4). Then there exist positive scalers $K, a \in \mathbb{R}$ such that

$$\|\Psi(t, \tau)\| \leq Ke^{-a(t-\tau)} \tag{B.5}$$

due to stability of (B.4), and $\mathcal{L}_o$ can be written as

$$\mathcal{L}_o(t) = \Psi(t, 0)\mathcal{L}_o(0) + \int_0^t \Psi(t, \tau)A_2(\tau)d\tau. \tag{B.6}$$

Note that $\mathcal{L}_o$ is bounded on $t \geq 0$ because

$$\begin{aligned}
\|\mathcal{L}_o(t)\| &\leq \|\Psi(t, 0)\| \cdot \|\mathcal{L}_o(0)\| + \int_0^t \|\Psi(t, \tau)\| \cdot \|A_2(\tau)\|d\tau \\
&\leq Ke^{-at}\|\mathcal{L}_o(0)\| + \int_0^t Ke^{-a(t-\tau)}\|A_2(\tau)\|d\tau \\
&\leq Ke^{-at}\|\mathcal{L}_o(0)\| + \frac{K}{a}(1 - e^{-at})\|A_2\| \\
&\leq K\|\mathcal{L}_o(0)\| + \frac{K}{a}\|A_2\|.
\end{aligned} \tag{B.7}$$

Continuous differentiability of $\mathcal{L}_\varepsilon(t)$ follows from its definition and continuity of the system matrices. To show the boundedness of $\mathcal{L}_\varepsilon(t)$, let us define $\Delta_\varepsilon(t)$ by (3.9). Note that $\Delta_\varepsilon(t)$ is the solution of

$$\dot{\Delta}_\varepsilon(t) = A_1(t)\Delta_\varepsilon(t) + G(t, \mathcal{L}_o(t) + \varepsilon\Delta_\varepsilon(t)) \tag{B.8}$$

with initial condition $\Delta_\varepsilon(0) = 0$, which can be verified by subtracting (3.7) from (3.4) and dividing by ε. This Δ_ε can be seen as a fixed point of mapping M defined by

$$M(Y)(t) = \int_0^t \Psi(t, \tau)G(\tau, \mathcal{L}_o(\tau) + \varepsilon Y(\tau))d\tau.$$

We will show that there exists a constant $c > 0$ such that, when $\varepsilon > 0$ is sufficiently small, M is a contraction mapping on

$$\mathbb{B}_o := \{\ Y \in \mathbb{B} : \|Y\| \leq c\ \}, \tag{B.9}$$

where $\mathbb{B}$ is the Banach space of continuous and bounded matrix-valued functions, defined on $t \in [0, \infty)$, and equipped with the supremum norm. Then Δ_ε is the unique fixed point satisfying

$$\Delta_\varepsilon = M(\Delta_\varepsilon), \quad \Delta_\varepsilon \in \mathbb{B}_o$$

and the boundedness of Δ_ε implies that of $\mathcal{L}_\varepsilon$ from (3.9).

To this end, use (B.5), go through calculations like (B.7), and bound G in (3.5) by the triangle inequality to obtain

$$\|M(Y)\| \leq \rho(\|\mathcal{L}_o + \varepsilon Y\|) \tag{B.10}$$

where ρ is defined by

$$\rho(x) := \frac{K}{a}\Big(\|B_2\| + \big(\|B_1\| + \|C_2\|\big)x + \|C_1\|x^2\Big).$$

Let c be chosen such that $c > \rho(\|\mathcal{L}_o\|)$. Then for sufficiently small $\varepsilon > 0$ and arbitrary $Y \in \mathbb{B}_o$, we have

$$\rho(\|\mathcal{L}_o + \varepsilon Y\|) \leq \rho(\|\mathcal{L}_o\| + \varepsilon c) \leq c$$

where the first inequality holds since $\rho(x)$ is increasing on $x > 0$. Thus, for such small ε, we have $M(Y) \in \mathbb{B}_o$ whenever $Y \in \mathbb{B}_o$. Finally, for $Y_1, Y_2 \in \mathbb{B}_o$, another inequality can be derived with the help of Lemma 4 as

$$\|M(Y_1) - M(Y_2)\| \leq \varepsilon(a + b\varepsilon) \cdot \|Y_1 - Y_2\|,$$

where $a, b \in \mathbb{R}$ are positive constants that depend on the norms of the system matrices and $\mathcal{L}_o$. Hence, for sufficiently small $\varepsilon > 0$, M is a contraction operator on $\mathbb{B}_o$. □

Lemma 6. *Consider the system*

$$\dot{x} = \Big(A(t) + M(t)\Big)x.$$

Suppose the system is exponentially stable when $M(t) \equiv 0$. Then there exists $\varepsilon > 0$ such that the system is exponentially stable for all $M(t)$ such that $\|M\| < \varepsilon$.

Proof. See Theorem 1 on p.205 of [6]. □

Lemma 7. *Consider the system*

$$\dot{x} = A_\varepsilon(t)x, \quad A_\varepsilon(t) := \varepsilon\Big(A(t) + \varepsilon M_\varepsilon(t)\Big) \tag{B.11}$$

with $\varepsilon \in \mathbb{R}$, where $A(t)$ is continuous and T-periodic, and $M_\varepsilon(t)$ is bounded for all $t \geq 0$ and $\varepsilon \in (0, \bar{\varepsilon}_1)$ with a given positive scalar $\bar{\varepsilon}_1$. Suppose the matrix

$$\mathfrak{B} := \int_0^T A(t)dt \tag{B.12}$$

is Hurwitz. Then there exists $\bar{\varepsilon}_2 > 0$ such that system (B.11) *is stable for all $\varepsilon \in (0, \bar{\varepsilon}_2)$.*

Proof. Based on the Peano-Baker series, the state transition matrix of system (B.11) can be written as

$$\Psi(t,\tau) = I + \int_\tau^t A_\varepsilon(\sigma)d\sigma + \sum_{k=1}^{\infty} \Psi_k(t,\tau),$$

$$\Psi_k(t,\tau) := \int_\tau^t A_\varepsilon(\sigma_1) \cdots \int_\tau^{\sigma_k} A_\varepsilon(\sigma_{k+1})d\sigma_{k+1} \cdots d\sigma_1.$$

Setting $t = \tau + T$, we have

$$\Psi(\tau + T, \tau) = I + \varepsilon\mathfrak{B} + \varepsilon^2\mathfrak{C}_\varepsilon(\tau),$$

$$\mathfrak{C}_\varepsilon(\tau) := \frac{1}{\varepsilon^2}\sum_{k=1}^{\infty} \Psi_k(\tau + T, \tau) + \int_\tau^{\tau+T} M_\varepsilon(\sigma_1)d\sigma_1,$$

Let H and P be matrices such that

$$H = P^{1/2}, \quad P = P^\intercal > 0, \quad P\mathfrak{B} + \mathfrak{B}^\intercal P < 0$$

and define

$$\hat{\Psi}(\tau) := H\Psi(\tau + T, \tau)H^{-1}, \quad \hat{\mathfrak{B}} := H\mathfrak{B}H^{-1}.$$

Then we have

$$\hat{\Psi}(\tau)^\intercal\hat{\Psi}(\tau) = I + \varepsilon(\hat{\mathfrak{B}} + \hat{\mathfrak{B}}^\intercal) + \varepsilon^2\mathfrak{D}_\varepsilon(\tau) \tag{B.13}$$

where $\mathfrak{D}_\varepsilon(\tau)$ is a quadratic function of $\mathfrak{B}$ and $\mathfrak{C}_\varepsilon(\tau)$. Now, let $a, m \in \mathbb{R}$ be positive scalars such that

$$\|A_\varepsilon\| \leq a\varepsilon, \quad \|M_\varepsilon\| \leq m, \quad \forall\ \varepsilon \in (0, \bar{\varepsilon}_1),$$

and define $\bar{\varepsilon}_3 := \min(1/(aT), \bar{\varepsilon}_1)$. Then, for $\varepsilon \in (0, \bar{\varepsilon}_3)$,

$$\|\mathfrak{C}_\varepsilon\| \le \frac{1}{\varepsilon^2} \sum_{k=1}^{\infty} (aT\varepsilon)^{k+1} + mT = \frac{(aT)^2}{1 - aT\varepsilon} + mT$$

which implies $\|\mathfrak{D}_\varepsilon\| < d$ for some constant $d \in \mathbb{R}$ independent of ε. Note that the eigenvalues of $\hat{\mathfrak{B}} + \hat{\mathfrak{B}}^\intercal$ are all real negative by construction, and denote the maximum and minimum by $-\lambda_M$ and $-\lambda_m$, respectively. Then, from (B.13),

$$\|\hat{\Psi}\|^2 \le 1 - \varepsilon\lambda_M + \varepsilon^2 d$$

for all $\varepsilon \in (0, \bar{\varepsilon}_4)$ where $\bar{\varepsilon}_4$ is the smaller of $\bar{\varepsilon}_3$ and $1/\lambda_m$. We now see that there exists $\bar{\varepsilon}_2 > 0$ such that $\|\hat{\Psi}\| < 1$ for $\varepsilon \in (0, \bar{\varepsilon}_2)$. Finally, for arbitrary $t_o \ge 0$ and positive integer n, we have

$$\Psi(t_n, t_o) = H^{-1} \left(\prod_{k=1}^{n} \hat{\Psi}(\tau_k) \right) H,$$
$$t_n := t_o + nT, \quad \tau_k := t_o + (k-1)T,$$

and hence $\|\Psi(t_n, t_o)\|$ converges to zero as $n \to \infty$, provided $\varepsilon \in (0, \bar{\varepsilon}_2)$, proving stability of (B.11). □

Lemma 8. *Let $n \times n$ real matrices M and K be given. Suppose $M + M^\intercal > 0$ and $K = K^\intercal \ge 0$. Let $\lambda \in \mathbb{C}$ be a nonzero generalized eigenvalue satisfying*

$$\det(\lambda M + K) = 0.$$

Then the real part of λ is negative.

Proof. Let M be expressed as $M = P + S$ with symmetric P and skew symmetric S. By definition, there exists a nonzero vector $v \in \mathbb{C}^n$ such that

$$\big(\lambda(P + S) + K\big)v = 0.$$

Let

$$p := v^* P v > 0, \quad q := v^* K v \ge 0, \quad j\omega := v^* S v,$$

where we noted that the first two are real positive and nonnegative since $M + M^\intercal$ and K are symmetric positive (semi)definite, and the last term is purely imaginary since S is skew symmetric. Then

$$v^*\big(\lambda(P+S)+K\big)v = \lambda(p+j\omega)+q = 0$$
$$\Rightarrow \quad \lambda = -\frac{q}{p+j\omega} \quad \Rightarrow \quad \Re[\lambda] = -\frac{pq}{p^2+\omega^2} < 0,$$

where q is positive since λ is nonzero. □

REFERENCES

[1] Brian Anderson, Robert R Bitmead, C Richard Johnson Jr, Petar V Kokotovic, Robert L Kosut, Iven MY Mareels, Laurent Praly, and Bradley D Riedle. *Stability of adaptive systems: Passivity and averaging analysis*. MIT press, 1986.

[2] K. Ahlborn B and R.W. Blake. Walking and running at resonance. *Zoology*, 105:165–174, 2002.

[3] K. Ahlborn B, R.W. Blake, and W.M. Megill. Frequency tuning in animal locomotion. *Zoology*, 109:43–53, 2006.

[4] Laurent Baratchart, Monique Chyba, and Jean-Baptiste Pomet. A Grobman-Hartman theorem for control systems. *Journal of Dynamics and Differential Equations*, 19(1):75–107, 2007.

[5] Richard Bellman. *Stability theory of differential equations*. Courier Corporation, 2013.

[6] R.W. Brockett. *Finite Dimensional Linear Systems*. John Wiley & Sons, Inc., 1970.

[7] Jonas Buchli, Fumiya Iida, and Auke J Ijspeert. Finding resonance: Adaptive frequency oscillators for dynamic legged locomotion. In *Intelligent Robots and Systems, 2006 IEEE/RSJ International Conference on*, pages 3903–3909. IEEE, 2006.

[8] G Cheron, M Duvinage, C De Saedeleer, T Castermans, A Bengoetxea, M Petieau, K Seetharaman, T Hoellinger, B Dan, T Dutoit, et al. From spinal central pattern generators to cortical network: integrated bci for walking rehabilitation. *Neural plasticity*, 2012, 2012.

[9] Michel Desmurget and Scott Grafton. Forward modeling allows feedback control for fast reaching movements. *Trends in cognitive sciences*, 4(11):423–431, 2000.

[10] A Earl and NORMAN LEVINSON. *Theory of ordinary differential equations*. McGraw-Hill New York:, 1955.

[11] D. Efimov, A.L. Fradkov, and T. Iwasaki. Exciting multi-DOF systems by feedback resonance. *Automatica*, 49(6):1782–1789, 2013.

[12] J Randall Flanagan, David J Ostry, and Anatol G Feldman. Control of trajectory modifications in target-directed reaching. *Journal of motor behavior*, 25(3):140–152, 1993.

[13] Christian Fleischer and Günter Hommel. Emg-driven human model for orthosis control. In *Human Interaction with Machines*, pages 69–76. Springer, 2006.

[14] A.L. Fradkov. Exploiting nonlinearity by feedback. *Physica D*, 128:159–168, 1999.

[15] Y. Futakata and T. Iwasaki. Formal analysis of resonance entrainment by central pattern generator. *J. Math. Biol.*, 57(2):183–207, 2008.

[16] Y. Futakata and T. Iwasaki. Entrainment to natural oscillations via uncoupled central pattern generators. *IEEE Trans. Auto. Contr.*, 56(5):1075–1089, 2011.

[17] Clément Gosselin, Thierry Laliberté, Boris Mayer-St-Onge, Simon Foucault, Alexandre Lecours, D Gao, and R Menassa. A friendly beast of burden: A human-assistive robot for handling large payloads. *IEEE Robotics & Automation Magazine*, 20(4):139–147, 2013.

[18] Rick Grush. The emulation theory of representation: Motor control, imagery, and perception. *Behavioral and brain sciences*, 27(03):377–396, 2004.

[19] N.G. Hatsopoulos and W.H. Warren Jr. Resonance tuning in rhythmic arm movements. *J. Motor Behavior*, 28(1):3–14, 1996.

[20] Geoffrey Hinton. Parallel computations for controlling an arm. *Journal of motor behavior*, 16(2):171–194, 1984.

[21] T. Iwasaki and M. Zheng. Sensory feedback mechanism underlying entrainment of central pattern generator to mechanical resonance. *Biological Cybernetics*, 94(4):245–261, 2006.

[22] Tetsuya Iwasaki. Multivariable harmonic balance for central pattern generators. *Automatica*, 44(12):3061–3069, 2008.

[23] Tetsuya Iwasaki, Jun Chen, and W Otto Friesen. Biological clockwork underlying adaptive rhythmic movements. *Proceedings of the National Academy of Sciences*, 111(3):978–983, 2014.

[24] Hami Kazerooni, J-L Racine, Lihua Huang, and Ryan Steger. On the control of the berkeley lower extremity exoskeleton (bleex). In *Robotics and automation, 2005. ICRA 2005. Proceedings of the 2005 IEEE international conference on*, pages 4353–4360. IEEE, 2005.

[25] Steven W Keele. Behavioral analysis of movement. *Comprehensive Physiology*, 1981.

[26] H.K. Khalil. *Nonlinear Systems*. Prentice Hall, 1996.

[27] S. Kohannim and T. Iwasaki. Analytical insights into optimality and resonance in fish swimming. *J. Royal Society Interface*, 11:20131073, 2014.

[28] H Igo Krebs, Neville Hogan, Mindy L Aisen, and Bruce T Volpe. Robot-aided neurorehabilitation. *IEEE transactions on rehabilitation engineering*, 6(1):75–87, 1998.

[29] Arthur D Kuo. Choosing your steps carefully. *IEEE Robotics & Automation Magazine*, 14(2):18–29, 2007.

[30] Xinmin Liu and Tetsuya Iwasaki. Design of coupled harmonic oscillators for synchronization and coordination. *IEEE Transactions on Automatic Control*, 2017. (To appear).

[31] Lennart Ljung. System identification. In *Signal analysis and prediction*, pages 163–173. Springer, 1998.

[32] Laura Marchal-Crespo and David J Reinkensmeyer. Review of control strategies for robotic movement training after neurologic injury. *Journal of neuroengineering and rehabilitation*, 6(1):20, 2009.

[33] Takamitsu Matsubara, Akimasa Uchikata, and Jun Morimoto. Full-body exoskeleton robot control for walking assistance by style-phase adaptive pattern generation. In *Intelligent Robots and Systems (IROS), 2012 IEEE/RSJ International Conference on*, pages 3914–3920. IEEE, 2012.

[34] Theodore E Milner. A model for the generation of movements requiring endpoint precision. *Neuroscience*, 49(2):487–496, 1992.

[35] Hiroyuki Miyamoto, Mitsuo Kawato, Tohru Setoyama, and Ryoji Suzuki. Feedback-error-learning neural network for trajectory control of a robotic manipulator. *Neural networks*, 1(3):251–265, 1988.

[36] G.N. Orlovsky, T.G. Deliagina, and S. Grillner. *Neuronal control of locomotion: from mollusc to man*. Oxford University Press, 1999.

[37] A Mehmet Oymagil, Joseph K Hitt, Thomas Sugar, and Jennifer Fleeger. Control of a regenerative braking powered ankle foot orthosis. In *Rehabilitation robotics, 2007. ICORR 2007. IEEE 10th international conference on*, pages 28–34. IEEE, 2007.

[38] GP Rosati Papini and Carlo Alberto Avizzano. Transparent force control for body extender. In *RO-MAN, 2012 IEEE*, pages 138–143. IEEE, 2012.

[39] L. Righetti and A.J. Ijspeert. Programmable central pattern generators: an application to biped locomotion control. *Proc. IEEE Int. Conf. Robotics and Automation*, pages 1585–1590, 2006.

[40] Ludovic Righetti, Jonas Buchli, and Auke Jan Ijspeert. Dynamic hebbian learning in adaptive frequency oscillators. *Physica D: Nonlinear Phenomena*, 216(2):269–281, 2006.

[41] Renaud Ronsse, Tommaso Lenzi, Nicola Vitiello, Bram Koopman, Edwin van Asseldonk, Stefano Marco Maria De Rossi, Jesse van den Kieboom, Herman van der Kooij, Maria Chiara Carrozza, and Auke Jan Ijspeert. Oscillator-based assistance of cyclical movements: model-based and model-free approaches. *Medical & biological engineering & computing*, 49(10):1173, 2011.

[42] Jacob Rosen, Moshe Brand, Moshe B Fuchs, and Mircea Arcan. A myosignal-based powered exoskeleton system. *Systems, Man and Cybernetics, Part A: Systems and Humans, IEEE Transactions on*, 31(3):210–222, 2001.

[43] Yoshiaki Sakagami, Ryujin Watanabe, Chiaki Aoyama, Shinichi Matsunaga, Nobuo Higaki, and Kikuo Fujimura. The intelligent asimo: System overview and integration. In *Intelligent Robots and Systems, 2002. IEEE/RSJ International Conference on*, volume 3, pages 2478–2483. IEEE, 2002.

[44] Daniel Sanz-Merodio, Manuel Cestari, Juan Carlos Arevalo, and Elena Garcia. Control motion approach of a lower limb orthosis to reduce energy consumption. *International Journal of Advanced Robotic Systems*, 9(6):232, 2012.

[45] Kenta Suzuki, Gouji Mito, Hiroaki Kawamoto, Yasuhisa Hasegawa, and Yoshiyuki Sankai. Intention-based walking support for paraplegia patients with robot suit hal. *Advanced Robotics*, 21(12):1441–1469, 2007.

[46] Nevio Luigi Tagliamonte, Fabrizio Sergi, Giorgio Carpino, Dino Accoto, and Eugenio Guglielmelli. Human-robot interaction tests on a novel robot for gait assistance. In *Rehabilitation Robotics (ICORR), 2013 IEEE International Conference on*, pages 1–6. IEEE, 2013.

[47] Ryosuke Tajima, Daisaku Honda, and Keisuke Suga. Fast running experiments involving a humanoid robot. In *Robotics and Automation, 2009. ICRA'09. IEEE International Conference on*, pages 1571–1576. IEEE, 2009.

[48] B.W. Verdaasdonk, H.F. Koopman, and F.C. Van der Helm. Resonance tuning in a neuro-musculo-skeletal model of the forearm. *Biological Cybernetics*, 96(2):165–180, 2007.

[49] C.A. Williams and S.P. DeWeerth. A comparison of resonance tuning with positive versus negative sensory feedback. *Biol. Cyb.*, 96:603–614, 2007.

[50] M.M. Williamson. Neural control of rhythmic arm movements. *Neural Networks*, 11:1379–1394, 1998.

[51] E Paul Zehr and Jacques Duysens. Regulation of arm and leg movement during human locomotion. *The Neuroscientist*, 10(4):347–361, 2004.

[52] J. Zhao and T. Iwasaki. Cpg control for assisting human with periodic motion tasks. In *2016 IEEE 55th Conference on Decision and Control (CDC)*, pages 5035–5040, Dec 2016.

[53] Adam B Zoss, Hami Kazerooni, and Andrew Chu. Biomechanical design of the berkeley lower extremity exoskeleton (bleex). *IEEE/ASME Transactions On Mechatronics*, 11(2):128–138, 2006.